Heteroleptic Copper(II) Chemotherapeutic Agents

Submitted in fulfilment of the requirements for the degree of

Master of Science

By

Njabulo Mbatha

BSc, (BSc Hons.) (UKZN)

November 2019

Declaration

I, Njabulo Mbatha, declare that:

i. This thesis/desitation is a presentation of my original research work. Wherever contribution of others are involved, effort is made to indicate this clearly, with due references to the literature, and acknowledgements.

ii. This thesis/desitation contain no material that has been submitted previously, in part or in whole, for the award of any other academic degree. Except where otherwise indicated, this thesis is my own work.

iii. This thesis/dissertation does not contain other persons' data, pictures, graphs or other information, unless specifically acknowledged as being sourced from other persons.

iv. This thesis/dissertation does not contain other persons' writing, unless specifically acknowledged as being sourced from other researchers. Where other written sources have been quoted, then:

   a) Their words have been re-written but the general information attributed to them has been referenced;
   b) Where their exact words have been used, their writing has been placed inside quotation marks, and referenced.

v. This dissertation/thesis does not contain text, graphics or tables copied and pasted from the internet, unless specifically acknowledged, and the source being detailed in the dissertation/thesis and in the References sections.

The work was done under the guidance of Professor M.P Akerman and Dr B.A Xulu, at the University of KwaZulu-Natal, Pietermaritzburg.

Signed: [redacted] Date: 3/12/2019

Njabulo Mbatha

In hereby certify that the above statements are true to the best of my knowledge.

Signed: [redacted] Date: 3/12/2019

Prof. M.P Akerman (Supervisor)

Signed: [redacted] Date: 3/12/2019

Dr B.A Xulu (Co-supervisor)

Acknowledgements

I would like to acknowledge and give thanks to my supervisor Prof M.P. Akerman, who made this work possible. His never ending patience, expert advice, guidance and assistance have been invaluable throughout the duration of this project. I also acknowledge his financial support.

Special thanks are due to Mr L. Hunter for his valuable suggestions throughout all stages of this work. His willingness to assist wherever possible is highly appreciated.

Furthermore, I am grateful to my co-supervisor, Dr B.A. Xulu for attaining the raw Electron Spin Resonance data.

My studies would not have been conceivable without my family. In particular, to my mother Nokukhanya Mbatha, who has made many sacrifices for me, I am forever grateful. Thank you for the motivation and encouragement through all ups and downs in my university career.

My thanks are extended to the University of KwaZulu-Natal, School of Chemistry and Physics for providing me with facilities required for this study.

Lastly, but most importantly, I am grateful to God for the strength and endurance that has made me the person I am today.

List of Abbreviations

%Diff.	percentage difference
Å	angstrom
°	degrees
A	absorbance
aq	aqueous
BC	before Christ
br	broad
Calc.	calculated
$CDCl_3$	deuterated chloroform
ctDNA	Calf Thymus DNA
d	doublet
DCM	dichloromethane
dd	doublet of doublets
DMF	*N, N'*-dimethylformamide
DMSO	Dimethyl sulfoxide
DMSO-d_6	Deuterated dimethylsulfoxide
DNA	deoxyribonucleic acid
DNA-EB	Deoxyribonucleic acid ethidium bromide
DPPZ	dipyrido[3,2-a:2',3'-c]phenazine
EB	ethidium bromide
IC_{50}	inhibitory concentration 50%
FTIR	fourier transform infrared
J	coupling constant
K	kelvin

K_{app}	apparent binding constant
K_{EB}	Ethidium bromide binding constant
m	multiplet/ medium intensity
m/z	mass to charge ratio
NMR	nuclear magnetic resonance
Phen	1,10-phenanthroline
Phendione	1,10-Phenanthroline-5,6-dione
Phen-NH_2	1,10-phenanthroline-5-amine
ppm	parts per million
s	singlet/ strong
t	triplet
THF	tetrahydrofuran
TOF	time of flight
UV	ultraviolet
vis	visible
w	weak
XRD	X-ray diffraction

List of Figures

Chapter 1

Chapter 2

Chapter 3

Chapter 4

Chapter 5

Chapter 6

Chapter 7

List of Tables

List of Schemes

ABSTRACT

In this study, a range of heteroleptic copper(II) chelates were synthesized as chemotherapeutic agents. Two primary heteroleptic copper(II) chelates, $[Cu(L)(H_2O)_2]NO_3$ and $[Cu(L1)(H_2O)_2]NO_3$ were successfully synthesized and characterized. These complexes had Schiff base ligands HL and HL1 coordinated, both with an *N,N',O* donor atom set which were synthesized by the reaction of 2-aminophenol with 2-pyridinecarbaldehyde for HL and the condensation of salicylaldehyde with 8-aminoquinoline for HL1. Both Schiff base ligands were synthesized *via* the eco-friendly solid state technique. The reaction between $(CuNO_3)_2$ and Schiff base HL yielded $[Cu(L)(H_2O)_2]NO_3$ which was further reacted with three co-ligands: 1,10-phenantroline (phen), 1,10-phenantroline-5-amine (phen-NH_2) and dipyrido[3,2-a:2',3'-c]phenazine (dppz) to afford three secondary heteroleptic copper(II) chelates. The secondary heteroleptic copper(II) complexes have been synthesized using a mechanochemical technique that is eco-friendly, efficient, simple and afforded excellent yields. The co-ligand dppz was prepared from the reaction of 1,10-phenanthroline-5,6-dione with *o*-phenylenediamine. The complex $[Cu(phen\text{-}NH_2)_2Cl]Cl$ was synthesized by reacting $CuCl_2$ with 1,10-phenantroline-5-amine.

The ligands have been characterised by mass spectrometry (MS), IR and NMR spectroscopy, while the chelates have been characterised by EPR, MS, elemental analysis as well as UV/vis spectroscopy. The solid state structures of three heteroleptic complexes were elucidated using single crystal X-ray diffraction. X-ray crystallography showed that $[Cu(L)(H_2O)_2]NO_3$ and $[Cu(L1)(H_2O)_2]NO_3$ complexes had square pyramidal geometries with various combinations of N and O-donor ligands. The solution state coordination geometry of copper(II) complexes $[Cu(L)(H_2O)_2]NO_3$, $[Cu(L)(phen)]NO_3$, $[Cu(L)(phen\text{-}NH_2)]NO_3$ and $[Cu(L)(dppz)]NO_3$ were found to be trigonal bipyramidal using EPR spectroscopy.

The DNA binding affinities of the chelates were measured using fluorescence competitive binding assays. The binding affinities range from 2.79×10^5 M^{-1} for $[Cu(L)(H_2O)_2]NO_3$ to 5.31×10^6 M^{-1} for $[Cu(phen\text{-}NH_2)_2(Cl)]Cl$. The order of all complexes in terms of increasing binding strength is: $[Cu(L)(H_2O)_2]NO_3$ < $[Cu(L)(phen)]NO_3$ < $[Cu(L)(dppz)]NO_3$ < $[Cu(L)(phen\text{-}NH_2)]NO_3$ < $[Cu(phen\text{-}NH_2)_2(Cl)]Cl$. The five copper(II) chelates synthesized were screened against a panel of four human cell lines. These cell lines are: HEK293 (healthy embryonic kidney cells) which was used as a control, MDA-MB (triple negative cancer cells), HELA (cervical cancer cells) as well as SHSY5Y (human neuroblastoma cells). From the cell screening, the EC_{50} values were calculated. The complex $[Cu(L)(dppz)]NO_3$ had the lowest EC_{50} values while $[Cu(L)(H_2O)_2]NO_3$ had the highest EC_{50} values. The results showed that four complexes are highly cytotoxic towards tumour cells, more so than the well-known chemothepeutic agent cisplatin. The complex $[Cu(L)(H_2O)_2]NO_3$ showed lower cytotoxicity, however, it has greater selectivity towards tumour cells.

The cytotoxicity of the compounds varies with different cells; hence each has a unique cytotoxicity profile and could be used for a specific type of cancer. There is little correlation between the binding affinities of complexes and their cytotoxicity, this suggest that the mechanism of action could include the production of ROS *in vitro*, which are known to cleave the DNA and induce apoptosis. Significantly, all the complexes synthesized in this work showed lower toxicity towards

the healthy cell line than the tumour cell lines. It was also shown that the combination of the Schiff base ligand and co-ligand was an important factor in the cytotoxicity. The redox activity of copper and the production of reactive oxygen species (ROS) are likely key in the cytotoxicity of the complexes.

TABLE OF CONTENTS

CHAPTER 1: INTRODUCTION

1.1 Preface

Cancer is a group of diseases characterised by the uncontrolled growth and spread of abnormal cells which can invade nearby tissues.[1] Cells generally become cancerous due to the accumulation of mutations in their DNA. Though cancer has been known since antiquity, most significant advances made in understanding it have been since the middle of the 20th century.[2] Some of the earliest evidence of human bone cancer dates to approximately 1600 B.C where it was found in mummified bodies in ancient Egypt. The world's oldest recorded case of breast cancer also hails from ancient Egypt in 1500 BC, where it was recorded that there was no treatment for the cancer, only palliative care.[3]

Cancer is a major health burden and remains the second leading cause of death globally after cardiovascular diseases. In 2015, there were an estimated 17.5 million new cancer cases of cancer with over 8.7 million deaths recorded. Prostate and lung cancer are the most common cancer in men while breast cancer is the leading cause of cancer deaths in women.[4] With these alarming statistical findings, there is clearly a need for developing improved intervention measures.

In recent decades, there has been an increase in the rate of cancer survival following the discovery of the anticancer activity of cis-diamminedichloroplatinum(II) (cisplatin).[5,6] Cisplatin is a widely used chemotherapeutic drug to treat different types of cancers such as testicular and ovarian cancer.[7] Although this drug is effective against cancer cells, the drug itself has clinical disadvantages. Cisplatin targets both healthy cells and cancer cells, without any distinction, in the same manner as most currently available chemotherapeutic drugs. The lack of cell selectivity leads to a variety of undesirable side effects such as anemia, myelotoxicity, nephrotoxicity and hair loss.[74] To overcome these sides effects new chemotherapeutic drugs, that should specifically and selectively target different types of cancer cells are needed. These would reduce side effects.[8,9]

Metals play a significant role in a number of biological processes including redox chemistry and facilating enzyme function. In the past 50 years, transition metals have increasingly become the focus in the development of novel cancer therapies.[9] Among all the metals studied, copper complexes are regarded as one of the most promising alternatives to cisplatin drugs.[90] The medicinal properties of copper have been known and used for centuries. The first recorded medical use was found in an Egyptian text, written between 2600 and 2200 B.C., in which copper was use to sterilize both drinking water and chest wounds.[10]

In this research study, the chemotherapeutic potential of Schiff base ligands with multiple N-heterocyclic aromatic ligands forming heteroleptic copper(II) complexes will be investigated. These copper-based compounds represent an exciting new prospect in the search for chemotherapeutics as the biologically accessible redox potential means they can catalytically produce reactive oxygen species (ROS) *in vivo*. These ROS can induce single and double-stranded DNA cleavage, hindering DNA replication. Thus a novel set of compounds with a unique mechanism of action are being developed and their cytotoxicity investigated.

1.2 Cancer

1.2.1 What is cancer?

Cancer is a number of diseases, potentially affecting almost all organs, and is characterized by uncontrolled cell growth that can potentially spread into the surrounding normal tissues, or to other body parts *via* the lymphatic system and/or blood stream.[51] This uncontrolled and accelerated growth results in the formation of a lump called a tumor; this is true for all cancers except leukaemia. Tumours can be malignant or benign: a malignant tumor tends to grow faster than a benign one and they have the ability to spread and destroy surrounding tissues. Malignant tumour cells can break off from the main (primary) tumour, invade healthy neighbouring tissues and spread to other body parts through the process of metastasis. The condition is hence known as metastatic cancer and the secondary sites are referred to as metastases, Figure 1.1. Benign tumours tend to grow more slowly, are rarely life threatening and do not spread to other parts of body.[52,53]

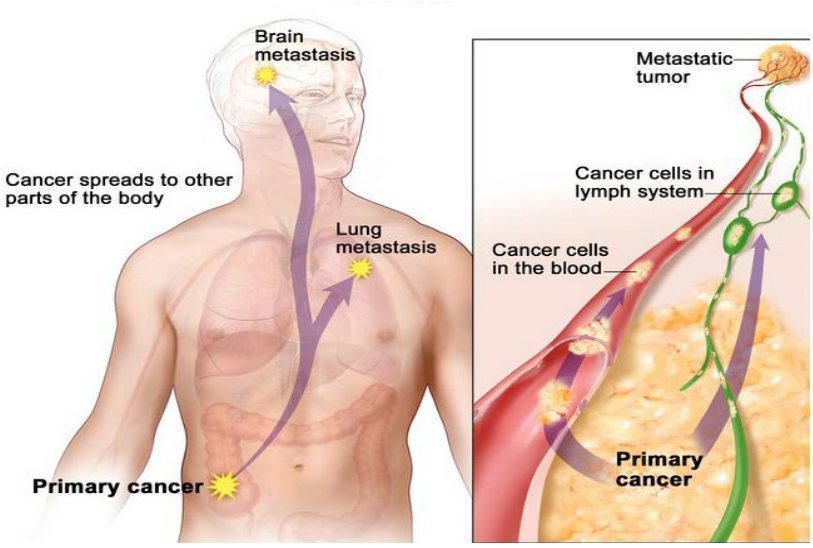

Figure 1.1: Metastasis process showing cancer cells traveling through the blood or lymph system, and forming new tumors (metastatic tumors) in other parts of the human body.[77]

1.2.2 Diagnosis

There is no single test that can diagnose cancer accurately. The complete evaluation process includes a physical examination and thorough medical history coupled with diagnostic testing. Many tests need to be done to determine whether a patient has cancer, or has another condition with symptoms similar to cancer. There are a wide range of cancer diagnostic methods these include, lab tests, diagnostic imaging, genetic tests, tumor biopsies and endoscopic exams.[53,57]

Diagnostic imaging is one of the main aspects of comprehensive cancer care. Imaging is not only used for detection, but it is also important in determining the stage and the precise location of cancer to assist in directing the surgery or cancer treatments. Imaging offers many advantages including accessibility without tissue destruction, real time monitoring, minimal or no invasiveness and can function over a wide range of size and time scales involved in pathological and biological processes.[79,80]

There are various imaging methods used for biological imaging, these include Positron Emission Tomography (PET), Magnetic Resonance Spectroscopy (MRS), Magnetic Resonance Imaging (MRI), Computed Tomography (CT), Single Photon Emission CT (SPECT), Ultrasound (US) and optical imaging. The majority of imaging in the clinical setting is currently performed only with PET and SPECT imaging, with each technique having advantages and disadvantages (Table 1.1).

Table 1.1: Advantages and disadvantages of PET and SPECT imaging techniques.

Technique	Advantage	Disadvantage	Common contrast agent	Example clinical application
PET	• Quantitative molecular imaging • Unlimited depth penetration • Whole body imaging possible • Can be combined with CT or MRI for anatomical information	• Radiation exposure • High cost • Low spatial resolution (1-2 mm; 4-8 mm^3) • Long acquisition times (minutes to hour)	• ^{11}C • ^{18}C • ^{64}Cu • ^{68}Ga	• ^{18}F-FDG-PET for cancer staging
SPECT	• Quantitative molecular imaging • Unlimited depth penetration • Theranostic: can combine imaging and radiotherapy • Can be combined with CT for anatomical information	• Radiation exposure • Low spatial resolution (0.3-1 mm; 12-15 mm^3) • Long acquisition time	• ^{99m}Tc • ^{123}I • ^{111}In • ^{177}Lu	• Radiotherapy of thyroid carcinoma with ^{131}I-iodide

The PET imaging produces a valuable overview of organs and body structure by the use of radiotracers that emit positrons, the counterparts of electrons. The gamma rays used for imaging are produced when the positron meets an electron inside the body of a patient, an encounter that annihilates both positrons and electrons and produces two gamma rays travelling in opposite directions.[85] Figure 1.2 shows that only coincident photons are registered and not scattered ones.

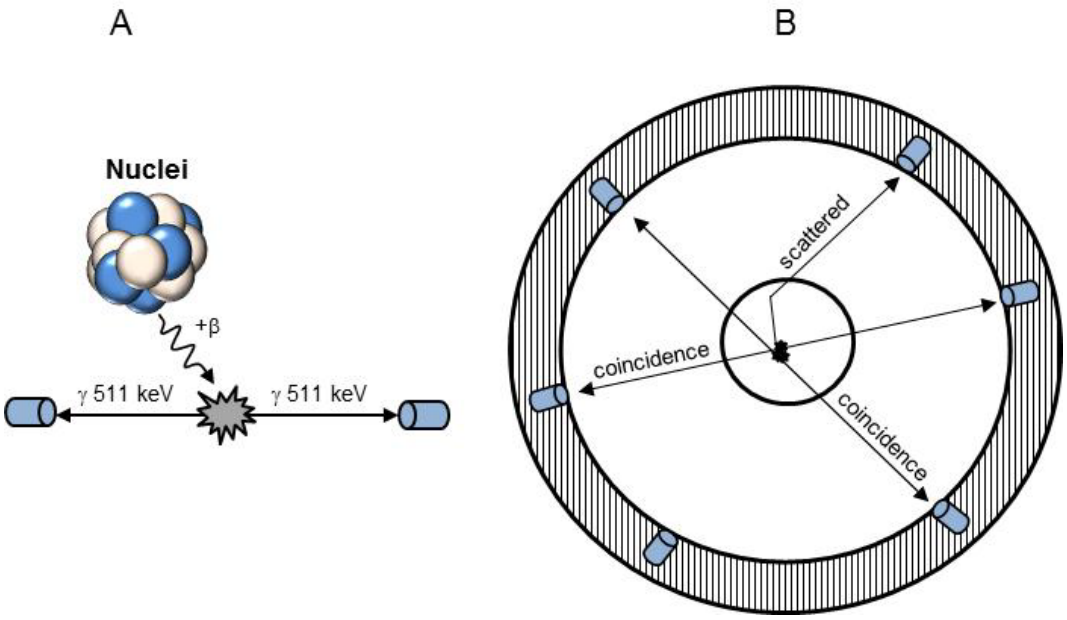

Figure 1.2: Schematic diagram of PET imaging basic principles. (A) The movement of a positron before annihilating with an electron, with emission of two 511 keV photons (this is the specific decay energy of the Cu-64 isotope) to each other; and (B) a PET camera with an acquisition system illustrating how the co-incident rays are used to map the position of a tumour.[89]

There is a great number of suitable positron emitting isotopes used in PET e.g. ^{18}F, ^{15}O, ^{13}N and ^{11}C. ^{18}F in particular, is used to make the radioactive analogue of glucose (^{18}F-labled 2-deoxy-d-glucose, FDG) which is an excellent probe of glucose metabolism. Since glucose has a huge role in many biological processes, ^{18}F-FDG is a versatile imaging agent that can be used widely in oncology. There is effective uptake of this compound by cancer cells making it an ideal tool for detection of tumours.[81,82]

Following the success of ^{18}F-FDG, there has been a considerable interest in the radiopharmaceutical sector and the search for new imaging agents labelled with ^{18}F as well as other radionuclides such as copper isotopes. Positron-emitting ^{64}Cu which has $t_{1/2}$ = 12.8 hours; B^+ = 0.655 MeV (19%); B^- = 0.573 MeV (40%) has shown promise in the development of new PET agents. ^{64}Cu has a relatively long half-life compared to commonly used radioisotopes for PET imaging: ^{11}C ($t_{1/2}$ =20.4 min) and ^{18}F ($t_{1/2}$ =109.7 min). Longer half-lives are favourable for imaging the *in vivo* behaviour of targeting monoclonal antibodies, antibody fragments, peptides, and nanoparticles which all take a longer time to reach their target. The longer half-life of ^{64}Cu also enables imaging up to 48 h post-injection while limiting the exposure of the patient to radiation, unlike longer lived radionuclides such as ^{89}Zr ($t_{1/2}$ =78.4 h). [83] Shorter-lived positron-emitting copper radioisotopes are also useful: ^{62}Cu ($t_{1/2}$ = 9.7 min), ^{60}Cu ($t_{1/2}$ = 23.7 min) and ^{61}Cu($t_{1/2}$ = 3.32 h), they have been used as perfusion agents such as Cu-ethylglyoxal bis(thiosemicarbazone) ETS.[84]

There are three general categories in which ^{64}Cu-labelled radiophamarceuticals can be grouped: small molecules, antibodies and peptides. Among small molecules, ^{64}Cu-PTSM (pyruvaldehyde bis(N_4-dimethylthiosemicarbazone)), shown in Figure 1.3, has proven to be an agent that can measure blood flow in the brain and heart, thus identifying blood flow abnormalities. Cu–ATSM (diacetylbis(N^4-methylthiosemicarbazone)) is another thiosemicarbarzone complex of Cu(II) with a similar structure to that of ^{64}Cu-PTSM (Figure 1.3) and has been shown to be trapped in hypoxic cells. In the presence of hypoxia, there is a reduction of Cu(II)-ATSM to Cu(I)-ATSM, which is then

trapped intracellularly, resulting in a very high and rapid tumor uptake post-injection. Clinical studies have shown that when ^{64}Cu-ATSM is administered in large quantities it can predict tumor response to therapy in non-small cell lung cancer and cervical cancer.[86]

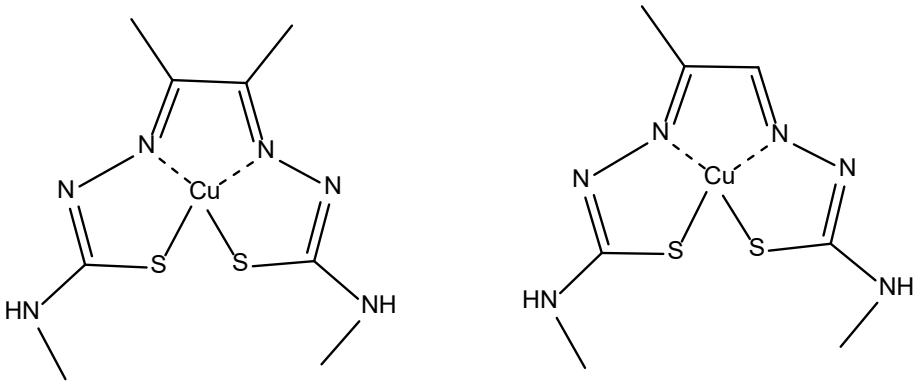

Figure 1.3: Structure of Cu-ATSM (Left) and Cu-PTSM (Right) (^{62}Cu or ^{64}Cu).[86]

Molecular imaging can play a huge role in the different areas of oncology including diagnosis, disease detection, personalized treatment, treatment monitoring, staging and follow-up.[87] However, the current status of clinical molecular imaging is limited to the use of PET and SPECT imaging, and a small number of highly specific applications for MRS/MRI, US, and optical imaging. There is thus a high demand for new strategies with improved imaging and screening protocols to enhance early disease detection, improve patient-specific treatment selection and therapy-specific monitoring. It is believed that these new strategies will improve success rates for curing deadly diseases such as cardiovascular disease and cancer and provide more specific treatment for other diseases such as Parkinson's and Alzheimer's.[88]

1.2.3 How is cancer treated?

Chemotherapy (chemo) refers to the use of, generally a small molecule, anticancer drugs to destroy cancer cells. The treatment may be given in different ways depending on the stage and the type of cancer being treated. Some common routes include oral, injection, intrathecal, infusion and topical application. Chemotherapy stops the growth of cancer cells, by either preventing cell division or killing the cells. It generally has a greater effect on cancer cells because they divide and grow faster than normal cells. Although chemotherapeutic agents are powerful, they can cause damage to healthy cells, affecting rapidly dividing cells such as hair follicles most significantly, which leads to undesirable sides effects.[54,55] A potential advantage of chemotherapy is that it is a systematic treatment circulating throughout the whole body *via* the bloodstream, thus it can treat cancer cells almost anywhere in the body. Chemotherapy is used to treat different types of cancers. For some types of cancer, this treatment can also be used in combination with other cancer treatments such as radiation and surgery. An example of this is the use of radiosensitizers which are chemotherapeutic drugs that make cancer cells more sensitive to radiation, thus increasing the efficacy of radiation therapy.[56]

Over the last few decades, the use of chemotherapeutic agents has resulted in the successful treatment of various types of cancer. However, to minimize the side-effects associated with chemotherapy new approaches are being studied, this includes the use of monoclonal and liposomal therapy to target specifically cancer cells, new combinations of drugs, chemoprotective agents and agents that overcome multidrug resistance.[57,58]

1.2.4 Aetiology of cancer

It is not easy to determine the specific cause and (or) treatment of cancer since there are more than 200 different types of cancer. The causes of cancer may be biological, physical or chemical. Major biological causes include infection with oncogenic viruses (such as hepatitis B virus), which can trigger mechanisms that lead to the deregulation of genes critical for survival and growth of malignant tissues. Physical causes include exposure to ionizing or ultraviolet radiation (sun exposure), whereas chemical carcinogenesis may take place due to the exposure to carcinogens, which may be occupational (e.g. bladder cancer by the exposure to nitrosamines); or environmental (e.g. exposure to cigarette smoke, asbestos, or benzene). Other factors which increase the risk of cancer include the intake of alcohol, lack of physical activity, obesity and a poor diet. [55,59,78]

1.3 Transition Metals in Medicine

Metal ions play a key role in most biological systems, participating in a number of biological processes including oxygen transportation, redox reactions and facilitating enzyme function.[9] Although important, either scarcity or excessive amounts of metals can cause fatal diseases. Well-known examples include anemia arising from iron deficiency and Wilson's disease due to excess copper accumulation.[11] As our understanding of metals in biological processes improves, we may develop a better understanding of the etiology of disease such as cancer and hence develop more effective intervention measures.[12]

The pharmaceutical sector has typically been dominated by organic compounds, however, in the last half century inorganic drugs have been getting increased attention.[13] Transition metal coordination complexes offer a number of advantages over standard organic molecules or free metal ions in the design of DNA-binding agents and chemotherapeutics. Transition metals have unique structural properties that allows them to organise other molecules (ligands) in a wide range of geometries.[14] They also have the ability to be transferred in the biological environment by ligand substitution reactions and redox reactions.[13] The history of metal-based drugs started with the discovery of the anticancer activity of cisplatin (cis-diamminedichloroplatinum(II)) in the 1960's. Cisplatin is used to treat a broad range of cancers, including testicular, cervical, lung, ovarian and bladder cancers. However, this anticancer-drug has significant flaws as it is prone to resistance in secondary tumors, and the lack of selectivity and specificity leads to undesirable biological activity. Another problem lies in the side effects (nephrotoxic, severe nausea and vomiting) associated with it's toxicity and interaction with other biomolecules.[9,15] It's mode of action has been linked with binding to DNA *via* both intrastand and interstrand cross linking; interfering with DNA replication and RNA transtription. This subsequently triggers apoptosis in cancer cells.[16]

To combat these cisplatin-related issues, other platinum based-complexes (Figure 1.4) have been synthesized and found clinical application for therapy and diagnosis. Satraplatin and iproplatin are Pt(IV) octahedral complexes that appear to be more effective and exhibit lower toxicity compared to Pt(II) complexes, this is due to their relative inertness and reduced reactivity towards biomolecules.[17] As illustrated in Figure 1.4, these platinum-based compounds are a good illustration of how small modifications in chemical structure can have a significant effect on biological activity. Cisplatin is structurally composed of four ligands surrounding the divalent

platinum ion. Ammine ligands form strong interactions with the platinum ion while the two chlorido ligands are weakly bonded rendering them an ideal leaving group thus allowing the platinum ion to form new bonds with DNA bases.[18] Carboplatin is another platinum(II)-based chemotherapeutic drug used for neck, head, lung and ovarian cancers. It has a similar mechanism of action to cisplatin, but differs in terms of toxicity and structure. Carboplatin has a bidentate ligand (cyclobutane decarboxylate group) replacing the two chlorido ligands associated with cisplatin.[19] Carboplatin has reduced neurotoxicity, nephrotoxic effects, vomiting and nausea experienced by patients, but it is known to be more myelotoxic. To address the problem associated with current platinum-based drugs, current research has focused on other metal-based anticancer drugs that have different mechanisms of action, hydrolytic rates and chemical behaviour.[20] Several metals including gold, palladium, ruthenium, copper and rhenium have been investigated as possible chemotherapeutic agents.[15,20] The applications of some of these metals in medicinal chemistry are evaluated in the following sections.

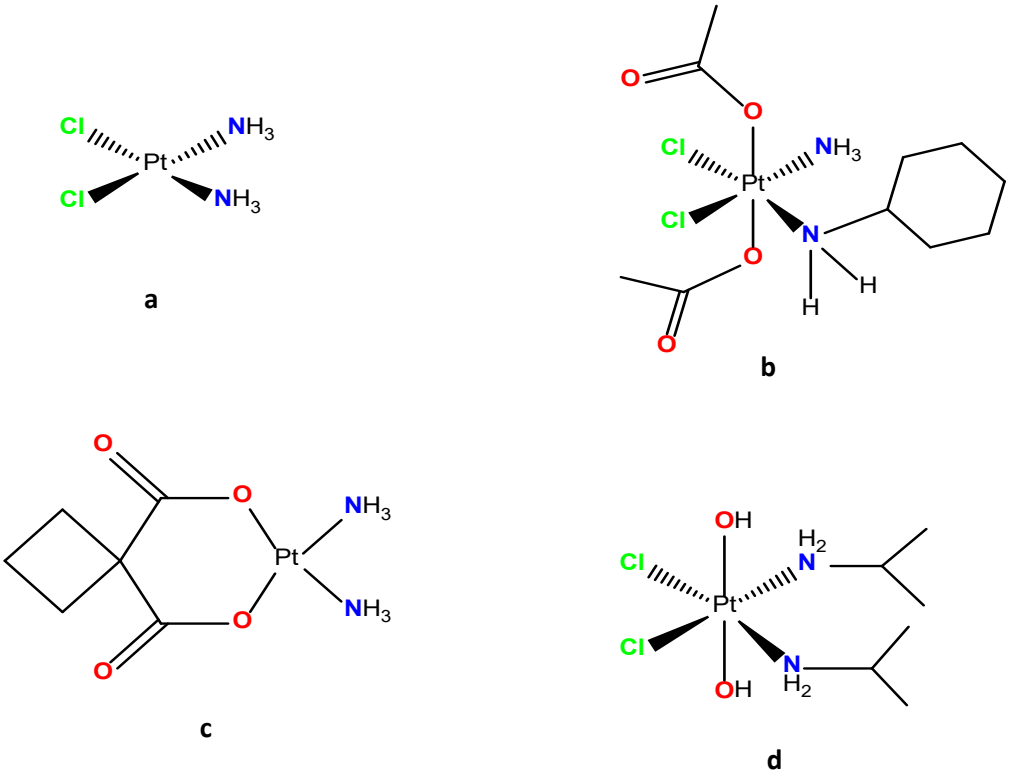

Figure 1.4: Platinum-based chemotherapeutic agents: a) Cisplatin, b) Satraplatin, c) Carboplatin, d) Iproplatin.[7]

1.3.1 Ruthenium

The history of ruthenium-based anticancer complexes started in 1980, when chloro-amine-Ru(III) compounds were discovered to have anticancer activity in rats.[21] However, its application was limited by poor solubility; *cis*-[$RuCl_2(dmso)_4$] was then developed and shown to be active against both primary and secondary cancer cells.[21,22] Ruthenium has variable oxidation states, Ru(II), Ru(III) and Ru(IV) which are all accessible under physiological conditions. Due to low energy barriers to interconversion between these oxidation states, there is a possibility of oxidation state changes within the cell which may enhance the cytotoxicity.[22] The interest in designing ruthenium chemotherapeutic drugs has been growing since KP1019 and NAMI-A (Figure 1.5) each successfully completed phase 1 clinical trials in 2008 and 2004, respectively.[20] KP1019 and NAMI-

A are structurally similar (both have Ru(III), heterocyclic ligands, chloride ion and heterocyclic counter ion) yet they display different cytotoxic profiles and anticancer activity. NAMI-A is found to be active against secondary cancer cells such as non-small cell lung cancer, whereas KP1019 is active against primary cancers, especially colorectal cancer.[22-24] Moreover, their mechanism differs in that KP1019 causes cell death *via* the formation of reactive ROS and intrinsic mitochondrial pathway, while NAMI-A interferes with the extracellular matrix, preventing further tumor metastasis.[25]

In comparison to platinum drugs, ruthenium compounds tend to cause fewer and less severe side effects, this is believed to be because of "Activation by Reduction". This theory is based on the understanding that ruthenium(II) complexes are more reactive than Ru(III), which can partially be attributed to the higher effective nuclear charge. Furthermore, cancerous cells tend to have a more chemically reducing environment compared to healthy cells, owing to their lower concentration of molecular oxygen (due to remoteness from blood supply and higher metabolic rate).[26] A less toxic ruthenium(III) compound can therefore be administered and is converted into the more toxic ruthenium(II) derivative only inside the reducing environment of the cancer cell.

Also, chemical similarities between iron and ruthenium (they are Group congeners) in binding to biological molecules, including serum proteins (e.g. albumin and transferiin) is believed to have an effect on the general toxicity of ruthenium-based drugs.[27] Absorption, solubility and tumor targeting are among the issues concerned in the design of novel ruthenium chemotherapeutic drugs.[24]

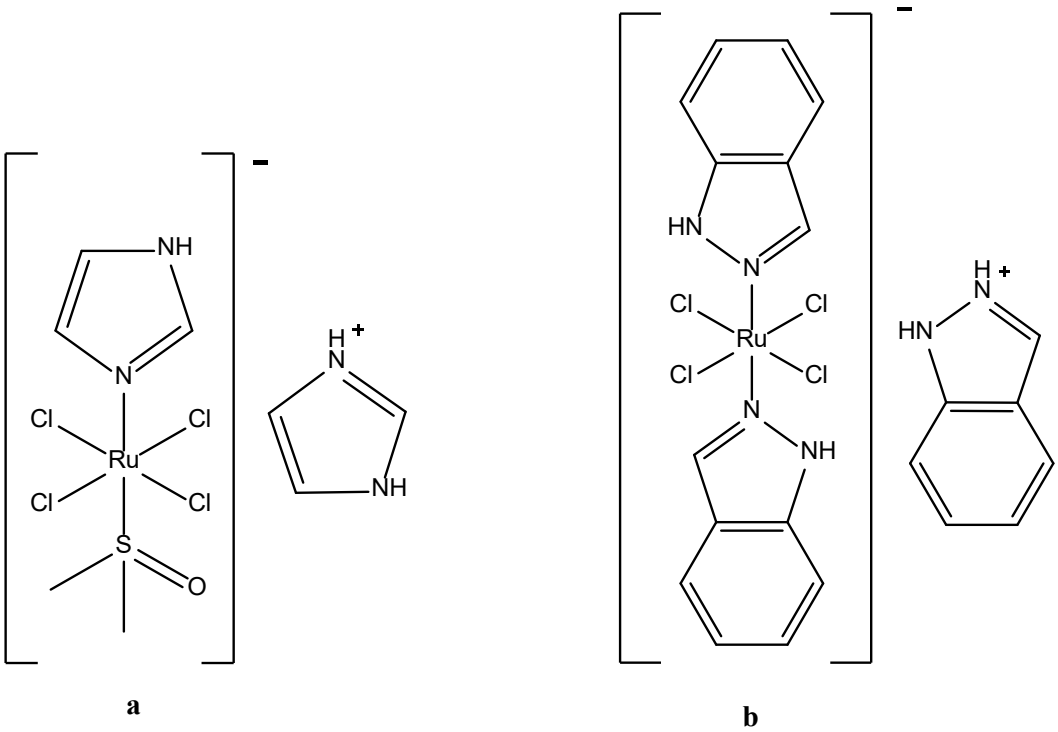

a b

Figure 1.5: Structures of Ru(III) complexes: NAMI-A (a) and KP1019 (b).[21]

1.3.2 Copper

1.3.2.1 Copper in Medicine

Copper (Cu) is an essential micronutrient in all living organisms.[29,30] It is required for a wide range of biological process such as respiration, energy production, metabolism of oxygen and iron, cell signalling and free radical eradication.[30] Due to the high redox activity of copper (Cu^{2+}/Cu^{+}), many enzymes harness this activity and hence copper plays a vital role in biological redox reactions. While the redox properties of copper ions are important for enzymatic reactions, this property can be potentially toxic.[28] The toxicity of copper has been attributed to its ability to catalyse the production of free radicals, leading to damage in lipids, proteins, DNA and other biomolecules. Additionally, copper can interfere and displace metals such as zinc from metalloproteins inhibiting their activity.[28-30]

A healthy 60 kg human body only contains about 100 mg of this vital element.[31] Copper is located in different regions of the body, the highest concentrations are in the liver, brain, central nervous system and heart.[32] Cu is absorbed within the gut and then transported to the liver (which is responsible for regulating and excretion of copper) before it is distributed to other tissues. Ceruloplasmin protein is involved in the transportation of Cu in the liver and also carries most Cu in the blood.[33]

In prokaryotes, more than 10 proteins have been identified to require copper for their function these are Cu/Zn–superoxide dismutase (SOD1, a cytosolic protein that speeds up the dismutation of superoxide) and cytochrome c oxidase (COX, the terminal mitochondrial electron carrier), for example.[28] In addition, Cu plays a vital role in many physiological functions of haematological, reproduction, cardiovascular and nervous systems.[34] The role of copper ions in the active site of different metallo-proteins has driven many researchers to synthesize and characterize new copper complexes as models to further the understanding of biological systems.

Although copper is an essential microelement, it has to be maintained at an optimum level. Any imbalance in copper bioavailability leads to various disorders in humans. Myeloneuropathy, leucopenia, Alzheimer's, dementia and anemia are among the disorders resulting from insufficient copper. An excess of copper also has negative effects on human health causing Menkes disease and Wilson's diseases.[35] Menkes disease also known as Menkes syndrome, is an X-linked disorder of copper metabolism resulting in severe neurodegenerative disease in early childhood.[35,91] Wilson's disease is a rare autosomal recessive disorder of copper metabolism resulting in neuronal degeneration and hepatic cirrhosis.[91]

1.3.2.2 Copper as an Antibiotic Agent

Copper has been used for hygienic purposes for centuries. The Greek physician Hippocrates used it to treat skin irritation and wounds, while the ancient Egyptians similarly used it to sterilize wounds and drinking water.[36] Storing contaminated water in copper pots for 16 h was proven to be sufficient to kill diarrhoeagenic bacteria (*Salmonella enterica Paratyphi*, *Vibrio cholera*, enteropathogenic *E. coli*, *Shigella flexneri* and *Salmonella enterica Typhi*). This decontamination process is very effective. [37,38]

Copper was recognised as a metallic antimicrobial agent by the US Environmental Protection Agency in 2008 and about 300 copper-containing compounds were registered as antimicrobial agents.[36] Since then, there has been renewed interest in the applications of the antimicrobial properties of copper such as piping material, water treatment and working surfaces.[36]

In addition, copper can be used in pesticides, fungicides and algaecides, but the feasibility of such practices must be monitored and carefully evaluated since high copper intake can be poisonous.[39,40] Unfortunately, the widespread use of copper containing compounds in agriculture, farming and medicine has led to prolonged exposure of bacteria to copper, resulting in the evolution of copper-tolerant/resistant strains, which limits the future application of copper compounds in the aforementioned fields.[41]

Generally, divalent copper compounds are utilized although Cu(I) also shows antibiotic activity. Copper(II) complexes normally bear a combination of ligands to enhance the activity of the drugs. The utilisation of 1,10-phenanthroline in Cu(II)-antibiotic complexes is found to increase the stability of the drug as in the case of lomefloxacin.[42,43]

1.3.2.3 Anticancer Activity of Copper Complexes

Copper complexes have been studied for various therapeutic purposes, such as antifungal, antimalarial and antibacterial agents, but more recent research has focused on their action as anticancer agents. The mechanism of action of these copper-based chemotherapeutics is not yet fully understood.[44] One well-supported pathway is based on the intracellular thiol-mediated reduction of copper(II) to copper(I) *via* the Haber-Weiss reaction, in the process catalysing the formation of hydroxyl radicals from hydrogen peroxide (see equations below).

$$HS\text{-}R\text{-}S^{-} + Cu^{2+} \rightarrow HS\text{-}R\text{-}S + Cu^{+}$$

$$HS\text{-}R\text{-}S^{\cdot} + O_2 \rightarrow S\text{-}S\text{-}R + H^{+} + O_2^{-\cdot}$$

$$2O_2^{-\cdot} + 2H^{+} \rightarrow H_2O_2 + O_2$$

$$Cu^{+} + H_2O_2 \rightarrow OH^{\cdot} + OH^{-} + Cu^{2+}$$

$$OH^{\cdot} + DNA \rightarrow Fragments$$

Scheme 1.1: The reaction equations for the formation of hydroxyl radicals catalysed by copper(II).

These reactive hydroxyl radicals have the ability to interact with most biological molecules by either removing an electron from an aromatic system or the hydrogen atom from an amino bearing carbon, forming a carbonated protein radical and unsaturated fatty acids to form a lipid radical. This can induce extensive oxidative damage in cells, but most importantly are known to produce DNA strand breaks which can ultimately lead to cell apoptosis.[45,46]

1.3.2.4 Copper Complexes with Phenanthroline Ligands

Phenanthroline (phen) is a neutral heterocyclic ligand that has two N-donor atoms. Phen and its derivatives display a wide range of physiological and biological activities. They have therefore attracted considerable interest from both medicinal and synthetic chemists.[47] It is also an appropriate ligand for DNA binding due to its hydrophobic, rigidly planar and heteroaromatic structure.[48] Copper-based complexes have been investigated for antitumor potential based on the assumption that endogenous metals may be less toxic than current metallodrugs based on platinum. They could also be tuned to specifically interact with pre-selected biological targets and thereby minimise the toxicity to healthy tissue.

The properties of copper-based complexes are largely determined by the nature of the coordinated ligands and the donor atoms bonded to the metal centre.[49] Copper complexes with phenanthroline are known to act as nucleases, causing oxidative damage and cleave nucleic acids. Additionally, Cu(II) complexes with Schiff base ligands are known to have strong interactions with DNA *via* intercalation or surface interactions and potential DNA cleavage properties *via* oxidative or hydrolytic mechanisms. Schiff bases also have unique properties (denticity, easy synthesis and stability) which makes them versatile and widely used in coordination chemistry.[48,50] Moreover, copper complexes with Schiff base ligands could inhibit *in vitro* tumor cell growth with the cytotoxicity of the Cu(II) complexes higher than that of the free ligands.[50]

1.3.2.5 Polynuclear Copper Complexes

Copper(II) tri- and dinuclear complexes have impressive antiangiogenic properties and cytotoxicity activities, mostly via ROS formation pathway.[7] However, DNA binding and intercalation pathways may also be relevant as in the case of a trimetallic species containing μ-amido-bridge ligands which was found to be active against lung and liver cancers.[7,48] Similar results have been reported for a trinuclear complex containing a disubstituted terpyridine ligands which shows that this complex can efficiently bind and break DNA strands, the cleavage activity is dependent on the number of copper atoms present in the complex, which increase in order: 1 < 2 < 3. This trimetallic complex was found to be highly active against leukemia, with good propensity to enter the cell and localize in its nucleus. Thus polypyridyl ligands can confer high cytotoxicity on copper(II) polynuclear species, although the mechanism of action differs depending on the type of ligands used.[7,42]

1.4 DNA Binding

1.4.1 DNA Structure

DNA was identified as one of the primary targets for a number of anti-cancer drugs currently in clinical trials. Hence the precise understanding of the DNA structure and the binding properties of transition metal complexes is of paramount importance in the process of designing potential chemotherapeutic drugs.[60] The three dimensional structure of DNA proposed by Watson and Crick (1953) consists of two antiparallel polymeric chains, with a hydrophobic core and a sugar phosphate hydrophilic backbone.[92] A major and minor grove is generated along the DNA chain as the two sugar-phosphates twist around the central stack of base pairs. These groves are due to *N*-gylcosidic bonds of the base pair that are not diametrically opposed to each other.[60]

The complementary strands of nucleotides that form the DNA double-helical structure are stabilized by hydrogen bonding between guanine and cytosine (G–C) and adenine and thymine (A–T) nucleic acids. In addition, electrostatic forces between the negatively charged phosphate groups and solvated ions play a vital role in stabilizing the DNA strands.[61]

1.4.2 Types of DNA interaction

A precise understanding of how transition metal complexes interact with DNA is key in the development of more specific and efficient therapeutics, with minimum or no side-effects. Since DNA was identified as one of the primary targets for different types of drugs, including metal

based drugs, binding small molecules to DNA is important in understanding the drug-DNA interactions. A small molecule that binds to DNA has the potential to inhibit and/or alter its function, interfere with replication, protein synthesis and disturb gene expression. The adduct formed upon binding to DNA can be stabilized through a series of interactions, such as hydrogen bonding, van der Waals interactions, π-stacking (of aromatic hetrocyclic groups between base pairs) and electrostatic interactions.[60-62]

The binding of molecules may be either covalent or non-covalent. Most of the chemotherapeutic agents currently in use such as cisplatin and nitrogen mustard exert their effect by covalent binding to DNA, forming an adduct through alkylation or intrastrand and interstrand crosslinking. This type of binding is irreversible and causes the complete inhibition of DNA function and induces apoptosis. The non-covalent binding of molecules to DNA includes major and minor groove binding (Figure 1.6), electrostatic interaction and intercalation between adjacent base pairs. This results in structural abnormalities and interference with normal DNA functions such as protein interaction and replication. Non-covalent binding is preferred over covalent adduct formation because it is considered to be reversible and less cytotoxic. However, the high binding strength of covalent interactions is a major advantage.[63,64,75]

The non-covalent binders are divided into two types: intercalators (acridine, doxorubicin, etc.) and groove binders (netropsin and distamycin). Intercalators are molecules that have a planar moiety usually comprising fused aromatic rings, which are inserted between adjacent DNA base pairs, which reduces the DNA helical twist and lengthens the DNA. The energy required for this process is low (approximately 4 kcal mol^{-1}) this is due to the favourable contributions (hydrogen bonding, van der waals forces, hydrophobic and ionic interactions) which stabilize the complex and results in association constants of 10^5 to 10^{11} M^{-1}.[76] Although intercalation is usually associated with molecules containing fused rings structures, atypical intercalators with non-fused ring system exist, Figure 1.7.[65,66,76]

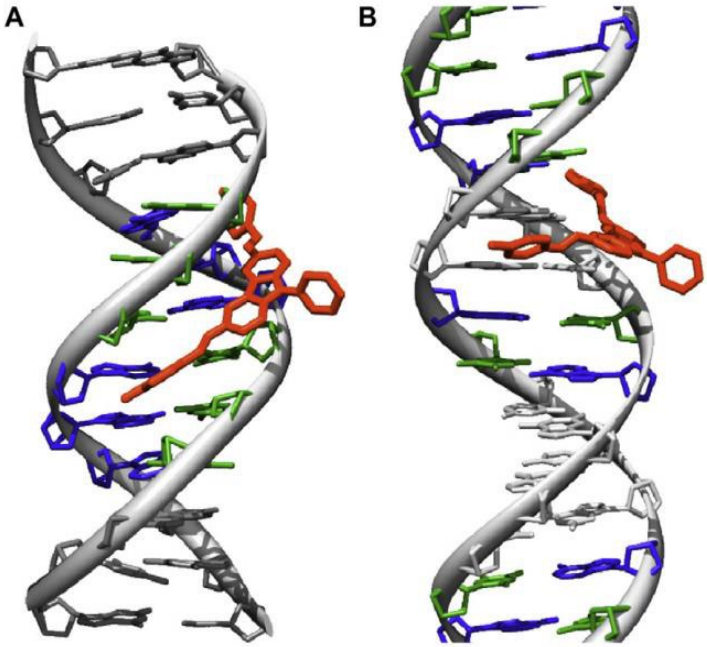

Figure 1.6: A) A molecule bound in the minor groove and (B) into the major groove of the DNA helix.[82]

Groove binders are usually crescent-shaped molecules that bind to DNA and do not induce large conformation changes in DNA like intercalators. Typically, they have larger association constants than intercalators (up to 10^{11} M^{-1}) this is because there is no energy required for the creation of a binding site. Notably, some compounds such as anthracyclines take advantage of both binding modes as they possess a grooving-binding side chain and an intercalative unit.[75,76]

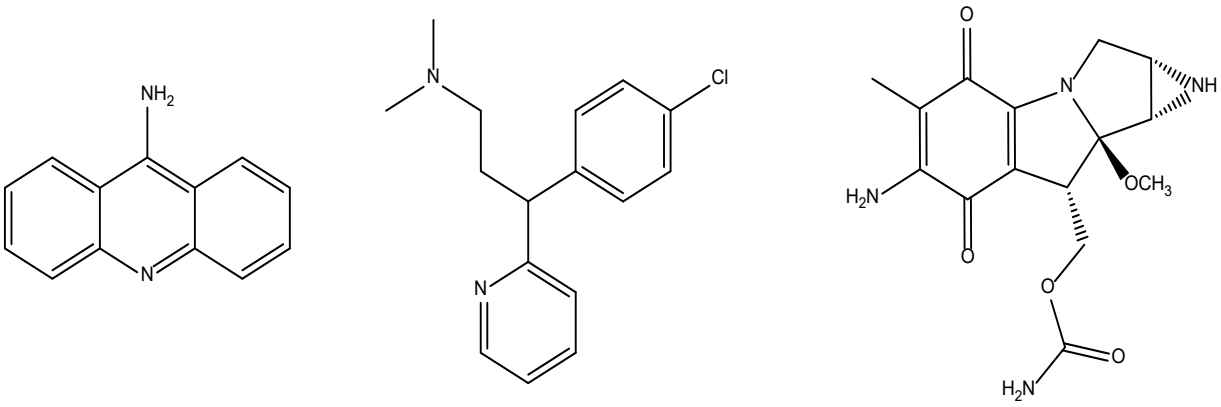

Figure 1.7: Structure of a typical intercalator (left), an atypical intercalator (centre), and a groove binder (right).

The structure of intercalating agents contains planar heterocylic moieties, which stack perpendicular to the DNA backbone. The intercalating agent stiffens, lengthens, stabilizes and unwinds the DNA double helix thus inhibiting DNA topoisomerase II, resulting in DNA strand breaks. For minor groove binders to interact with DNA they need to have electron-accepting and electron-donating groups capable of forming hydrogen bonds. In addition, minor groove binders have to have a concave-shaped aromatic framework that fits in the convex DNA minor groove.[60,65-67].

The basis for designing DNA binding drugs with improved affinity and specificity lies in the ability to identify key structural features of the drug that are responsible for the stabilization of the Drug-DNA complex and for the specificity of the binding.[75] Commercially available intercalators (such as DOXIL and daunorubicin) are found to have similar structural features which are responsible for the DNA intercalation process. These include, a planar aromatic region, hydrogen bonding region and a charged group which allow for interaction with the negatively charged phosphate backbone of the DNA helix thus stabilising the DNA/drug conjugate and increasing binding affinity. Figure 1.8 below illustrates the key structural fixtures of DOXIL.

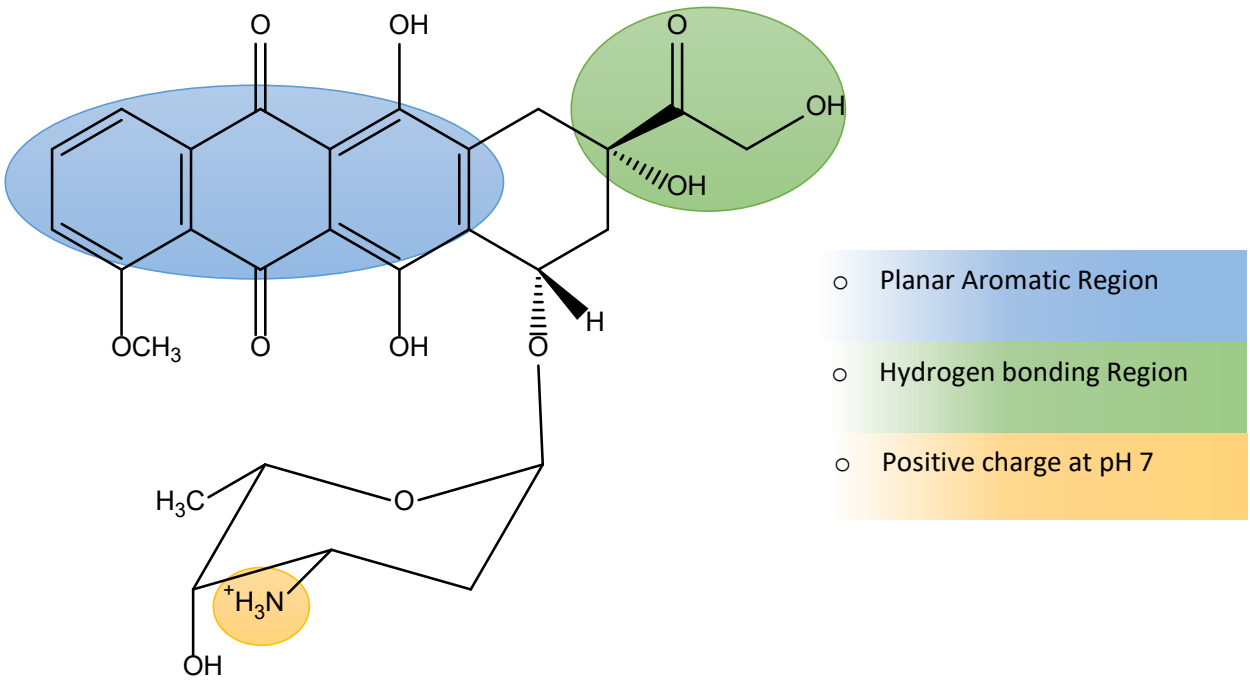

Figure 1.8: Key structural features of DOXIL highlighted.

1.5 Biological Activity of Schiff Bases

Compounds having an azomethine or imine (-C=N-) functional group are known as Schiff bases and were first reported by the German chemist, Hugo Schiff, in 1864.[68] As shown in Figure 1.9, Schiff bases are prepared by the condensation reaction of primary amines and carbonyl compounds with the concomitant elimination of water. It has been demonstrated through several studies that the lone pair of electrons in the sp^2 hybridized orbital of nitrogen atom is of considerable biological and chemical importance.[68,69] They impart excellent chelating ability when in combination with one or more donor atoms in close proximity to the azomethine group.

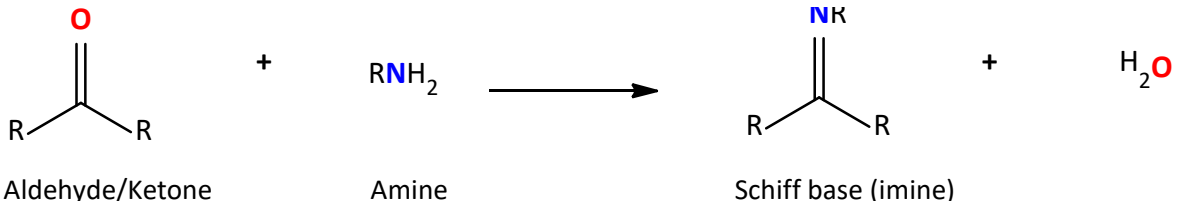

Figure 1.9: Formation of a Schiff base.

Schiff bases form the backbone for a large number of organic compounds and have been studied extensively because of their enormous applications in many fields. They are known to have potential biological activities including anticancer, analgesic, anti-inflammatory, antioxidant and antimicrobial. The biological importance of such compounds may be due to the formation of hydrogen bonds between the azomethine group and active sites of cell constituents, which interferes with normal cellular processes.[69,70]

Several studies have shown that biological activity of chelating compounds is enhanced upon metal ion coordination. Therefore, the interaction between metal ions and biologically active compounds represents an important route in the design of novel metal-based anticancer,

antibacterial and antifungal therapies against different kinds of viruses, bacteria and fungi that are resistant to current (predominantly) organic drugs. [71]

1.6 Objectives and Motivation

The biologically accessible redox potential of copper complexes has made it one of the most studied metallonucleases.[28-30] Copper is known to accumulate in tumors due to the selective permeability of the cancer cell membrane to copper compounds. Polypyridyl ligands (terpyridines, phenantrolines, bipyridines, etc.), comprise a class of ligands that have been widely used in the synthesis of metal complexes as therapeutic agents due to their interaction with DNA via intercalation and their anticancer activity. In the case of copper complexes with polypyridyl ligands, it has been reported that those with 1,10-phenanthrolines offer some of the most promising anticancer activities, and are thus explored in this research study. The anticancer activity was due to the intercalation of the complex between the base pairs of DNA, and the interference with the normal function of the enzyme topoisomerase II that was involved in the releasing and breaking of DNA strands. It seems, therefore important to synthesize compounds that have potential intercalative moieties.[7,72] The copper(II) ion with the above mentioned biologically accessible redox potential may also catalyse the production of ROS *in vivo* through the Haber Weiss or Fenton mechanism. These radicals are capable of inducing single and double-stranded DNA breaks and thus inducing cell apoptosis.

Schiff base ligands derived from N-heterocyclic aromatic rings are expected to yield planar metal complexes due to the rigidity in the aromatic ligand framework. Hence, it appears to be of considerable importance to conduct a study of copper(II) complexes involving Schiff base ligands derived from 2-aminophenol and 2-pyridinecarboxaldehyde which contains basic N-donor atoms and possess planar aromatic regions, which are known to be of importance for π-π stacking effects with pyrimidine and purine bases of DNA. Moreover, since the cleavage of DNA through the production of ROS requires the compound to first bind to DNA, this Schiff base is expected to enhance the binding affinity and therefore DNA cleavage ability of the copper complexes.

In this research study, the chemotherapeutic potential of Schiff base ligands with N-heterocyclic aromatic rings as well as heteroleptic copper(II) chelates will be investigated. Bidentate ligands with *N,N'* and tridentate *N,N',O* donor Schiff base ligands will be synthesized and chelated to copper(II). The copper(II) chelates are anticipated to exert their cytotoxicity *via* DNA binding and subsequent cleavage through ROS catalysis. DNA binding affinities of the copper(II) chelates will be measured using fluorescence competitive binding assays and chelates will be screened against a panel of human tumor cell lines to determine their efficacy and to understand the significance of the second ligand on the cytotoxicity of heteroleptic compounds. Triplicate screening on one cell will be averaged to obtain mean cytotoxicity.

Previous work on the copper chelate $[(Cu(L)(Cl)_2]$ (Figure 1.10.) conducted by the Akerman research group shows enhanced activity against the TK-10 cell line, with the mean cytotoxicity (IC_{50} =5.60 μM), even higher than that of cisplatin and carboplatin.[93] However, they show a lack of selectivity between unhealthy and normal cells, thus in this present study we incorporate a similar Schiff base ligand (Figure 1.11 (a)) and various co-ligands, including biotin-based ligands (Figure 1.11 (b)) which are expected to improve the selectivity of the compounds towards neoplastic tissue.

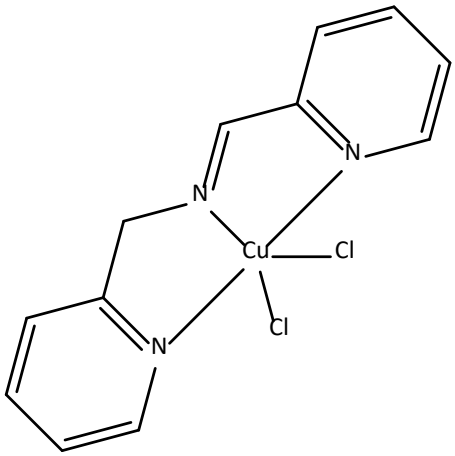

Figure 1.10: Structure of dichloro-(*E*)-1-(1,6-dihydropyridin-2-yl)-*N*-(1,2-dihydropyridin-2-ylmethyl)methanimine copper(II) [Cu(L)(Cl_2)].

The *N,N',O* schiff base ligand will be synthesized, chelated to copper(II) and then characterized by mass spectrometry, FT-IR spectroscopy, X-ray crystallography and UV/Vis spectroscopy. The copper(II) complex of the Schiff base ligand will be further reacted with different co-ligands to form a range of heteroleptic complexes (Figure 1.12). These are 1,10-phenanthroline (d), 5-amino-1,10-phenanthroline (e) and DPPZ (c). The co-ligands 1,10-phenanthroline and 5-amino-1,10-phenanthroline will be purchased.

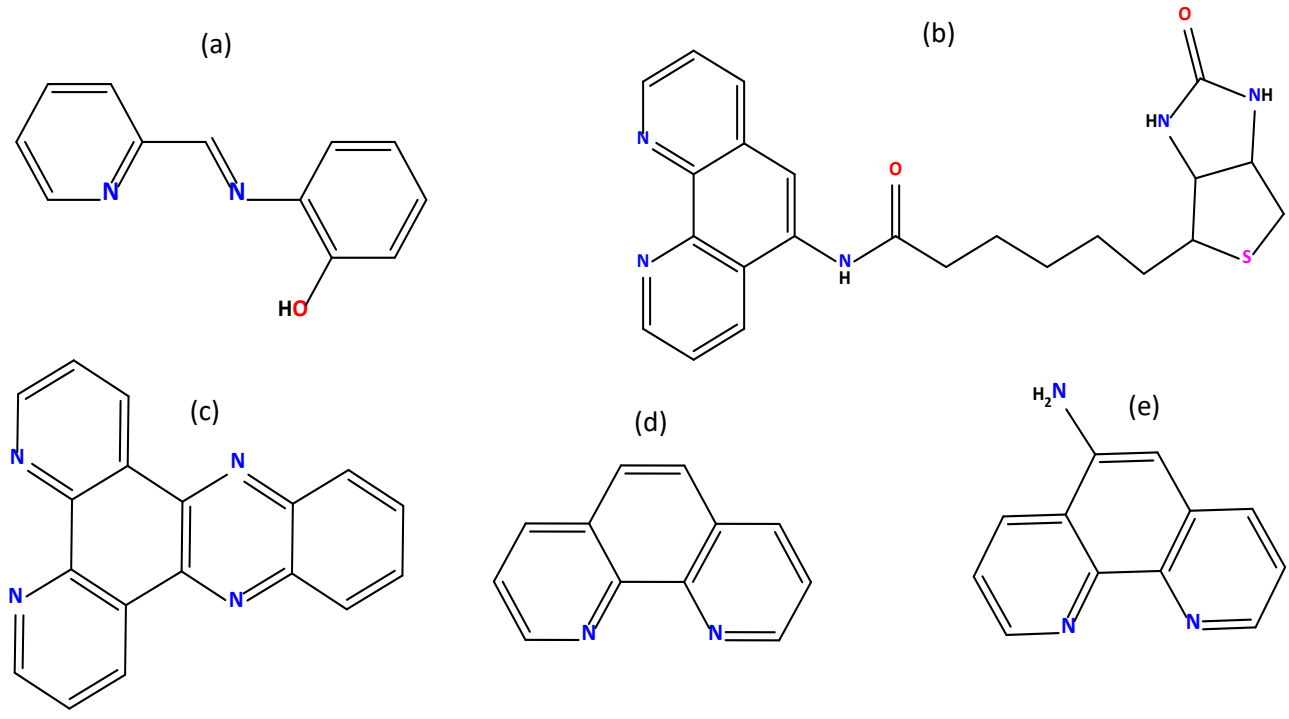

Figure 1.11: Ligands to be chelated to copper(II).

The purpose of the aforementioned co-ligands is to compare the bioactivity of single-ligand copper(II) chelates to heteroleptic copper(II) chelates. The nature of co-ligands affect hydrophobicity, planarity and coordination geometry of the copper chelate and enhance the DNA

binding affinity and potentially chemotherapeutic activity as well as tumour cell specificity.[74] The 5-amino-1,10-phenanthroline and phen-biotin co-ligands will be chelated to copper(II) forming copper(II) chelates (Figure 1.12 (a) and (f)). If the uptake in neoplastic versus healthy tissue can be increased then it is anticipated that the side-effects of the drug candidates may be reduced. This is based on the premise that the majority of side-effects are the result of a lack of target specificity.

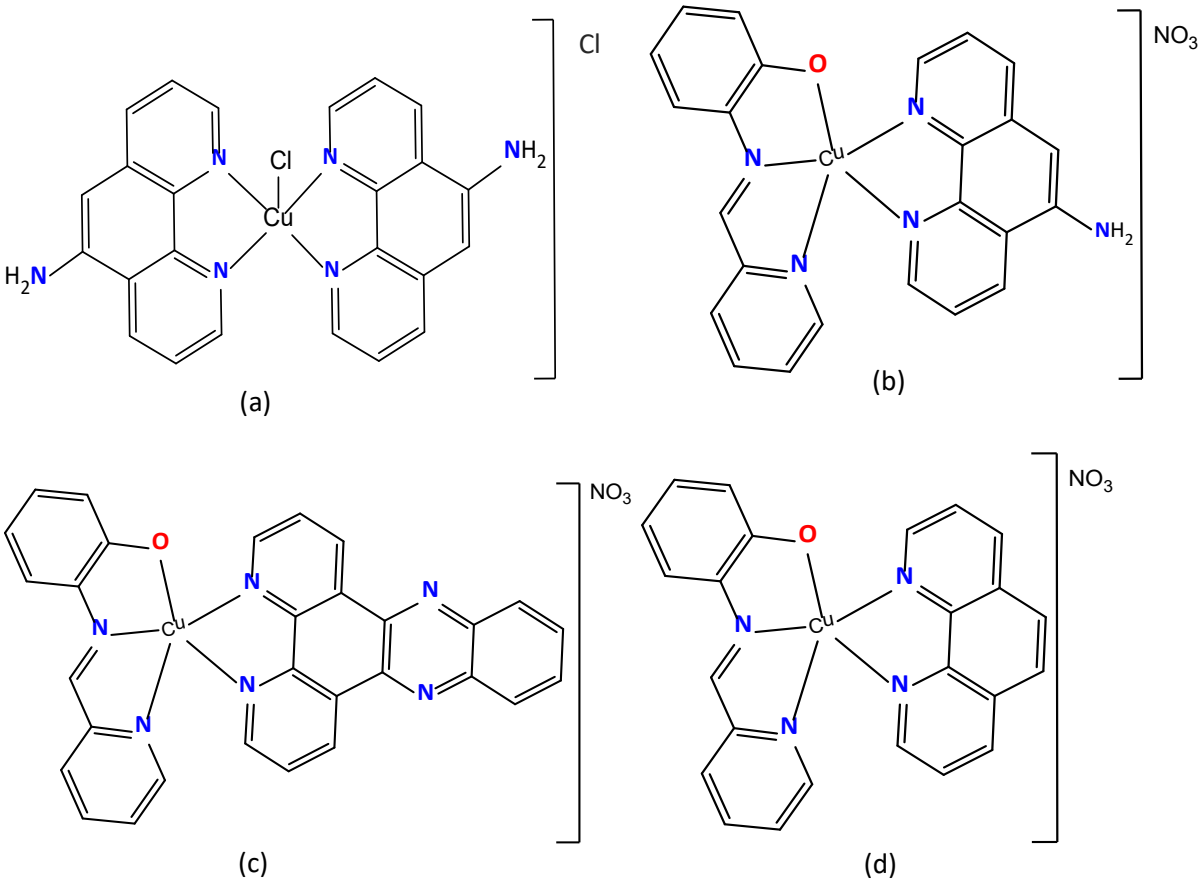

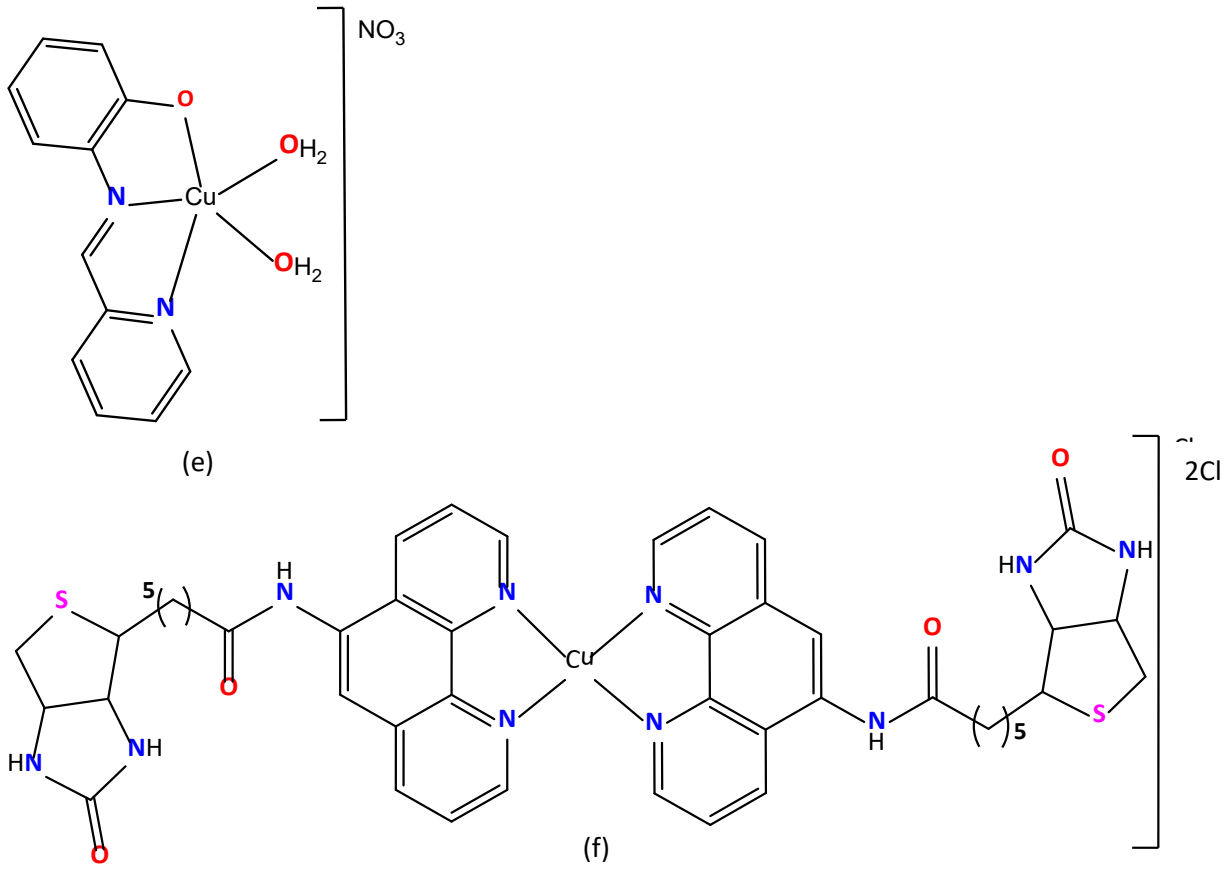

Figure 1.12: Proposed copper(II) chelates to be synthesized in this study.

The DNA binding affinity of the complexes toward calf-thymus DNA (CT-DNA) will be determined by competitive titration with ethidium bromide, which will give an indication of the intercalative ability of the copper complexes for human DNA. DNA intercalation is a key step in the DNA cleavage process and understanding this may provide insight into the activity of each compound. Determining the cytotoxicity and selectivity is a critical component in the drug discovery process. In this study it will be investigated by screening against a panel of human cells. This will show the effect of structural modification of ligands on the cytotoxicity of the copper(II) chelates.

1.7 References

1. https://www.cancerresearchuk.org/about-cancer/what-is-cancer (What is cancer?).
2. https://www.britannica.com/science/cancer-disease (Cancer Disease).
3. Sudhakar, A., 2009. History of cancer, ancient and modern treatment methods. *Journal of Cancer Science & Therapy*, *1*(2), pp.1-3.
4. Fitzmaurice, C., Allen, C., Barber, R.M., Barregard, L., Bhutta, Z.A., Brenner, H., Dicker, D.J., Chimed-Orchir, O., Dandona, R., Dandona, L. and Fleming, T., 2017. Global, regional, and national cancer incidence, mortality, years of life lost, years lived with disability, and disability-adjusted life-years for 32 cancer groups, 1990 to 2015: a systematic analysis for the global burden of disease study. *Journal of the American Medical Association oncology*, *3*(4), pp.524-548.
5. Gomez-Ruiz, S., Maksimović-Ivanić, D., Mijatović, S. and Kaluđerović, G.N., 2012. On the discovery, biological effects, and use of cisplatin and metallocenes in anticancer chemotherapy. *Bioinorganic Chemistry and Applications*, *2012*, pp.1-13.
6. Faithfull, S., Burton, C., Clarke, S., Kirby, M., Lyon, A., Levitt, G. and Walter, F., 2017. Mitigating risk of cardiovascular disease in people living with and beyond cancer. *Cancer Nursing Practice*, *16*(1), pp.18-23.
7. Medici, S., Peana, M., Nurchi, V.M., Lachowicz, J.I., Crisponi, G. and Zoroddu, M.A., 2015. Noble metals in medicine: Latest advances. *Coordination Chemistry Reviews*, *284*, pp.329-350.
8. Oun, R., Moussa, Y.E. and Wheate, N.J., 2018. The side effects of platinum-based chemotherapy drugs: a review for chemists. *Dalton Transactions*, *47*(19), pp.6645-6653.

9. Spencer, J. and Walden, B., 2018. Special focus: metals in medicine. *Future Medicinal Chemistry, 10*(6), pp.607-609.
10. Grass, G., Rensing, C. and Solioz, M., 2011. Metallic copper as an antimicrobial surface. *Applied and Environmental Microbiology*, *77*(5), pp.1541-1547.
11. Lippard, S.J., 1994. Metals in medicine. *Bioinorganic Chemistry*, pp.505-583.
12. Al-Fartusie, F.S. and Mohssan, S.N., 2017. Essential Trace Elements and Their Vital Roles in Human Body. *Indian Journal of Advances in Chemical Science*, *5*(3), pp.127-136
13. Sekhon, B.S. and Gandhi, L., 2006. Medicinal uses of inorganic compounds-1. *Resonance*, *11*(4), pp.75-89.
14. Ashfaq, M., Najam, T., Shah, S.S.A., Ahmad, M.M., Shaheen, S., Tabassum, R. and Rivera, G., 2014. DNA binding mode of transition metal complexes, a relationship to tumor cell toxicity. *Current Medicinal Chemistry*, *21*(26), pp.3081-3094.
15. Guo, Z. and Sadler, P.J., 1999. Metals in medicine. *Angewandte Chemie International Edition*, *38*(11), pp.1512-1531.
16. Dasari, S. and Tchounwou, P.B., 2014. Cisplatin in cancer therapy: molecular mechanisms of action. *European Journal of Pharmacology*, *740*, pp.364-378.
17. Wang, X. and Guo, Z., 2013. Targeting and delivery of platinum-based anticancer drugs. *Chemical Society Reviews*, *42*(1), pp.202-224.
18. Goodsell, D.S., 2006. The molecular perspective: cisplatin. *The Oncologist*, *11*(3), pp.316-317.
19. Dasari, S. and Tchounwou, P.B., 2014. Cisplatin in cancer therapy: molecular mechanisms of action. *European Journal of Pharmacology*, *740*, pp.364-378.
20. Lazarević, T., Rilak, A. and Bugarčić, Ž.D., 2017. Platinum, palladium, gold and ruthenium complexes as anticancer agents: Current clinical uses, cytotoxicity studies and future perspectives. *European Journal of Medicinal Chemistry*, *142*, pp.8-31.
21. Bergamo, A. and Sava, G., 2011. Ruthenium anticancer compounds: myths and realities of the emerging metal-based drugs. *Dalton Transactions*, *40*(31), pp.7817-7823.
22. Page, S. and Wheeler, R., 2012. Ruthenium compounds as anticancer agents. *Education in Chemistry*, *49*(1), pp.26-29.
23. Antonarakis, E.S. and Emadi, A., 2010. Ruthenium-based chemotherapeutics: are they ready for prime time?. *Cancer Chemotherapy and Pharmacology*, *66*(1), pp.1-9.
24. Muhammad, N. and Guo, Z., 2014. Metal-based anticancer chemotherapeutic agents. *Current Opinion in Chemical Biology*, *19*, pp.144-153.
25. Hartinger, C.G., Zorbas-Seifried, S., Jakupec, M.A., Kynast, B., Zorbas, H. and Keppler, B.K., 2006. From bench to bedside–preclinical and early clinical development of the anticancer agent indazolium trans-[tetrachlorobis (1H-indazole) ruthenate (III)](KP1019 or FFC14A). *Journal of Inorganic Biochemistry*, *100*(5-6), pp.891-904.
26. Vincent, J.B. and Love, S., 2012. The binding and transport of alternative metals by transferrin. *Biochimica et Biophysica Acta (BBA)-General Subjects*, *1820*(3), pp.362-378.
27. Page, S.M., Boss, S.R. and Barker, P.D., 2009. Tuning heavy metal compounds for anti-tumor activity: is diversity the key to ruthenium's success?. *Future Medicinal Chemistry*, *1*(3), pp.541-559.
28. Denoyer, D., Masaldan, S., La Fontaine, S. and Cater, M.A., 2015. Targeting copper in cancer therapy:'Copper That Cancer'. *Metallomics*, *7*(11), pp.1459-1476.

29. do Lago, L.C.C., Matias, A.C., Nomura, C.S. and Cerchiaro, G., 2011. Radical production by hydrogen peroxide/bicarbonate and copper uptake in mammalian cells: modulation by Cu (II) complexes. *Journal of Inorganic Biochemistry*, *105*(2), pp.189-194.
30. Kidane, T.Z., Farhad, R., Lee, K.J., Santos, A., Russo, E. and Linder, M.C., 2012. Uptake of copper from plasma proteins in cells where expression of CTR1 has been modulated. *Biometals*, *25*(4), pp.697-709.
31. https://www.copper.org/consumers/health/cu_health_uk.html (Copper in Human health).
32. Angelova, M., Asenova, S., Nedkova, V. and Koleva-Kolarova, R., 2011. Copper in the human organism. *Trakia Journal of Sciences*, *9*(1), pp.88-98.
33. Al-Fartusie, F.S. and Mohssan, S.N., 2017. Essential Trace Elements and Their Vital Roles in Human Body. *Indian Journal of Advances in Chemical Science*, *5*(3), pp.127-136.
34. Osredkar, J. and Sustar, N., 2011. Copper and zinc, biological role and significance of copper/zinc imbalance. *Journal of Clinical Toxicology S*, *3*(2161), pp.1-18.
35. Desai, V. and Kaler, S.G., 2008. Role of copper in human neurological disorders. *The American Journal of Clinical Nutrition*, *88*(3), pp.855S-858S.
36. Vincent, M., Hartemann, P. and Engels-Deutsch, M., 2016. Antimicrobial applications of copper. *International Journal of Hygiene and Environmental Health*, *219*(7), pp.585-591.
37. Sudha, V.P., Ganesan, S., Pazhani, G.P., Ramamurthy, T., Nair, G.B. and Venkatasubramanian, P., 2012. Storing drinking-water in copper pots kills contaminating diarrhoeagenic bacteria. *Journal of Health, Population, and Nutrition*, *30*(1), pp.17-21.
38. Thomas, D.R., Sunil, B., Latha, C. and Chacko, B., 2014. Microbiological Quality of Water Stored in Copper, Earthenware and Stainless Steel Vessels. *International Journal of Agriculture, Environment and Biotechnology*, *7*(1), pp.25-28.
39. Parada, J., Rubilar, O., Diez, M.C., Cea, M., da Silva, A.S.A., Rodríguez-Rodríguez, C.E. and Tortella, G.R., 2019. Combined pollution of copper nanoparticles and atrazine in soil: Effects on dissipation of the pesticide and on microbiological community profiles. *Journal of Hazardous Materials*, *361*, pp.228-236.
40. Palza, H., 2015. Antimicrobial polymers with metal nanoparticles. *International Journal of Molecular Sciences*, *16*(1), pp.2099-2116.
41. Hobman, J.L. and Crossman, L.C., 2015. Bacterial antimicrobial metal ion resistance. *Journal of Medical Microbiology*, *64*(5), pp.471-497.
42. Gugala, N 2018, *Biomedical Applications of Metals*, Springer International Publishing AG, Calgary.
43. Fernandes, P., Sousa, I., Cunha-Silva, L., Ferreira, M., de Castro, B., Pereira, E.F., Feio, M.J. and Gameiro, P., 2014. Synthesis, characterization and antibacterial studies of a copper (II) lomefloxacin ternary complex. *Journal of Inorganic Biochemistry*, *131*, pp.21-29.
44. Lakovidis, I., Delimaris, I. and Piperakis, S.M., 2011. Copper and its complexes in medicine: a biochemical approach. *Molecular Biology International*, *2011,* pp.1-6.
45. Kehrer, J.P., 2000. The Haber–Weiss reaction and mechanisms of toxicity. *Journal of Toxicology*, *149*(1), pp.43-50.
46. Marzano, C., Pellei, M., Tisato, F. and Santini, C., 2009. Copper complexes as anticancer agents. *Anti-Cancer Agents in Medicinal Chemistry (Formerly Current Medicinal Chemistry-Anti-Cancer Agents)*, *9*(2), pp.185-211.
47. Bonacorso, H.G., Andrighetto, R., Frizzo, C.P., Zanatta, N. and Martins, M.A., 2016. Recent advances in the chemistry of 1, 10-phenanthrolines and their metal complex derivatives:

Synthesis and promising applications in medicine, technology, and catalysis. *Societa Chimica Italiana*, pp.1-27.
48. Selvaganapathy, M. and Raman, N., 2016. Pharmacological activity of a few transition metal complexes: A short review. *Journal of Chemical Biology & Therapeutics*, *1*(02), pp.2572-0406.
49. Parada, J., Rubilar, O., Diez, M.C., Cea, M., da Silva, A.S.A., Rodríguez-Rodríguez, C.E. and Tortella, G.R., 2019. Combined pollution of copper nanoparticles and atrazine in soil: Effects on dissipation of the pesticide and on microbiological community profiles. *Journal of Hazardous Materials*, *361*, pp.228-236.
50. Reddy, P.R., Rajeshwar, S. and Satyanarayana, B., 2016. Synthesis, characterization of new copper (ii) Schiff base and 1, 10 phenanthroline complexes and study of their bioproperties. *Journal of Photochemistry and Photobiology B: Biology*, *160*, pp.217-224.
51. Weinberg, R.A., 1996. How cancer arises. *Scientific American*, *275*(3), pp.62-70.
52. Cooper, G.M. and Hausman, R.E 2000. *The cell: a molecular approach*, ASM press, Washington DC.
53. https://www.cancer.org/cancer/cancer-basics/what-is-cancer.html (What is cancer?).
54. Misra, R., Upadhyay, M. and Mohanty, S., 2014. Design considerations for chemotherapeutic drug nanocarriers. *Pharmaceutica Analytica Acta*, *5*, pp.1-6.
55. Airley, R 2009. *Cancer chemotherapy: Basic Science to the Clinic*, John Wiley & Sons, Chichester.
56. https://www.cancer.org/treatment/treatments-and-side-effects/treatment-types/radiation/basics.html (Radiation therapy Basics).
57. Sudhakar, A., 2009. History of cancer, ancient and modern treatment methods. *Journal of Cancer Science & Therapy*, *1*(2), p.1-4.
58. Baskar, R., Lee, K.A., Yeo, R. and Yeoh, K.W., 2012. Cancer and radiation therapy: current advances and future directions. *International Journal of Medical Sciences*, *9*(3), p.193.
59. Lennan, E., 2010. Cancer Chemotherapy: Basic Science to the Clinic. *Cancer Nursing Practice*, *9*(2), pp.8-9.
60. Topală, T., Bodoki, A., Oprean, L. and Oprean, R., 2014. Experimental techniques employed in the study of metal complexes-DNA–interactions. *Experimental Techniques*, *62*, pp.1049-1052.
61. Pages, B.J., Ang, D.L., Wright, E.P. and Aldrich-Wright, J.R., 2015. Metal complex interactions with DNA. *Dalton Transactions*, *44*(8), pp.3505-3526.
62. Rehman, S.U., Sarwar, T., Husain, M.A., Ishqi, H.M. and Tabish, M., 2015. Studying non-covalent drug–DNA interactions. *Archives of Biochemistry and Biophysics*, *576*, pp.49-60.
63. Shaikh, S.A. and Jayaram, B., 2014. DNA drug interaction. *Journal of Biomedicine and Biotechnology, 2*(1), pp.1-9.
64. Chaires, J.B., 1998. Drug—DNA interactions. *Current Opinion in Structural Biology*, *8*(3), pp.314-320.
65. Faddeeva, M.D. and Beliaeva, T.N., 1991. DNA intercalators: their interaction with DNA and other cell components and their use in biological research. *Journal of Cytology*, *33*(10), pp.3-31.
66. Brana, M.F., Cacho, M., Gradillas, A., Pascual-Teresa, B.D. and Ramos, A., 2001. Intercalators as anticancer drugs. *Current Pharmaceutical Design*, *7*(17), pp.1745-1780.

67. Karimi Goftar, M., Moradi Kor, N. and Moradi Kor, Z., 2014. DNA intercalators and using them as anticancer drugs. *International Journal of Advanced Biological and Biomedical Research*, *2*(3), pp.811-822.
68. Schiff, H., 1864. Mittheilungen aus dem Universitätslaboratorium in Pisa: eine neue Reihe organischer Basen. *Justus Liebigs Annalen der Chemie*, *131*(1), pp.118-119.
69. Tobriya, S.K., 2014. Biological Applications of Schiff base and its Metal Complexes-A Review. *International Journal of Science and Research, 3*(9), pp.1254-1256.
70. Al Zoubi, W., Kandil, F. and Chebani, K., 2014. Active transport of metal ions by using Schiff bases. *Physical Sciences Research International*, *2*(1), pp.12-23.
71. Mruthyunjayaswamy, B.H.M., 2017. Synthesis, spectroscopic characterization, electrochemistry and biological activity evaluation of some metal (II) complexes with ONO donor ligands containing indole and coumarin moieties. *Journal of Saudi Chemical Society*, *21*, pp.S202-S218.
72. Reddy, P.R. and Shilpa, A., 2012. 2-Hydroxynaphthalene-1-carbaldehyde-and 2-(Aminomethyl) pyridine-Based Schiff Base CuII Complexes for DNA Binding and Cleavage. *Chemistry & Biodiversity*, *9*(10), pp.2262-2281.
73. Dumat, B., Bordeau, G., Faurel-Paul, E., Mahuteau-Betzer, F., Saettel, N., Bombled, M., Metgé, G., Charra, F., Fiorini-Debuisschert, C. and Teulade-Fichou, M.P., 2011. N-phenyl-carbazole-based two-photon fluorescent probes: Strong sequence dependence of the duplex vs quadruplex selectivity. *Biochimie*, *93*(8), pp.1209-1218.
74. Lian, W.J., Wang, X.T., Xie, C.Z., Tian, H., Song, X.Q., Pan, H.T., Qiao, X. and Xu, J.Y., 2016. Mixed-ligand Copper (II) schiff base complexes: The role of the co-ligand in DNA binding, DNA cleavage, protein binding and cytotoxicity. *Dalton Transactions*, *45*(22), pp.9073-9087.
75. Cohen, S.M. and Lippard, S.J., 2001. Cisplatin: From DNA damage to cancer chemotherapy. *Progress in Nucleic Acid Research and Molecular Biology, 67*, pp.93-130.
76. Palchaudhuri, R. and Hergenrother, P.J., 2007. DNA as a target for anticancer compounds: methods to determine the mode of binding and the mechanism of action. *Current Opinion in Biotechnology*, *18*(6), pp.497-503.
77. https://www.cancer.gov/about-cancer/understanding/what-is-cancer (Metastasis).
78. Vanita P, Subrahmanyam V, Jhansi K., 2011. A Short Note on Cancer. *Journal of Carcinogene and Mutagene*, *4*(2) pp.2-128.
79. Fass, L., 2008. Imaging and cancer: a review. *Molecular Oncology*, *2*(2), pp.115-152.
80. Kircher, M.F., Hricak, H. and Larson, S.M., 2012. Molecular imaging for personalized cancer care. *Molecular Oncology*, *6*(2), pp.182-195.
81. Ossenkoppele, R., Rabinovici, G.D., Smith, R., Cho, H., Schöll, M., Strandberg, O., Palmqvist, S., Mattsson, N., Janelidze, S., Santillo, A. and Ohlsson, T., 2018. Discriminative accuracy of [^{18}F] flortaucipir positron emission tomography for Alzheimer disease vs other neurodegenerative disorders. *Journal of the American Medical Association, 320*(11), pp.1151-1162.
82. Dumat, B., Bordeau, G., Faurel-Paul, E., Mahuteau-Betzer, F., Saettel, N., Bombled, M., Metgé, G., Charra, F., Fiorini-Debuisschert, C. and Teulade-Fichou, M.P., 2011. N-phenyl-carbazole-based two-photon fluorescent probes: Strong sequence dependence of the duplex vs quadruplex selectivity. *Biochimie*, *93*(8), pp.1209-1218.
83. Lewis, J.S., Lewis, M.R., Cutler, P.D., Srinivasan, A., Schmidt, M.A., Schwarz, S.W., Morris, M.M., Miller, J.P. and Anderson, C.J., 1999. Radiotherapy and dosimetry of 64Cu-TETA-

Tyr3-octreotate in a somatostatin receptor-positive, tumor-bearing rat model. *Clinical Cancer Research*, *5*(11), pp.3608-3616.

84. Jiang, L., Tu, Y., Hu, X., Bao, A., Chen, H., Ma, X., Doyle, T., Shi, H. and Cheng, Z., 2017. Pilot Study of ^{64}Cu (I) for PET Imaging of Melanoma. *Scientific Reports*, *7*(1), p.2574.
85. Bhattacharyya, S. and Dixit, M., 2011. Metallic radionuclides in the development of diagnostic and therapeutic radiopharmaceuticals. *Dalton Transactions*, *40*(23), pp.6112-6128.
86. Bhattacharyya, S. and Dixit, M., 2011. Metallic radionuclides in the development of diagnostic and therapeutic radiopharmaceuticals. *Dalton Transactions*, *40*(23), pp.6112-6128.
87. Kircher, M.F., Hricak, H. and Larson, S.M., 2012. Molecular imaging for personalized cancer care. *Molecular Oncology*, *6*(2), pp.182-195.
88. Pysz, M.A., Gambhir, S.S. and Willmann, J.K., 2010. Molecular imaging: current status and emerging strategies. *Clinical Radiology*, *65*(7), pp.500-516.
89. Lázaro, G.G.F., 2013. 'Development of metal-based radiopharmaceuticals for positron emission tomography imaging: production of zinc-63 and molecular design for gallium-68 labeled probes'. PhD thesis, Chiba University, Chiba.
90. Tabti, R., Tounsi, N., Gaiddon, C., Bentouhami, E. and Désaubry, L., 2017. Progress in Copper Complexes as Anticancer Agents. *Journal of Medicinal Chemistry*, *7*, pp.875-879.
91. Schaefer, M. and Gitlin, J.D., 1999. IV. Wilson's disease and Menkes disease. American *Journal of Physiology-Gastrointestinal and Liver Physiology*, 276(2), pp.G311-G314.
92. Pray, L., 2008. Discovery of DNA structure and function: Watson and Crick. *Nature Education*, *1*(1), p.100.
93. Chatturgoon, T 2016, 'Synthesis, Characterisation and Biological Activity of a Series of Single-Ligand and Heteroleptic Copper(II) Schiff Base Complexes: Potential Chemotherapeutic Agents'. Master's Thesis, University of KwaZulu-Natal, Pietermaritzburg.

CHAPTER 2: EXPERIMENTAL

2.1 General Methods and Instrumentation

All starting materials and organic solvents used in the syntheses were purchased from Sigma–Aldrich (Germany) and used as received. Dry solvents were prepared using a Puresolv^{TM} MD 7 purification system from Innovative Technologies. NMR spectra were recorded with a Bruker Avance III 400 MHz spectrometer equipped with a Bruker magnet (9.395 T) using a 5 mm TBIZ probe at frequencies of 400 MHz and 100 MHz for the ^{1}H and ^{13}C spectra, respectively. The chemical shifts are reported in ppm with coupling constants calculated from peak separations and measured in Hertz (Hz). The spectra were recorded at 30 °C. All NMR experiments were conducted using Bruker Topspin 3.5, patch level 7. All proton and carbon chemical shifts are quoted relative to $CDCl_3$: ^{1}H, 7.26 ppm and ^{13}C, 77.16 ppm and DMSO-d_6: ^{1}H, 2.50 ppm and ^{13}C, 39.52 ppm.

FT-IR spectra were recorded using a Bruker Alpha FTIR spectrometer with ATR platinum Diamond 1 Reflectance accessory. The machine acquired the information in 32 scans with a spectral resolution of 1.0 cm^{-1} in the frequency range 4 000 to 400 cm^{-1}. The abbreviations used in the text are as follows; br, broad; s, strong; m, medium and w, weak signals. Electronic spectra were recorded using a Shimadzu UVPC-1800 double beam UV/Vis scanning spectrometer (1.0 cm path

length cuvette). Spectra were recorded from 800 to 200 nm. High resolution mass spectra were recorded with a Waters Acquity-LCT Premier coupled high performance liquid chromatograph-mass spectrometer (time-of-flight) using electrospray ionization in positive mode. Elemental analyses were done using a Thermo Scientific Flash 2000.

2.2 Synthesis of 1,10-Phenanthroline Precursor

2.2.1 Synthesis of 1,10-Phenanthroline-5,6-dione (phendione).

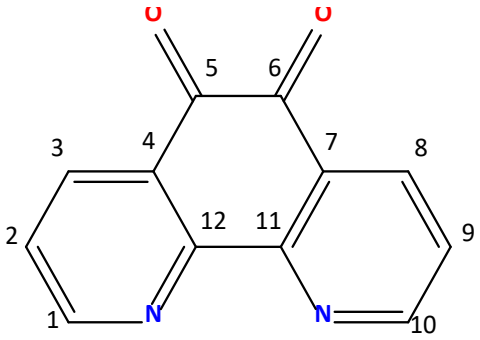

Figure 2.1: Structure of 1,10-phenanthroline-5,6-dione showing the atom numbering scheme.

Caution: Phendione is a flocculent solid and is a mucous membrane irritant. To reduce the exposure, wear protective face mask.

Phendione was prepared according to a literature method with slight modification.[1] 1,10-phenanthroline (1.00 g, 5.55 mmol) and potassium bromide (1.00 g, 8.40 mmol) were mixed and added to a mixture of H_2SO_4 (10.00 mL) and HNO_3 (5.00 mL) on ice. The mixture was slowly allowed to warm up to room temperature, while stirring and then heated to reflux for 16 hours. The mixture was cooled to room temperature and 100.00 g of ice was added followed by the slow

addition of NaOH to bring the pH to about 6, this yielded a yellow precipitate. The precipitate was collected by gravity filtration and washed with boiling water. The compound remaining in the aqueous solution was recovered using solvent extraction with DCM (5 × 40.00 mL). The DCM fractions were then dried using anhydrous magnesium sulphate. DCM was removed using a rotary evaporator under reduced pressure. The yellow solid was recrystallized from methanol and dried in an oven for 2 hours. Yield (0.90 g, 77%).

Characterization data:

^{1}H NMR (400 MHz, DMSO-*d6*, 298 K) [δ, ppm]: 8.98 (2H, dd, J= 4.61 Hz, J= 1.73 Hz, **1, 10**), 8.39 (2H, s, **2, 9**), 7.67 (2H, dd, J= 7.85 Hz J= 4.6 Hz, **3, 8**). **^{13}C NMR** (100 MHz, DMSO-*d6*, 303 K): 177.68 (C-**5, 6**); 154.26 (C-**1, 10**); 152.10 (C-**12, 11**); 135.76 (C-**3, 8**), 129.06 (C-**4, 7**), 125.29 (C-**2, 9**). **FT-IR** (cm^{-1}): 3063 ν(C-H) aromatic, 1680 ν(C=O), 1559 ν(C=N), 734 ν(C=C-H) out of plane bending. **Solubility**: MeOH, DMF, H_2O (partially). **Melting point** (mp) 260-262 °C.

2.3 Synthesis of Ligands

2.3.1 Synthesis of dipyrido[3,2-a:2′,3′-c]phenazine (DPPZ).

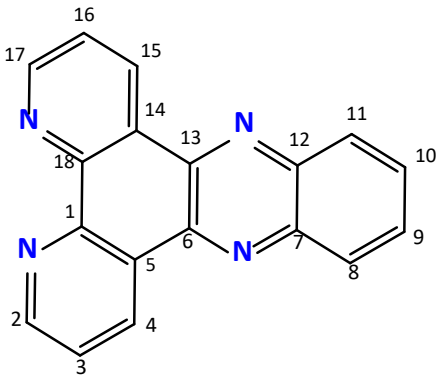

Figure 2.2: Structure of dipyrido[3,2-a:2′,3′-c]phenazine showing the atom numbering scheme.

DPPZ was prepared according to the method previously reported by Molphy *et al.*, with some modification.[1] The ethanolic solution (15.00 mL) of phendione (0.50 g, 2.38 mmol) was heated until fully dissolved. A warm ethanolic solution (15.00 mL) of *o*-phenylenediamine (0.26 g, 2.41 mmol) was prepared and added to the ethanolic solution of phendione and the resulting mixture

heated to reflux for 4 hours and then stirred at room temperature for 12 hours. The resulting mixture was filtered, and the precipitate was recrystallized from methanol to give a cream solid and dried in an oven for 2 hours. Yield (0.50 g, 75%).

Characterization data:

^{1}H NMR (400 MHz, DMSO-*d6*, 298 K) [δ, ppm]: 9.54 (2H, dd, J= 1.76 Hz, J= 8.08 Hz, **2, 17**), 9.21 (2H, dd, J= 1.76 Hz, J= 4.41 Hz, **8, 11**), 8.39 (2H, dd, J= 3.44 Hz, J= 6.52 Hz, **4, 15**), 8.06 (2H, dd, J= 3.40 Hz, J= 6.52 Hz, **3, 16**), 7.95 (2H, dd, J= 4.44 Hz, J= 8.12 Hz, **9, 10**). **^{13}C NMR** (100 MHz, DMSO-*d6*, 303 K): 152.3 (C-**2, 17**); 147.8 (C-**6, 13**); 141.7 (C-**7, 12**); 140.8 (C-**4, 15**); 133.0 (C-**8, 11**); 131.3 (C-**1, 18**); 129.2 (C-**5, 14**); 126.9 (C-**9, 10**); 124.5 (C-**3, 16**). **FT-IR (cm^{-1})**: 3413 ν(C-H), 1625 ν(C=N), 1573 ν(C=N), 738 ν(C-H). **Solubility**: DMF, DMSO (partially), EtOH. **Melting point** (248-250 °C).**TOF-MS^{+}**: 305.08 $(M+Na)^{+}$.

2.3.2 Synthesis of 6-(2-oxohexahydro-1H-thieno[3,4-d]imidazol-4-yl)-N-(1,10-phenanthrolin-5-yl)hexanamide.

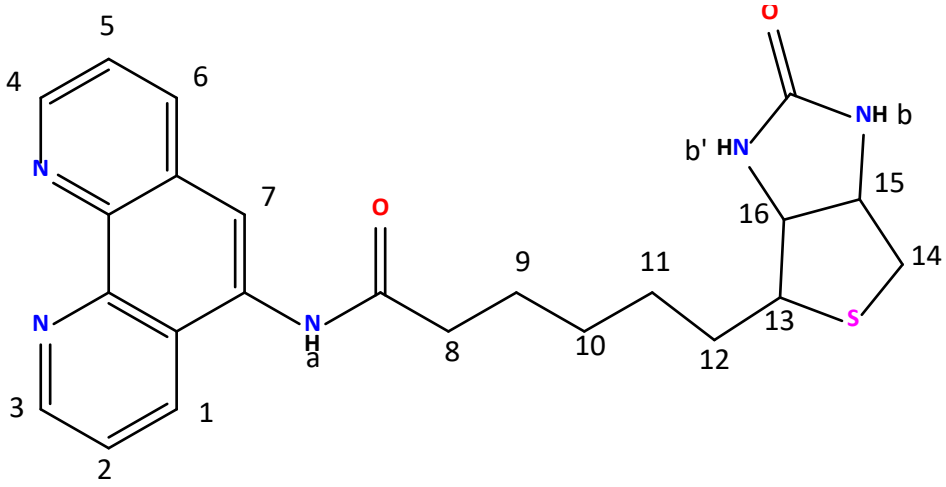

Figure 2.3: Structure of 6-(2-oxohexahydro-1H-thieno[3,4-d]imidazol-4-yl)-N-(1,10-phenanthrolin-5-yl)hexanamide.

This compound was prepared according to a previously reported procedure.[2] Biotin (0.15 g, 0.34 mmol) was dissolved in $SOCl_2$ (5.00 mL, 68.92 mmol) and stirred under nitrogen atmosphere for 1 hour, after which the excess thionyl chloride was remove *in vacuo*. The resulting residue was dissolved in dry dichloromethane (10.00 mL), then a solution of 5-amino-1,10-phenantroline (0.10

g, 0.51 mmol) and DMAP (17.00 mg, 0.14 mmol) in dry DCM (10.00 mL) was added. The mixture was stirred at room temperature for 24 h; this led to the formation of a yellow precipitate. The precipitate was collected by gravity filtration and washed with diethyl ether. Yield (0.09 g, 41 %).

Characterization data:

^{1}H NMR (400 MHz, DMSO-*d6*, 298 K) [δ, ppm]: 9.26 (1H, d, J= 8.45 Hz, **4**); 9.10 (1H, d, J= 7.78 Hz **1**); 8.81 (1H, dd, J= 6.30 Hz, J= 1.67 Hz, **3**); 8.21 (s, NH, **a**); 8.09 (1H, dd, J= 4.25 Hz, J= 1.71 Hz, **6**); 8.03 (1H, dd, J= 5.38 Hz, J= 3.26 Hz, **7**); 7.09 (1H, s, **2**); 6.98 (2H, d, J= 8.27 Hz, **5**); 4.30 (NH, t, J= 7.18 Hz, **b** and **b'**); 4.14 (2H, dd, J= 5.67 Hz, J= 2.13 Hz, **15** and **16**); 2.82 (1H, dd, J= 8.22 Hz, J= 2.31 Hz, **14**); 3.09 (2H, t, J= 7.15 Hz, **11**); 2.58 (1H, d, J= 6.78 Hz, **13**); 2.29 (2H, t, J= 6.89 Hz, **8**); 1.53 (4H, m, **9** and **12**) and 1.33 (2H, m, **10**).

2.3.3 Synthesis of 2-((pyridine-2-ylmethylene)amino)phenol (HL).

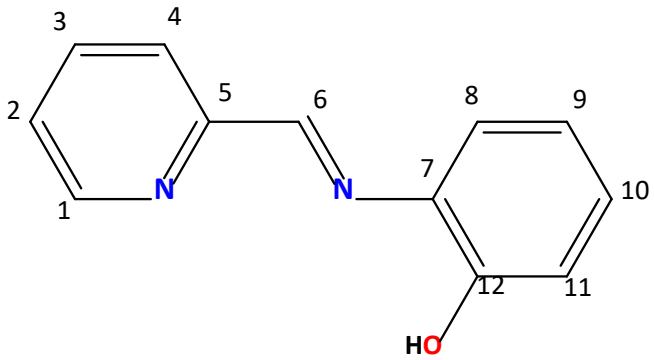

Figure 2.4: Structure of 2-((pyridine-2-ylmethylene)amino)phenol showing the atom numbering scheme.

This compound was synthesized according to the method previously reported by Akerman *et al.*, with some modification.[3] 2-Pyridinecarbaldehyde (0.87 mL, 9.15 mmol) and 2-aminophenol (1.00 g, 9.16 mmol) were added to an agate mortar and ground gently with a pestle at ambient temperature for 20-30 min. The mixture became a paste. The reaction produces a solid yellow powder after 30 min and was left for 12 hours to dry at room temperature to remove the waters of condensation released while forming the azomethine bond. The crude product was crystallized from methanol to give a yellow crystalline powder. Yield (1.71g, 98%).

Characterization data:

^{1}H NMR (400 MHz, DMSO-*d6*, 298 K) [δ, ppm]: 8.75 (1H, s, **6**) 8.64 (1H, dq, J= 4.8Hz, J= 0.84 Hz, **1**), 8.05 (1H, d, J= 7.92 Hz, **4**), 7.72 (1H, td, J= 1.51 Hz, J= 7.65 Hz, **3**); 7.29 (2H, td, J= 1.11 Hz, J= 4.80 Hz, **2,9**); 7.18 (1H, t, J= 7.61 Hz, **10**); 6.99 (1H, d, J= 8.01 Hz, **8**); 6.86 (1H, t, J=7.68 Hz, **11**). **^{13}C NMR** (100 MHz, DMSO-*d6*, 298 K): 159.32(C-**12**), 154.51(C-**6**), 151.45(C-**5**), 149.45(C-**1**), 136.85(C-**7**), 136.78(C-**3**), 128.27(C-**10**), 125.35(C-**8**), 121.56(C-**4**), 137.12(C-**11**) 119.62 (C-**9**), 116.35(C-**2**). **FT-IR** (cm^{-1}): 3364 ν(O-H), 3045 ν(C-H), 1583 ν(C=N), 1467 ν(C=C), 1146 ν(C-O), 734 ν(C-H bend). **UV** (λ_{max}, ε) [nm, M^{-1}]: 290, 9588; 359, 8178.

2.4 Synthesis of Copper(II) Chelates

2.4.1 Synthesis of diaqua-2-((pyridine-2-ylmethylene)amino)phenol copper(II) nitrate [Cu(L)(H_2O)$_2$](NO_3).

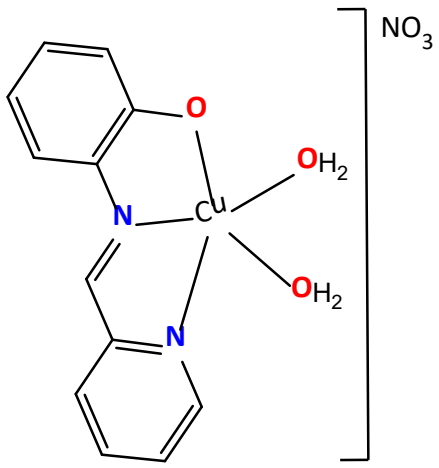

Figure 2.5: Structure of diaqua-2-((pyridine-2-ylmethylene)amino)phenol copper(II) nitrate, [Cu(L)(H_2O)$_2$](NO_3).

This compound was prepared according to previously reported procedure.[4] The ligand HL (0.10 g, 0.50 mmol), was dissolved in methanol (25.00 mL) and a solution of copper(II) nitrate (0.12 g, 0.50 mmol) dissolved in methanol (15.00 mL) was added. The solution was heated to reflux for 3 hours

followed by stirring at room temperature for 24 hours. This reaction mixture was allowed to slowly evaporate at room temperature, dark red crystals grew and were washed with diethyl ether. Yield (0.17 g, 94 %).

Characterisation data:

FT-IR (cm^{-1}): 3341 ν(C-H), 3084 ν(O-H), 1454 ν(C=N), 1266 ν(C=C), 762 ν(C-H bend), 1356 ν(NO_3^-). **UV** (λ_{max}, ε) [nm, M^{-1} cm^{-1}]: 210, 14646; 266, 3235; 302, 3491; 315, 2743; 435, 1087.**TOF-MS**$^+$: 260.01m/z. **Elemental analysis:** Calculated for $C_{12}H_9CuN_3O_4$: C, 44.64; N, 13.02; H, 2.81. (Found: C, 44.65; N, 13.02; H, 2.80).

2.4.2 Synthesis of (1,10-phenanthroline)-2-((pyridine-2-ylmethylene)amino)phenol copper(II) nitrate [Cu(L)(Phen)](NO_3).

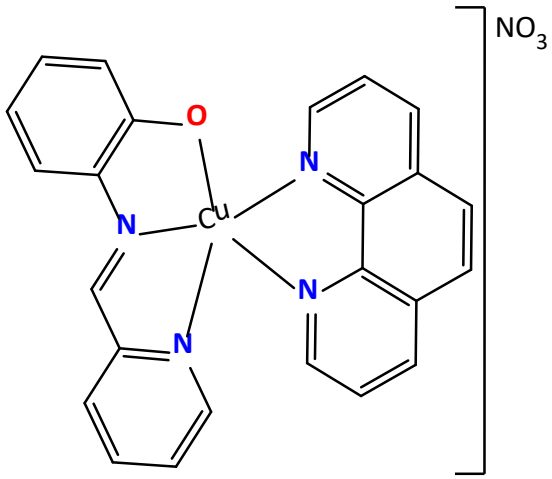

Figure 2.6: Structure of (1,10-phenanthroline)-2-((pyridine-2-ylmethylene)amino)phenol copper(II) nitrate [Cu(L)(Phen)](NO_3).

A mixture of [Cu(L)(H_2O)$_2$](NO_3) (99.30 mg, 0.278 mmol) and 1,10-phenanthroline (50.00 mg, 0.28 mmol) were mixed and ground into a paste using a mortar and pestle for 30 min. A microcrystalline powder of the dark brown product was obtained and washed with a minimum of diethyl ether. Yield (0.27 g, 97%).

Characterisation data:

FT-IR (cm^{-1}): 3051 ν(C-H), 1581 ν(C-N), 1512 ν(C-N), 710 ν(C-H), 1343 ν(NO_3^-). **TOF-MS**: 440.11 m/z.**UV** (λ_{max}, ε) [nm, M^{-1}]:225, 41099; 270, 26561; 294, 13025; 345, 5417; 435, 2732; 510,4146. **Elemental Analysis:** Calculated for $C_{24}H_{17}CuN_6O_4$: C, 57.29; N, 13.93; H, 3.41. (Found: C, 57.38; N, 13.84; H, 3.45).

2.3.3 Synthesis of (1,10-phenanthroline-5-amine)-(2)-((pyridine-2-ylmethylene)amino)phenol copper(II) nitrate [Cu(L)(Phen-NH_2)](NO_3).

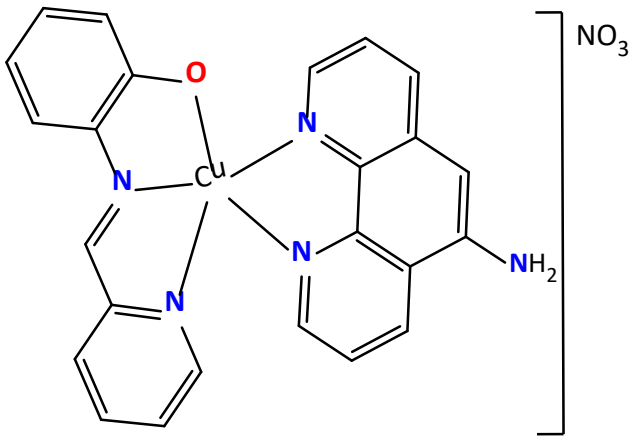

Figure 2.7: Structure of (1,10-phenanthroline-5-amine)-2-((pyridine-2-ylmethylene)amino)phenol copper(II) nitrate, [Cu(L)(Phen)](NO_3).

A solution of 1,10-phenanthroline-5-amine (97.90 mg, 0.50 mmol) dissolved in minimum methanol (~0.20 mL) was added to [Cu(L)(H_2O)$_2$](NO_3) (0.20 g, 0.56 mmol). The mixture was ground into a paste for 20 min using a mortar and pestle and then allowed to dry. The crude product was washed with DCM and evaporated to dryness. Yield (0.22 g, 85 %).

Characterisation data:

FT-IR (cm^{-1}): 1622 ν(C=N), 1589 ν(C=N), 1296 ν(C=C), 722 ν(C-H), 1356 ν(NO_3^-). **TOF-MS**: 455.13 m/z.**UV** (λ_{max}, ε) [nm, M^{-1}]: 204, 69366; 258, 22455; 289, 25799, 340, 10082; 450, 4764. **Elemental Analysis:** Calculated for $C_{24}H_{18}CuN_6O_4$: C, 55.63; N, 16.23; H, 3.50. (Found: C, 55.61; N, 16.33; H, 3.54).

2.3.4 Synthesis of (dipyrido[3,2-a:2′,3′-c]phenazine)-(2)-((pyridine-2-ylmethylene)amino)phenol copper(II) nitrate [Cu(L)(DPPZ)](NO_3).

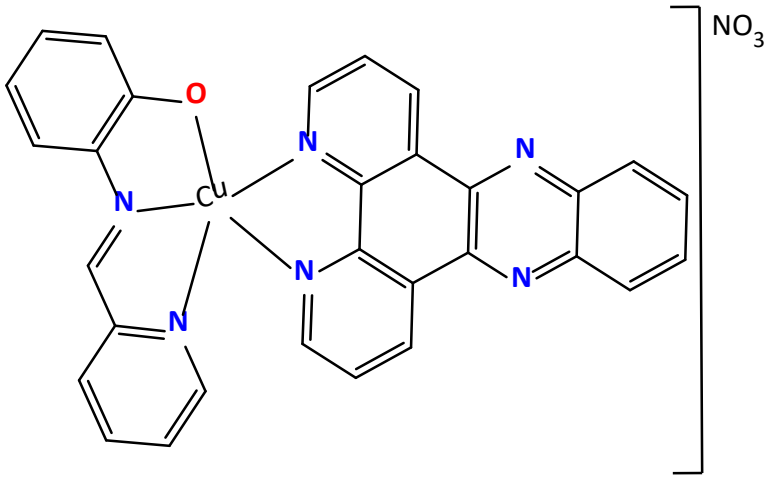

Figure 2.8: Structure of (dipyrido[3,2-a:2′,3′-c]phenazine)-2-((pyridine-2-ylmethylene)amino)phenol copper(II) nitrate, [Cu(L)(Dppz)](NO_3).

This compound, [Cu(L)(Dppz)](NO_3)was synthesized using the procedure that was employed to prepare (1,10-phenanthroline-5-amine)-2-((pyridine-2-ylmethylene)amino)phenol copper(II) nitrate as described above using DPPZ (0.13 g, 0.45 mmol) and [Cu(L)(H_2O)$_2$](NO_3) (0.20 g, 0.56 mmol). The crude product was dissolved in chloroform and filtered to remove excess insoluble [Cu(L)(H_2O)$_2$](NO_3). Chloroform was removed via rotary evaporation, yielding the final product as a deep red powder (0.25g, 92% yield).

Characterisation data:

FT-IR (cm^{-1}): 3061 ν(C-H), 1583 ν(C=N), 1274 ν(C=C), 727 ν(C-H), 1353 ν(NO_3^-). **TOF-MS**: 542.47 m/z. **UV** (λ_{max}, ε) [nm, M^{-1} cm^{-1}]: 209, 6052; 276, 5208; 359, 1260; 376, 1383; 431, 647). **Elemental Analysis:** Calculated for $C_{30}H_{19}CuN_7O_4$: C, 59.53; N, 16.21; H, 3.17. (Found: C, 59.56; N, 16.47; H, 3.43).

2.3.5 Synthesis of bis-1,10-phenantroline-5-amine copper(II) chloride [Cu(phen-NH_2)$_2$](Cl)]Cl.

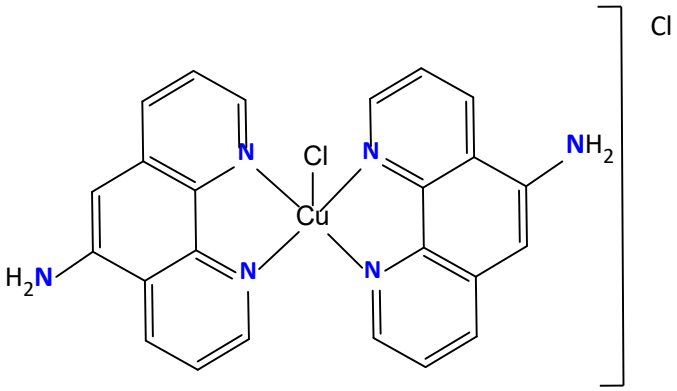

Figure 2.9: Structure of bis-1,10-phenantroline-5-amine copper(II) chloride [Cu(phen-NH_2)$_2$(Cl)]Cl.

This compound was synthesized according to the literature method reported, with slight modification.[5] The ligand 1,10-phenantroline-5-amine (phen-NH_2) (0.50 g, 2.56 mmol), was dissolved in methanol (20 mL) and a solution of $CuCl_2$ (0.22 g, 1.28 mmol) in methanol (30.00 mL) was added dropwise for 30 minutes, this led to the formation of a dark green precipitate. The solution was heated to reflux for 3 hours followed by further stirring at room temperature for an hour. After this period, methanol was removed under reduced pressure to afford a dark-green semi-crystalline precipitate of [Cu(phen-NH_2)$_2$(Cl)]Cl. Suitable crystals for X-ray diffraction were grown by slow evaporation of a dichloromethane solution of the target compound and were collected by gravity filtration. Yield (0.66 g, 92 %).

Characterisation data:

FT-IR (cm^{-1}): 3190 v(C-H), 1594 v(C=N), 1425 v(C=C), 722 v(C-H). **TOF-MS**: 454.96 m/z. **UV** (λ_{max}, ε) [nm, M^{-1} cm^{-1}]: 210, 3560; 258, 2167; 290, 2439; 343, 615. **Elemental Analysis:** Calculated for $C_{24}H_{18}Cl_2CuN_6O_4$: C, 54.90; N, 16.02; H, 3.46. (Found: C, 54.66; N, 16.14; H, 3.45).

2.5 References

1. Molphy, Z., Prisecaru, A., Slator, C., Barron, N., McCann, M., Colleran, J., Chandran, D., Gathergood, N. and Kellett, A., 2014. Copper phenanthrene oxidative chemical nucleases. *Inorganic Chemistry*, *53*(10), pp.5392-5404.
2. Slim, M. and Sleiman, H.F., 2004. Ruthenium (II)−phenanthroline−biotin complexes: synthesis and luminescence enhancement upon binding to avidin. *Bioconjugate Chemistry*, *15*(5), pp.949-953.
3. Akerman, M.P. and Chiazzari, V.A., 2014. An X-ray crystallographic and DFT study of the complementary hydrogen bonding of bidentate pyrrolide-imine Schiff base ligands. *Journal of Molecular Structure*, *1058*, pp.22-30.
4. Bhaumik, P.K., Jana, S. and Chattopadhyay, S., 2012. Synthesis and characterization of square planar and square pyramidal copper (II) compounds with tridentate Schiff bases: Formation of a molecular zipper via H-bonding interaction. *Inorganica Chimica Acta*, *390*, pp.167-177.
5. Yanick Gaelle, D.S., Ondoh Agwara, M., Yufanyi, D.M., Nenwa, J. and Jagan, R., 2017. Crystal structure and antimicrobial properties of a copper (II) complex with 1, 10-phenanthroline and azide co-ligand. *Inorganic and Nano-Metal Chemistry*, *47*(4), pp.618-625.

CHAPTER 3: ANALYSIS OF SYNTHETIC METHODS

3.1 Synthesis of Schiff base ligand HL

The primary ligand used in this study contains an imine bond, which is a bond formed from the reaction of a primary amine and a compound that has a carbonyl functional group: either ketone or aldehyde. In this case, 2-aminophenol (amine) and 2-pyridinecarbaldehyde (aldehyde) reacted producing the Schiff base 2-((pyridine-2-ylmethylene)amino)phenol and water as a by-product.

As illustrated below (Scheme 3.1), the first step in the Schiff base mechanism involves the lone pair electrons of the amine nitrogen attacking the carbonyl carbon. This is followed by the transfer of a proton from the ammonium ion to the alkoxide group. This results in the formation of carbinolamine, a neutral tetrahedral intermediate which exists in equilibrium with two protonated forms. The final step involves the elimination of water from the oxygen-protonated intermediate resulting in a protonated imine which forms a (N=C) double bond by losing a proton.

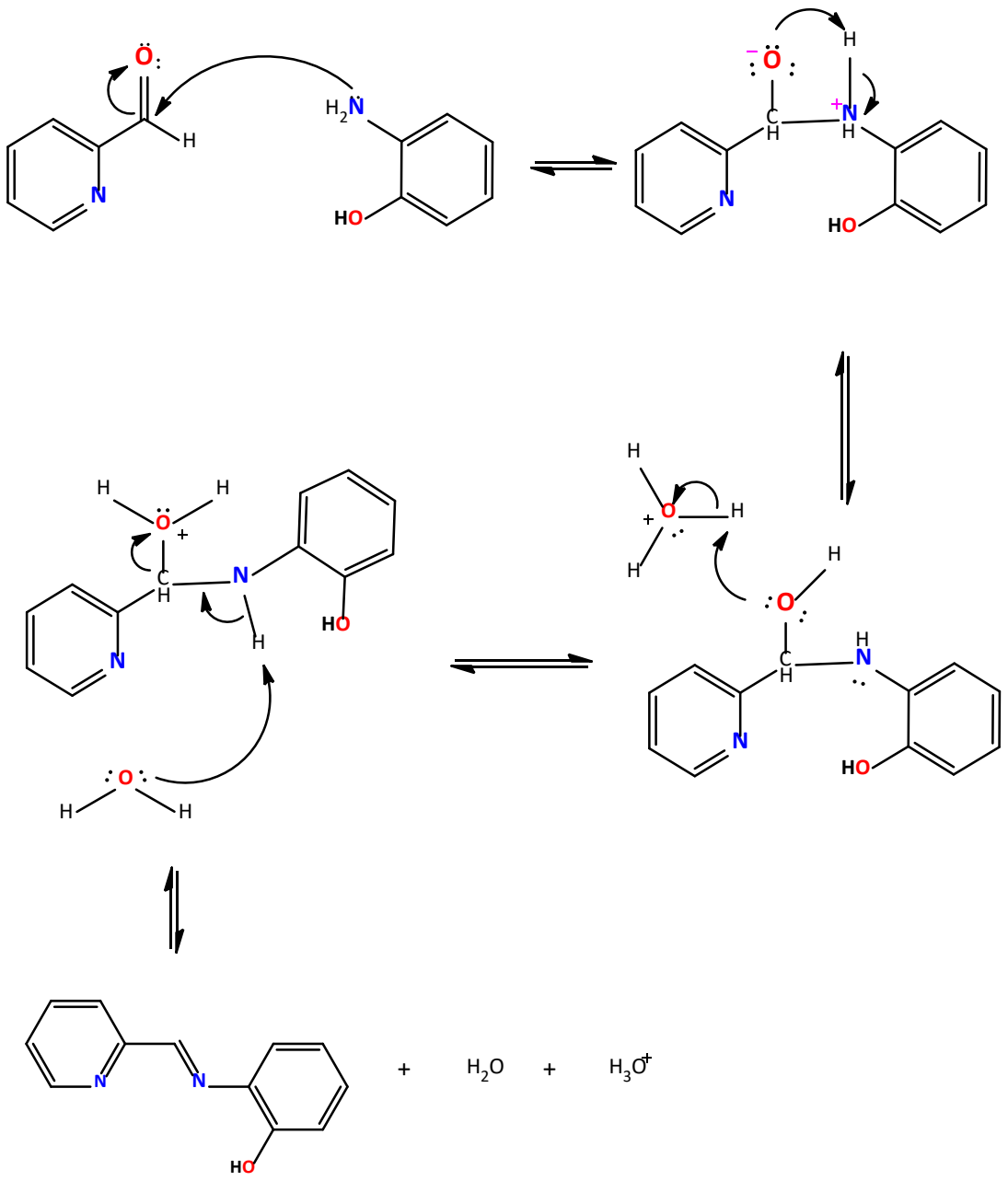

Scheme 3.1: Reaction mechanism for the acid-catalysed synthesis of 2-((pyridine-2-ylmethylene)amino)phenol.

The first approach to synthesize the Schiff base ligand was the traditional reflux of reagents in methanol for three hours. This approach was not the most efficient as it produced low yields (40 %) and an impure compound, hence a solid-state reaction was tested. 2-Pyridinecarbaldehyde and 2-aminophenol were placed in a mortar and pestle (Figure 3.1(a)), ground together for 20-30 min forming a yellow paste (Figure 3.1(b)). The crude product (Figure 3.1(c)) was crystallized in methanol and dried at room temperature producing a clean yellow crystalline powder at a high yield of (98 %). The solid state reaction therefore offers a number of advantages. In addition to being high yielding, the final product is of high purity requiring minimal purification. This reduction in synthetic steps and the solvent-free reaction method suggests that this could be classified as a "green" method for imine synthesis.

(a) (b) (c)

Figure 3.1: Solid-state reaction for the synthesis of Schiff base ligand (HL).

3.2 Synthesis of dipyrido[3,2-a:2’,3’-c]phenazine (DPPZ)

Phen (Figure. 3.2) is a well-known N-heterocyclic ligand with two pyridine rings fused to a benzene ring that belongs to the phenanthrene family. It can be described as a tricyclic molecule which is a bidentate ligand that coordinates through two nitrogen atoms.

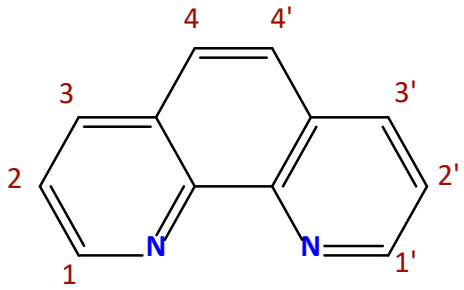

Figure 3.2: Structure and numbering of 1,10-phenantroline.

The study carried out by Cogan on 1,10-phenanthroline (The numbering used in Figure 3.2 is the same as that in the Cogan study) reports that the position related to nucleophilic substitution were assigned to position 1 and 3.[1] Position 1 and 1’ are nucleophilic due to the strong electron withdrawing effect of nitrogen atoms. Position 3 and 3’ are both adjacent to quartenary carbons that are experiencing electron withdrawing hence favours nucleophilic substitution. Due to higher electron density at position 2, 4, 4’ and 2’ these positions are electrophilic.[1]

The synthesis of the co-ligand dipyrido[3,2-a:2’,3’-c]phenazine (dppz) first requires the synthesis of the precursor, phendione. This was done by the oxidation of phen under acidic conditions in the presence of potassium bromide at room temperature (Figure 3.3). The phen and potassium bromide were directly added to a mixture of nitric and sulphuric acid. This reaction was done at low temperature (0 °C) as the mixture of acids produces heat during the oxidation reaction. After the reaction mixture was stirred for 24 hours, phendione is extracted and purified, resulting a

yellow crystalline powder in a 77% yield. A general scheme for the synthesis of phendione is shown in Figure 3.3.

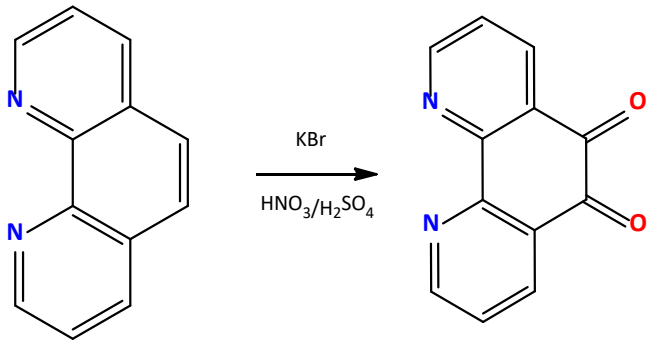

Figure 3.3: Synthesis of phendione.

After the diketone (phendione) was produced, the next step in the synthesis of dipyrido[3,2-a:2',3'-c]phenazine is the formation of imine bonds by replacing oxygen with nitrogen atoms forming a heterocycle. This reaction involves the addition of 1,2-phenylenediamine to a solution of phendione in methanol followed by heating to reflux. The mechanism begins with the nucleophilic attack on the carbonyl carbon by the lone pair on the nitrogen of an amine. This is followed by proton transfer and subsequently the protonation of the hydroxyl group. The final two steps involve the removal of water followed by deprotonation. Since 1,2-phenylenediamine contains two amine groups, two imine bonds are formed resulting in a closed heterocyclic ring. This is shown in Scheme 3.2.

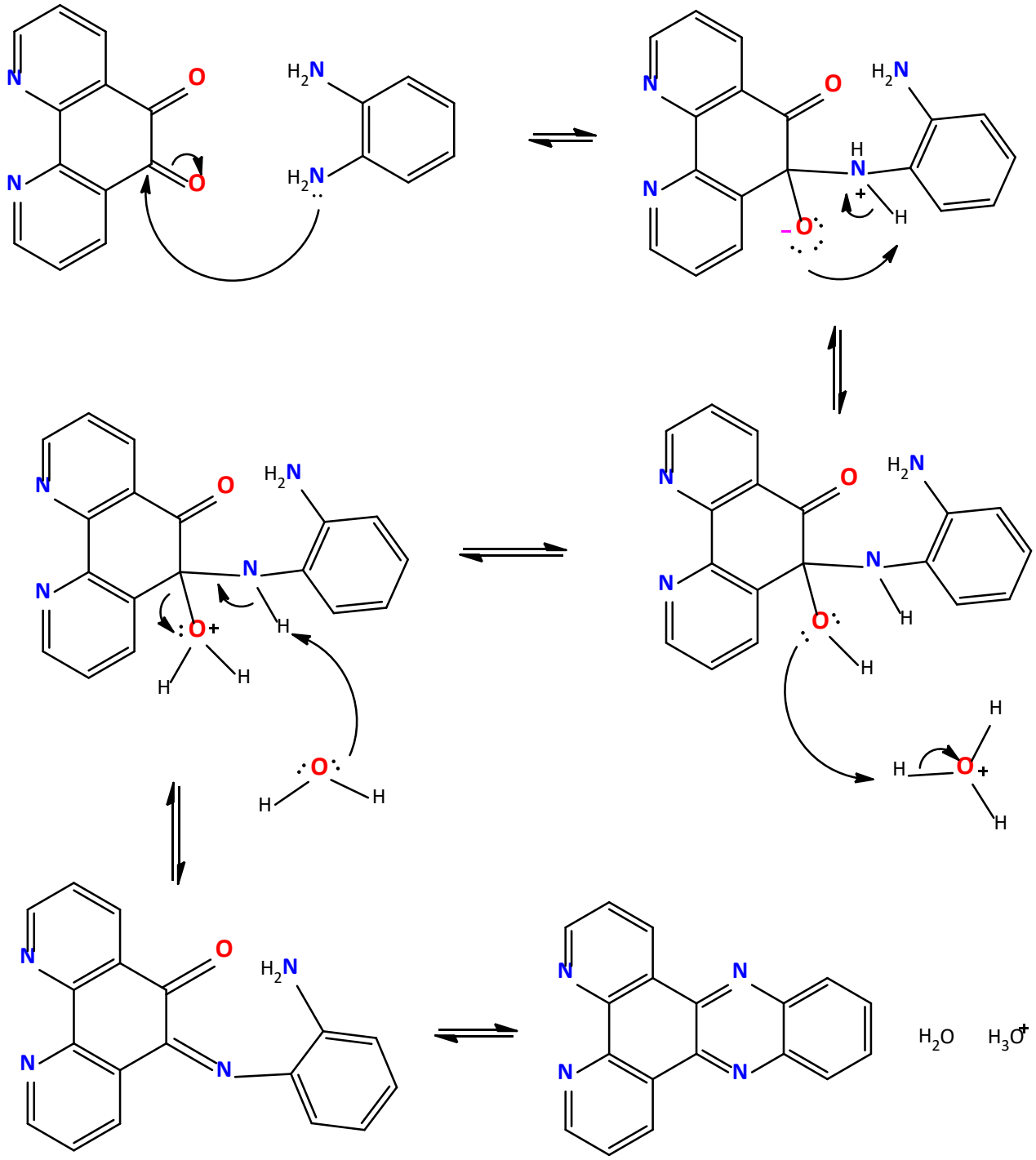

Scheme 3.2: Reaction mechanism for the formation of dipyrido[3,2-a:2',3'-c]phenazine.

3.3. Synthesis of Biotin Ligand

The synthesis of biotin ligand first requires the conversion of the carboxylic group of biotin to an acyl chloride by reaction with thionyl chloride ($SOCl_2$) under inert atmosphere (nitrogen). Thionyl chloride acts as both the solvent and reagent. In the presence of moisture, the acyl chloride is susceptible to hydrolysis back to the carboxylic acid.[2] Therefore, the product of this reaction was not isolated, but used directly in the next step. As shown in the general scheme Figure 3.4, this reaction also yields HCl and SO_2.

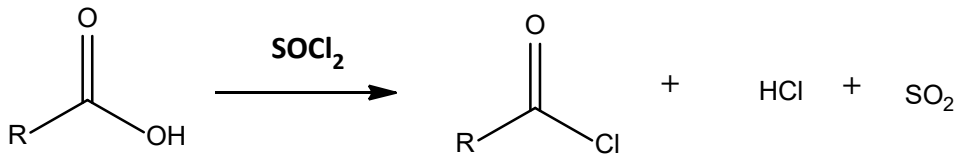

Figure 3.4: General reaction scheme for acyl chloride formation from a carboxylic acid using thionyl chloride.[2]

The second step involves the formation of an amide bond using the desired amine (1,10-phenathroline-5-amine) and an acyl chloride in the presence of a base, 4-dimethylaminopyridine (DMAP). DMAP is required to firstly trap the HCl formed and to accelerate the reaction. Trapping of HCl prevent the conversion of the amine into its unreactive salt.[3] A general reaction scheme for the synthesis of an amide from an acyl chloride and primary amine is shown in Figure 3.5.

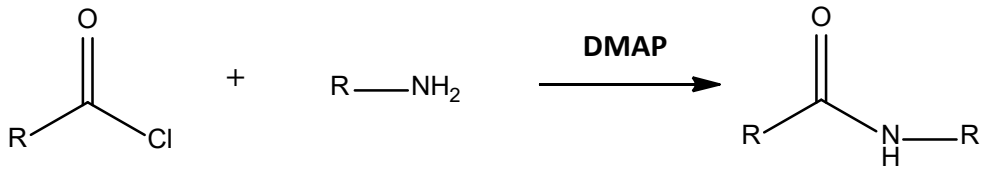

Figure 3.5: General reaction scheme for amide formation from acyl chloride.[2]

3.4. Synthesis of Metal Chelates

The copper(II) complexes synthesized in this study comprise three primary copper(II) complex ($[Cu(L)(H_2O)_2]NO_3$, $[Cu(L1)(H_2O)_2]NO_3$, and $Cu(phen\text{-}NH_2)_2Cl]Cl$) and three secondary copper(II) complexes ($[Cu(L)(phen)]NO_3$, $[Cu(L)(phen\text{-}NH_2)]NO_3$ and $[Cu(L)(dppz)]NO_3$. Copper(II) nitrate and copper(II) chloride were used in the synthesis of complexes. The complex $Cu(L)(H_2O)_2]NO_3$ and $[Cu(L1)(H_2O)_2]NO_3$ was synthesised by reacting a stoichiometric amount of copper(II) nitrate and the corresponding Schiff base ligand under reflux for three hours in methanol. The phenolic OH group of the Schiff base deprotonates during the metallation and the ligand coordinates through two nitrogen atoms and the anionic oxygen atom forming a five-coordinate square pyramidal complex with two water molecules bonded to the metal centre and nitrate as a counter ion (refer to Figure 3.6).

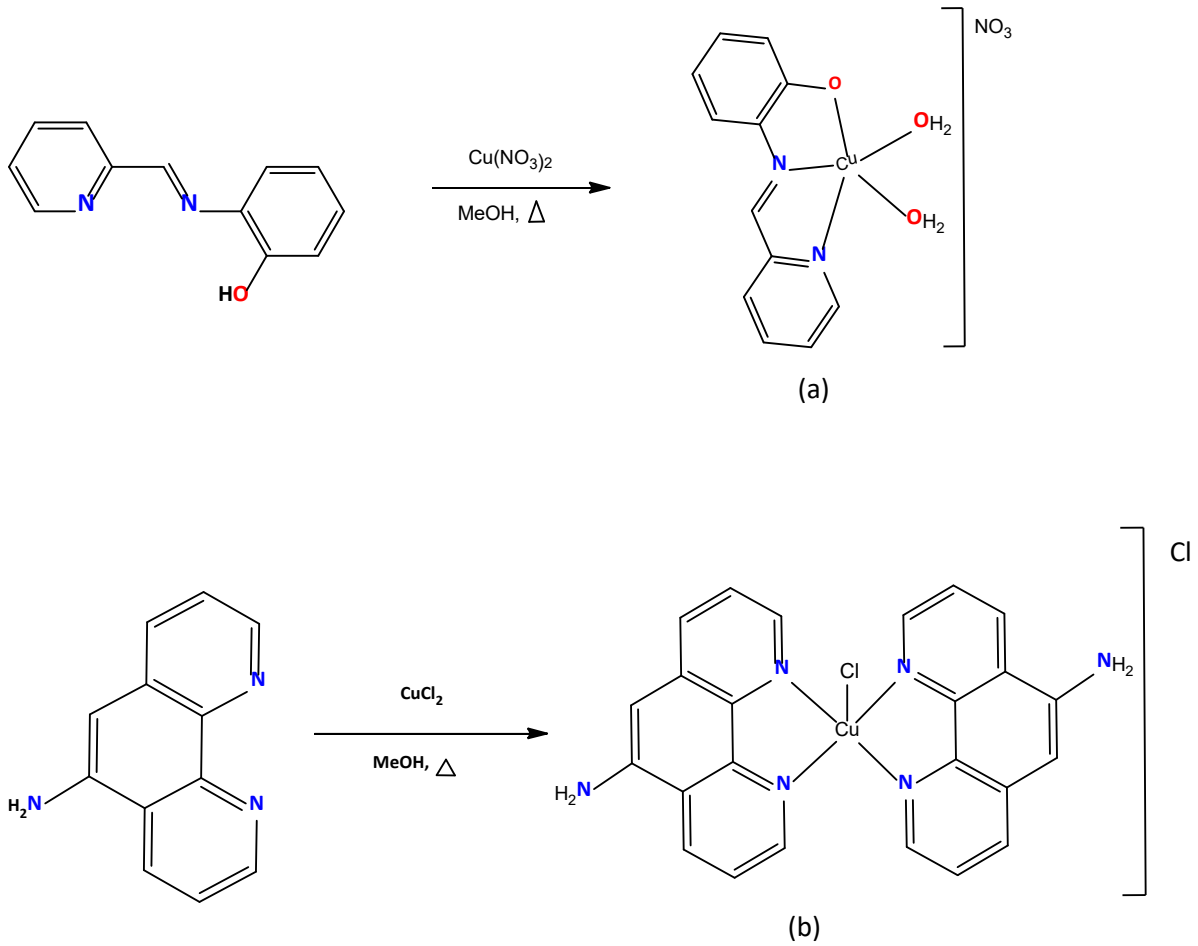

Figure 3.6: Synthesis of $[Cu(L)(H_2O)_2]NO_3$ (a) and $[Cu(phen\text{-}NH_2)_2Cl]Cl$ (b).

The synthesis of the complex $[Cu(phen\text{-}NH_2)_2Cl]Cl$ used similar reaction conditions as described above, using 1,10-phenathroline-5-amine ($Phen\text{-}NH_2$) and copper chloride in a 2:1 molar ratio. The purpose of synthesizing this complex is to determine which structural features are most significant with respect to cytotoxicity towards cancer cells. Figure 3.5 presents the synthetic procedure of these complexes. This reaction yields a five-coordinate copper(II) complex with coordination sites occupied by two bidentate ligands ($Phen\text{-}NH_2$), an axial chlorido ligand and one outer sphere chlorido ion.

Refluxing the primary complex ($[Cu(L)(H_2O)_2]NO_3$) with a co-ligand was not an ideal synthetic route for the synthesis of secondary heteroleptic copper(II) complexes ($[Cu(L)(phen\text{-}NH_2)]NO_3$, $[Cu(L)(phen)]NO_3$ and $Cu(L)(dppz)]NO_3$. This synthetic approach results in numerous side reactions taking place, making the isolation of the target compound difficult. The secondary 0heteroleptic complexes were, rather unusually, synthesized *via* a solid state reaction by adding the desired co-ligand and the copper-coordinated Schiff base, $[Cu(L)(H_2O)_2]NO_3$ to the mortar and ground together (see Figure 3.7). $[Cu(L)(dppz)]NO_3$ and $[Cu(L)(phen\text{-}NH_2)]NO_3$ require the addition of minimum solvent (methanol) to enhance the speed and efficiency of the reaction. In this process, water molecules are displaced by the neutral bidentate ligand leading to the formation of the desired heteroleptic copper(II) complexes as shown in Figure 3.7.

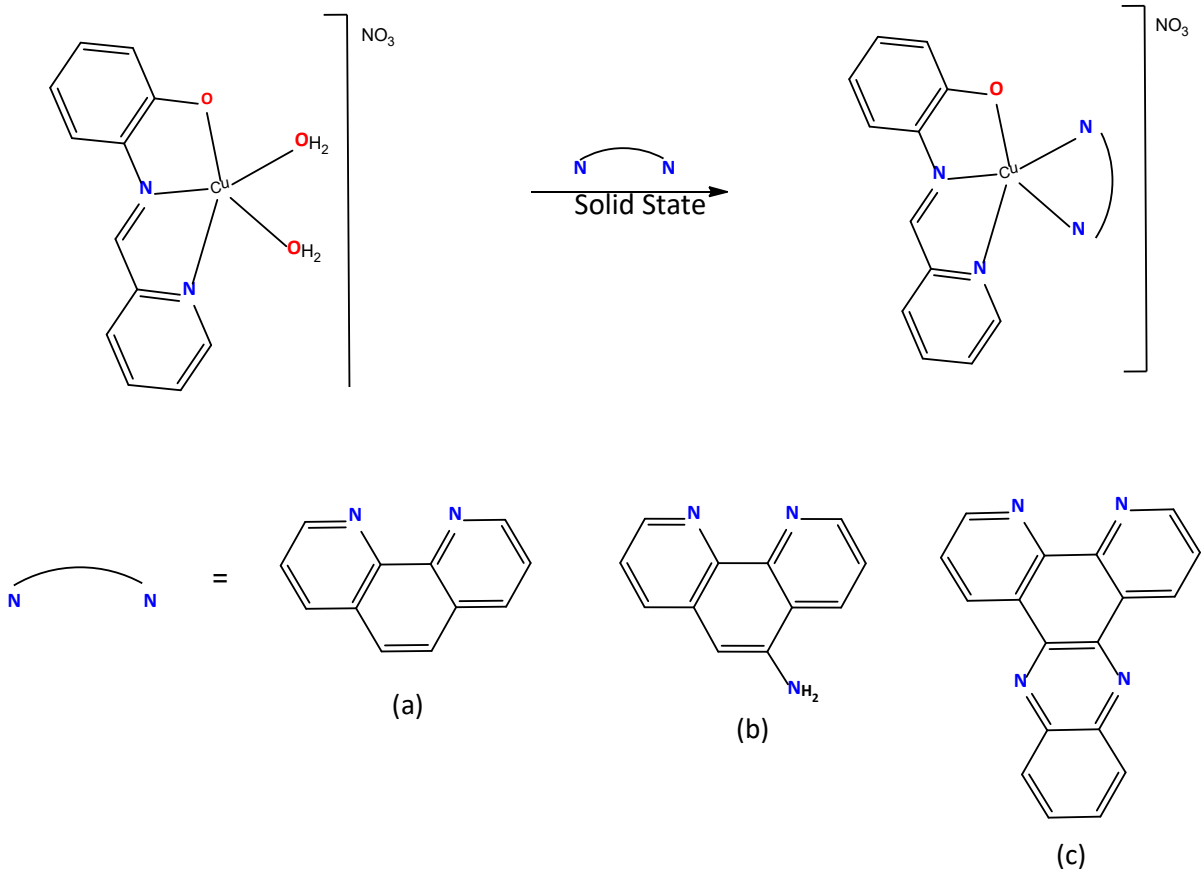

Figure 3.7: Synthesis of heteroleptic complexes [Cu(L)(phen)]NO_3, [Cu(L)(phen-NH_2)]NO_3 and [Cu(L)(dppz)]NO_3 using three different co-ligands (a) 1,10-phenantroline, (b) 1,10-phenantroline-5-amine and (c) DPPZ.

The formation of heteroleptic complexes in solution upon refluxing in methanol could not be detected; hence an unusual solid state synthetic route was applied. This solid state reaction is of considerable importance in the field of Green Chemistry as it produces quantitative yields with minimal solvent use and very few synthetic steps. Although relatively well established in organic syntheses, the use of solid state reactions in coordination chemistry is limited. Sufficient amounts of high purity compounds were easily obtained from this method for a broad-range of complexes. Furthermore, this novel synthetic process is fast, cost effective and leads directly to products in the solid form. Hence, the compound is ready for different applications without the need of post-synthetic processing. The purity of the compounds was established using elemental analysis. Figure 3.8 shows the solid-state reaction before and after grinding.

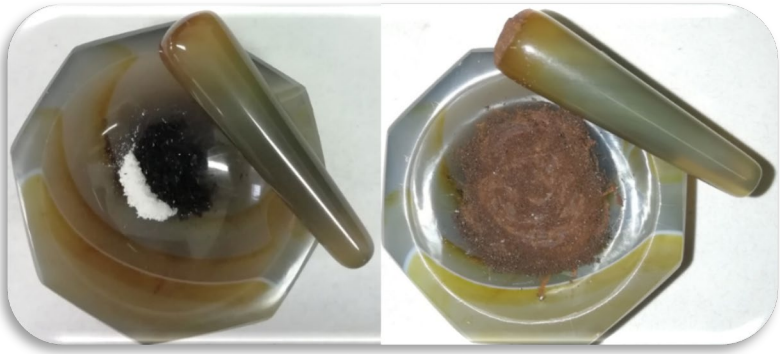

(a) (b)

Figure 3.8: Solid-State reaction for the synthesis of [Cu(L)(Phen)](NO_3). (a) Shows the two reagents before grinding and (b) shows the final microcrystalline product.

A mixture of [Cu(L)(H_2O)$_2$](NO_3) (Black) and 1,10-phenanthroline (White) (Figure 3.8 (a)) were mixed and ground together for 30 min. A microcrystalline powder of dark brown product (Figure 3.8 (b)) was obtained in a 97 % yield. The copper(II) Schiff base chelate ([Cu(L)(H_2O)$_2$)]NO_3) is the ideal precursor for this reaction owing to the presence of aqua ligands. As these ligands are displaced by the bidentate ligands they act as a solvent and then quickly evaporate.

The Schiff base ligand and secondary heteroleptic copper(II) chelates ([Cu(L)(phen)]NO_3, [Cu(L)(phen-NH_2)]NO_3 and [Cu(L)(dppz)]NO_3) were successfully synthesized *via* solid-state reactions, which offer significant improvements over conventional procedures with the short reaction time, excellent yields and reduced formation of undesired side products. The identity and purity of the chelates were confirmed using a range of spectroscopic techniques (FT-IR, TOF-MS, EPR and UV spectra as well as elemental analysis).

3.4 References.

1. Cogan, R., 2009. 'Synthesis, Characterisation and Anti-Candida Activity of Inorganic and Organic Derivatives of 1, 10-Phenanthroline'. Master's thesis, Dublin Institute of Technology, Dublin.
2. Bruice, P. Y 2007. *Organic Chemistry*, 5th edn, Pearson International Edition, Lincon.
3. Montalbetti, C.A. and Falque, V., 2005. Amide bond formation and peptide coupling. *Tetrahedron*, *61*(46), pp.10827-10852.

CHAPTER 4: SPECTROSCOPY

4.1 Electromagnetic Spectrum

Spectroscopy is the study of light interacting with matter. Light is a type of electromagnetic (EM) radiation which is made up of little packets of energy called photons with both particle and wave-like properties.[1,2] The EM radiation spans a wide range of frequencies and wavelengths. This enormous range is known as the electromagnetic spectrum. As shown in Figure 4.1, the EM spectrum is generally divided into seven regions, in order of increasing frequency and energy and decreasing wavelength.

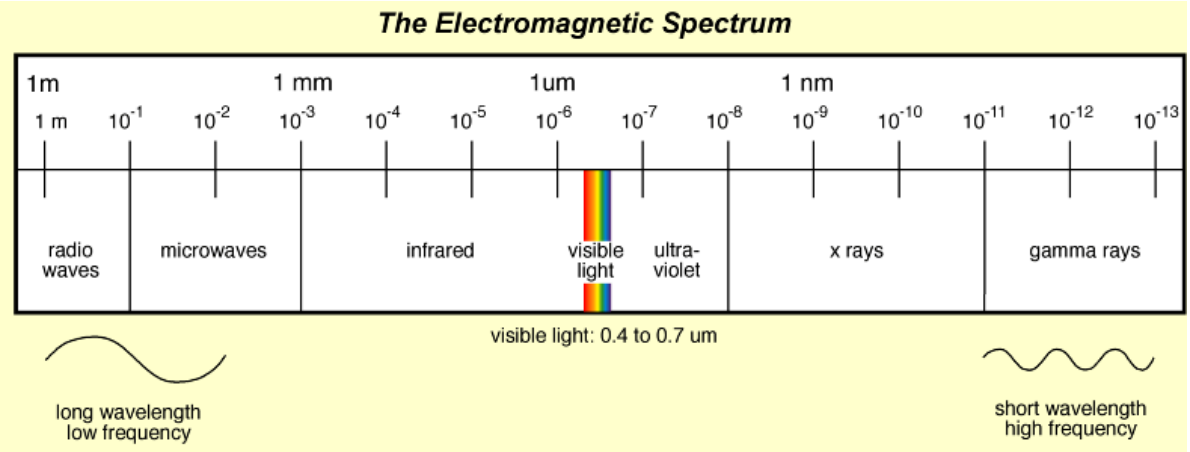

Figure 4.1: Electromagnetic spectrum showing the wavelengths of the different regions.[9]

Gamma rays and X-rays have short wavelengths (billionths or trillionths of meters) while radio and microwaves lie at the far left end of the spectrum with longer wavelengths (millimeters and centimeters to meters and kilometers). The light in the visible region (~400 to 700 nm) makes up only a small region of the entire spectrum of electromagnetic radiation.

Since it is impossible to physically visualize molecules and atoms, scientists use light-matter interactions to provide detailed information on their structure, interactions and composition. The technique used for measuring and interpreting the interaction of matter with light is referred to as spectroscopy.[15] There are many different types of spectroscopic techniques which can be used to solve a wide range of analytical problems. The methods used vary based on the species to be analysed (such as atomic or molecular spectroscopy), the type of radiation-matter interaction to be monitored (such as diffraction, emission, or absorption), and the region of the EM spectrum used in the analysis. Spectroscopic methods can give a lot of information and are widely used for both qualitative and quantitative analyses.[10,15]

Common spectroscopic methods that are based on the emission and absorption of radiation include infrared (IR), ultraviolet (UV), visible (Vis) and radio (nuclear magnetic resonance, NMR). In each of these methods the amount of emitted or absorbed radiation by the analyte is measured and used to gain insight into the structural properties. The above methods differ with respect to the wavelength of radiation used. Each wavelength of light interacts differently with a chemical sample and yields different structural information. A summary of various wavelengths and their corresponding spectroscopic technique is presented in Table 4.1.

Table 4.1: Electromagnetic spectrum region, type of energy transfer, and the associated spectroscopic technique.

Type of Energy Transfer	Region of the Electromagnetic Spectrum	Spectroscopic Technique
Emission (thermal excitation)	UV/vis	Atomic emission
Absorption	Radio waves	Nuclear magnetic resonance (NMR)
	Microwave	Microwave
		Electron spin resonance (ESR)
	Infrared	Infrared (IR)
		Raman
	UV-Vis	UV/Vis
		Atomic absorption
	X-ray	X-ray absorption
	γ-ray	Mössbauer
Photoluminescence	X-ray	X-ray fluorescence
	UV-Vis	Fluorescence
		Phosphorescence
		Atomic fluorescence

4.2 Infrared (IR) spectroscopy

4.2.1 Introduction

Infrared spectroscopy is a technique which uses electromagnetic radiation in the infrared region (4000 to 400 cm^{-1}) to perform structural analysis. Different types of information can be obtained from infrared spectroscopy, this includes the type of atoms comprising the molecule and types of bonds between atoms. For quantitative purposes infrared spectroscopy is well known for its power, flexibility and reliability. There are three defined IR regions as shown in Figure 4.2 (near, mid and far), the boundaries between them are not well defined, but broadly they are categorised as: Near infrared (12820-4000 cm^{-1}), Mid-infrared (4000-400 cm^{-1}) and Far Infrared (400-33 cm^{-1}).[11,12]

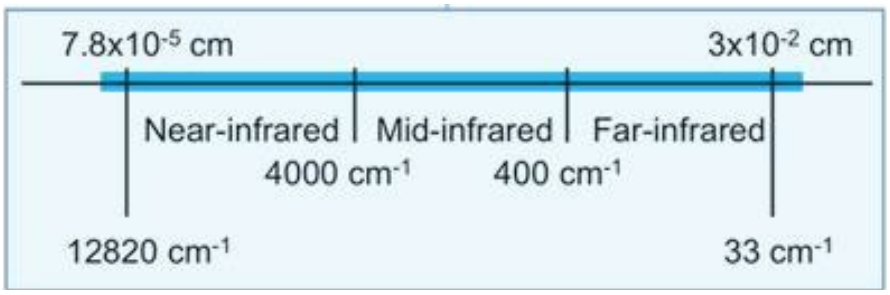

Figure 4.2: The Infrared region of electromagnetic spectrum.[12]

Infrared radiation is relatively low in energy and is not sufficient to cause electronic transitions, however, it causes changes in the amplitude of molecular vibrations. When the energy of the radiant light source matches that of a specific molecular vibration, the absorption occurs. The vibrational energy of a bond is characteristic of the nature of the two bonded atoms. Hence by measuring the frequency of the absorbed energy, the type of bond or functional groups in a compound can be determined. The vibrations are also influenced by neighbouring bonds of that particular molecule. Therefore the IR spectra of any given compound provides information about the kind of functional groups in said compound.[15] IR spectroscopy is an important technique in this work as the target copper(II) compounds are paramagnetic, which precludes NMR as a characterisation technique. IR spectroscopy was therefore used as the first line of characterization to identify key functional groups in the ligand to indicate successful synthesis and metal ion chelation.

4.2.2: Results and Discussion

In the synthesis of the phendione precursor, the replacement of atoms within the molecule was monitored using IR spectroscopy. In this case two hydrogen atoms at the five and six position have been replaced by two oxygen atoms forming phendione. The IR spectra of phendione (Figure. 4.3) reveals an absorption peak at 1559 cm^{-1} which is due to a C=C stretch, while the peak at 1411 cm^{-1} corresponds to C-H bends. The carbonyl stretching frequency is distinct and in a region of the IR spectrum in which typically few other groups resonate. The IR spectrum confirms the presence of carbonyl peaks at 1680 cm^{-1} specific to phendione, confirming phen was oxidized. Phendione has been synthesized by Molphy *et al.* and all the absorption peaks are comparable with those reported.[19]

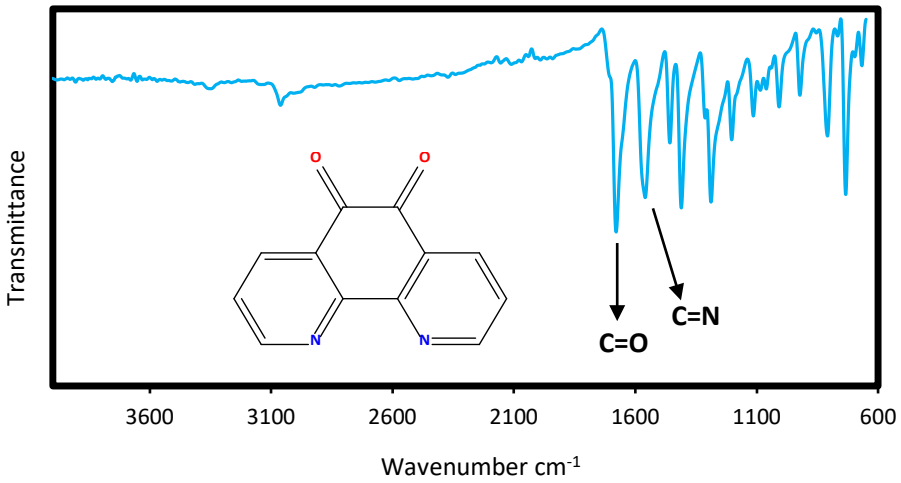

Figure 4.3: IR spectrum of phendione showing the characteristic carbonyl stretching frequency at 1680 cm^{-1} indicating successful oxidation.

In order to study the binding mode of the Schiff base ligand (HL) and co-ligands (phen, phen-NH_2 and dppz) to the metal ion in the complexes ($[Cu(L)(phen)]NO_3$, $[Cu(L)(phen\text{-}NH_2)]NO_3$ $[Cu(L)(dppz)]NO_3$) the IR spectra of the free ligands was compared with the spectra of the complexes. The FT-IR data of the free HL ligand and the complex $[Cu(L)(H_2O)_2]NO_3$ are shown in Figure 4.4 (a) and (b), respectively. The spectra of HL showed a strong band at 3364 cm^{-1} due to the presence of the phenolic group which is assigned to ν(O-H) stretching vibrations. This characteristic peak of ν(O-H) is absent in the IR spectra of the copper complex, indicating the hydroxyl groups are deprotonated during the coordination. The broader band centered at 3084 cm^{-1} is assigned to the O-H stretch of the water molecules, and there is another peak at 762 cm^{-1}, which is evidence for the existence of coordinated water molecules. The split peak at 1293 cm^{-1} is associated with the nitrate anion present in the structure. The complex showed a shift to lower wavenumber for the C=N bond. This is due to the electron withdrawing effect of the metal ion which lowers the bond order of the imine which therefore resonates at a lower frequency. Again, absorption peaks are comparing favourably to similar previously reported compounds.[20]

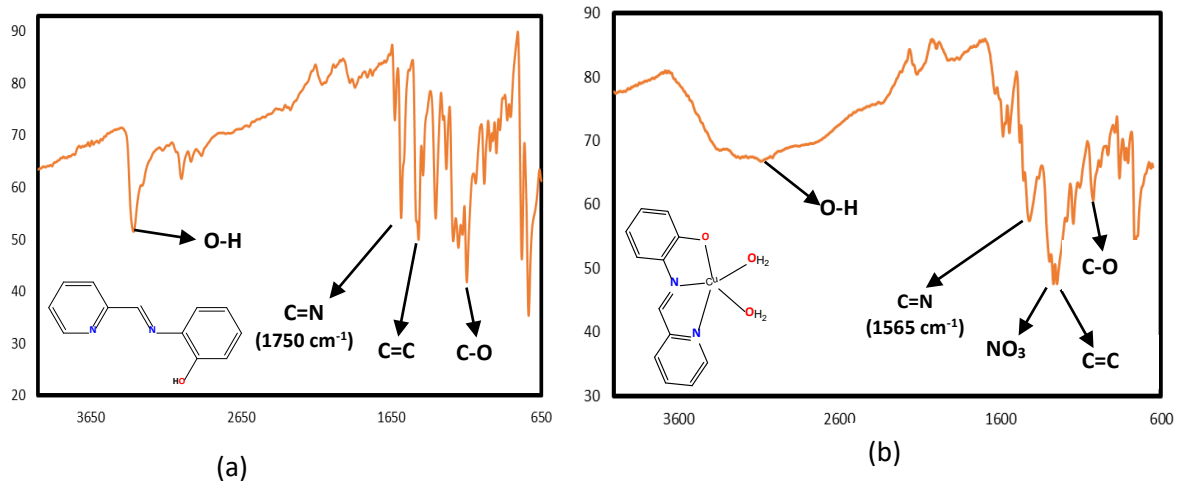

Figure 4.4: IR spectrum of (a) HL and (b) $[Cu(L)(H_2O)_2]NO_3$.

The intense vibration band at 1467 cm^{-1} and 1583 cm^{-1} are assigned to C=N which underwent a shift to lower wavenumbers of about 15-20 cm^{-1} in the complex, confirming the coordination of the N atom of the azomethine to copper ions. The absorption peaks in the region 400-600 cm^{-1} are assigned to the vibration of Cu-N and Cu-O coordinated bonds. The decrease in frequency for the same bond stretch is attributed to the electron withdrawing nature of the copper(II) metal center. The oxidised copper ions are electron deficient and they remove electron density from the ligands, this results in a weakening of the bonds in the region of the coordination sphere. This manifests as a shift to lower frequencies of the ν(C-N) stretching mode for the complexes.[21]

Table 4.2 below compares the frequencies of the bond (C-N) of the co-ligand before and after chelation to study the effect of chelation on the vibrational frequency of the molecule.

Table 4.2: Comparison of imine stretching vibrations of the free co-ligand and secondary heteroleptic chelates.

Co-ligand	Frequency of free co-ligand (cm^{-1})	Frequency of secondary heteroleptic chelate (cm^{-1})
Phen	1641	1581
	1614	1512
Phen-NH_2	1633	1622
	1610	1589
DPPZ	1625	1583
	1573	1456

When coordination of the co-ligand occurs, there is a characteristic shift of the imine bond to lower wavenumber (Table 4.2). This is due to the electron withdrawing effect of the metal centre. Oxidised metal ions draw electrons from the ligand to the metal hence weakening bonds in the region of the coordination sphere. In this case the C=N bond weakens because of this phenomenon. All the IR data suggest the copper ions are coordinated to the Schiff base *via* the imino-nitrogen, pyridine nitrogen and phenolic oxygen.

4.3: Nuclear Magnetic Resonance (NMR)

4.3.1: Introduction

NMR was discovered shortly after the Secord Word War, since then it has found a widespread application in different areas of science. NMR spectroscopy is based on the fact that nuclei of atoms are positively charged and they spin on an axis, creating a magnetic field. This magnetic property can be utilized to yield chemical information. Without any external applied magnetic field, the nuclear spins remain in random directions (Figure 4.5 (a)), however when an external magnetic field is present they align themselves with or against the applied magnetic field (Figure 4.5 (b)). Nuclei that align with the external magnetic field (B_o) are in a low energy state (α-spin state) while those nuclei that align against the field are in a higher energy state (β-spin state). The energy (E) difference between two states depends on the applied magnetic field (B_o), the greater the strength of B_o, the larger the energy difference between the two spin states.[16]

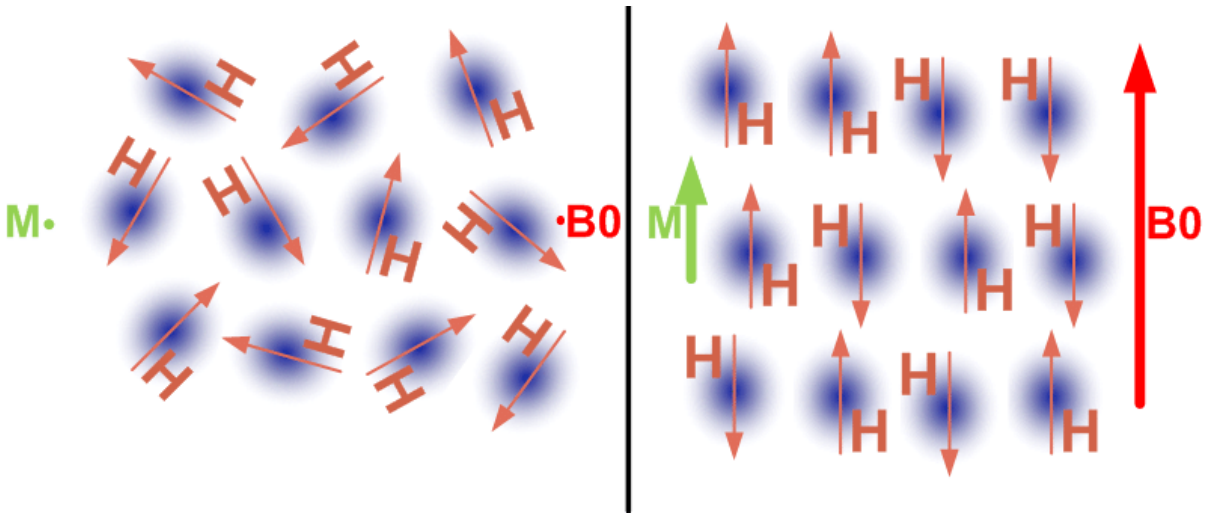

(a) (b)

Figure 4.5: (a) The nuclei are energetically degenerate with a random arrangement, (b) nuclei align with (low energy) or against (high energy) the applied magnetic field (B_o).[13]

The sample in the applied magnetic field is exposed to energy in the form of radio waves, nuclei absorb energy at a specific frequency and make a spin transition. Not all nuclei in a molecule absorb energy at the same frequency. This is due to the slight differences in magnetic environments resulting from the differing electron density surrounding the nuclei. Thus all nuclei in a molecule with a different electron density surrounding them are in a slightly different chemical environment with different electronic shielding, which consequently results in a slightly different resonance frequency and hence different chemical shift.[13,15]

In this research study, ^{1}H and ^{13}C NMR were used as characterization techniques. Both NMR techniques were only used to characterise ligands and not their complexes, this was due to the paramagnetic nature of copper(II) chelates. Hence, EPR was used to characterise the copper(II) complexes (*vide infra*)

4.3.2 Results and Discussion

The ^{1}H NMR spectrum (Figure 4.6) of the Schiff base ligand was recorded in $CDCl_3$ at room temperature.

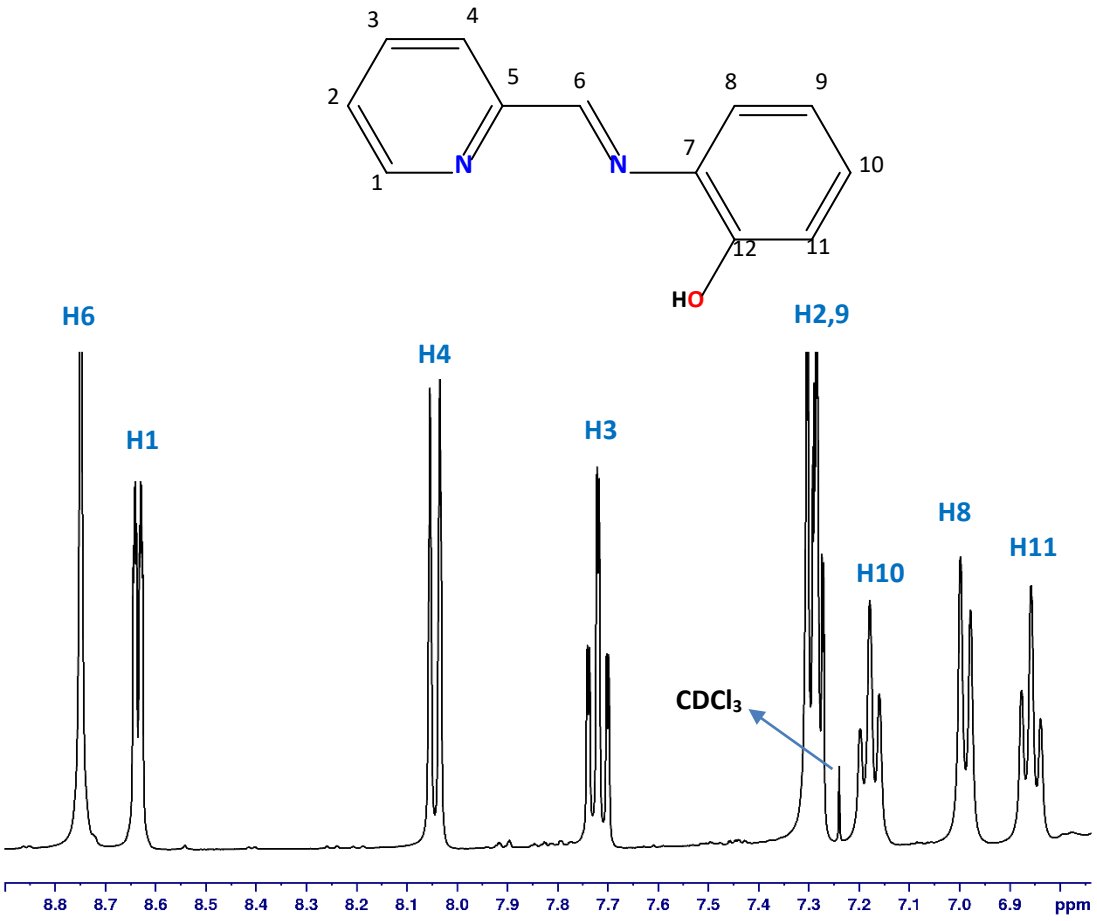

Figure 4.6: ^{1}H NMR spectrum of the aromatic region of 2-((pyridine-2-ylmethylene)amino)phenol.

The ^{1}H NMR spectrum of HL was characterized by a singlet signal corresponding to the azomethine group (CH=N) appearing at 8.75 ppm. Multiple signals at 6.82-8.85 ppm corresponding to the quinolone and aromatic ring are also present.[20,21] The characteristic signal of the OH hydrogen atom is absent. This may be due to rapid exchange. The O-H is evident if the spectrum was recorded in DMSO or other aprotic solvents. Chloroform is technically aprotic, but due to the stability of the CCl_3^- ion it is slightly acidic and thus it has a replaceable proton. It is also possible that the OH signal is obscured by the peak associated with the residual water in the chloroform.

The 1,10-phenanthroline was used as a co-ligand and building block of 1,10-phenanthroline-5,6-dione (phendione) precursor which is used in the synthesis of the DPPZ ligand. Scheme 3.1 (Chapter 3) shows the synthetic strategy, the experimental section (Chapter 2) fully assigns the ^{1}H and ^{13}C spectra of ligands, while the full spectra for each compound are in Appendix B.

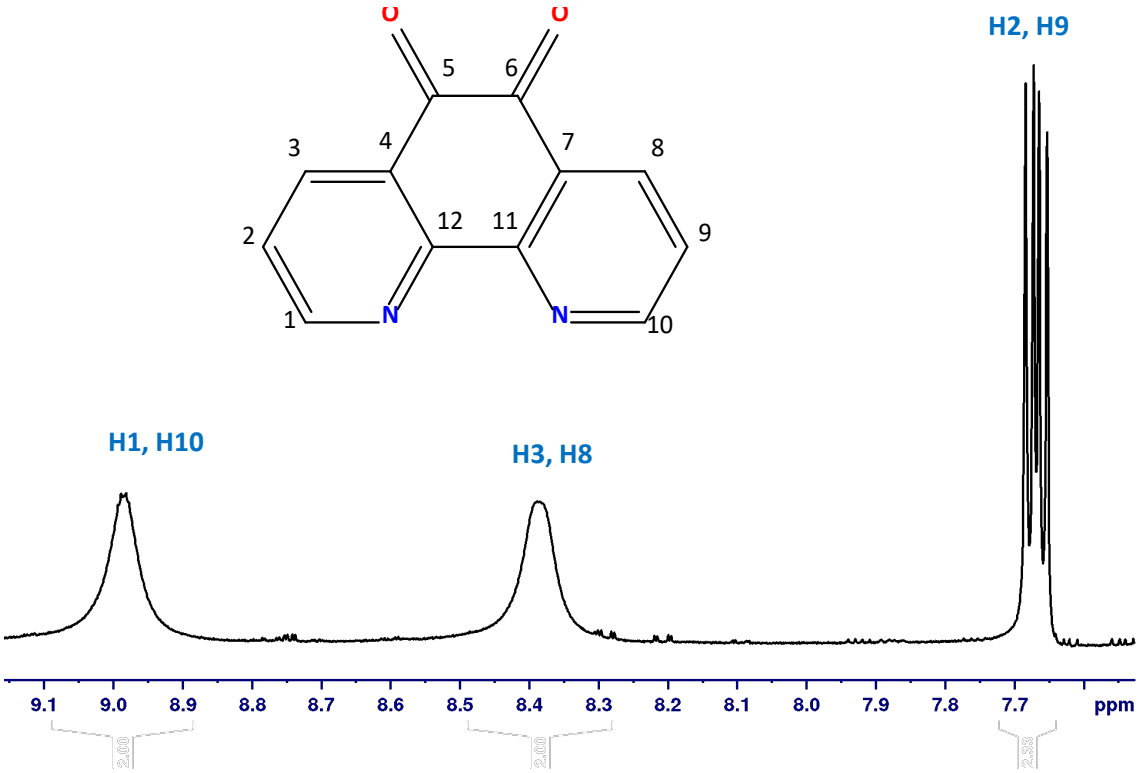

Figure 4.7: ^{1}H NMR spectrum of the aromatic region of 1,10-phenanthroline-5,6-dione.

The ^{1}H NMR spectrum of phendione (Figure 4.7) which was recorded in DMSO-d6 shows three signals at 8.98, 8.39 and 7.67 ppm, confirming the oxidation of 1,10-phenathroline. A considerable degree of symmetry is present in this compound so that the hydrogen atoms in the two halves of the molecule are magnetically equivalent. These three non-equivalent signals are due to protons 1, 2, 3 of the phendione ring, respectively. The doublet of doublet peak labelled "H2 and H9" is due to the coupling of the respective hydrogen atoms at position 3 and 1.[19]

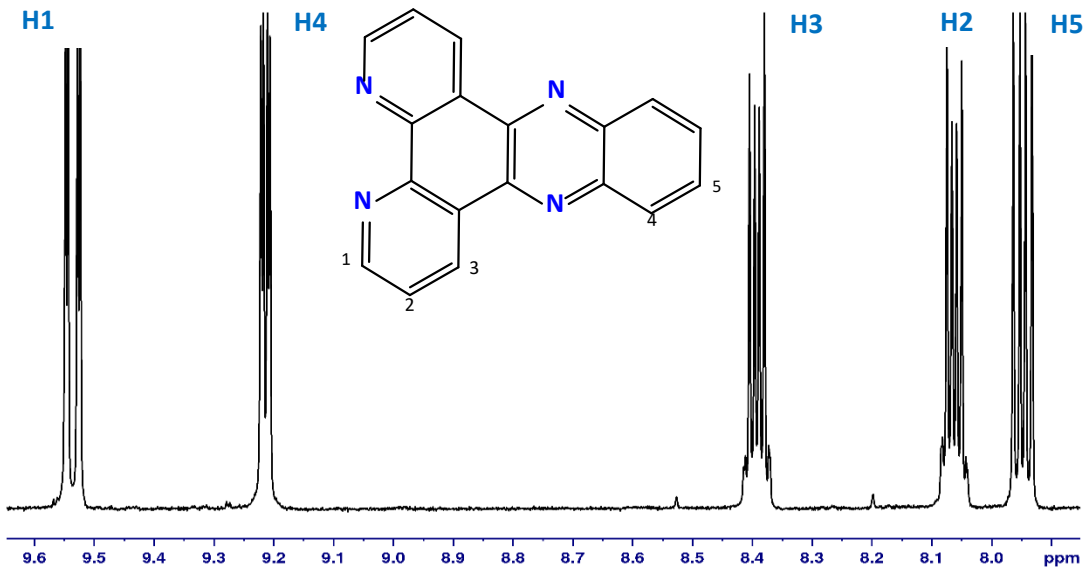

Figure 4.8: ^{1}H NMR spectrum of the aromatic region of co-ligand Dipyrido[3,2-a:2',3'-c]phenazine (dppz).

The ^{1}H NMR spectra of DPPZ (Figure 4.8) reveals one set of aromatic protons again confirming the high symmetry of the ligand. The signal appearing at 9.54 ppm represents H1 and is highly deshielded due to the electron withdrawing effect of the adjacent nitrogen atom. The H5 hydrogen atom is shielded with respect to the other hydrogen atoms its signal appear at 7.95 ppm, other aromatic hydrogen atoms signals appear at 8.02-9.25 ppm.[19]

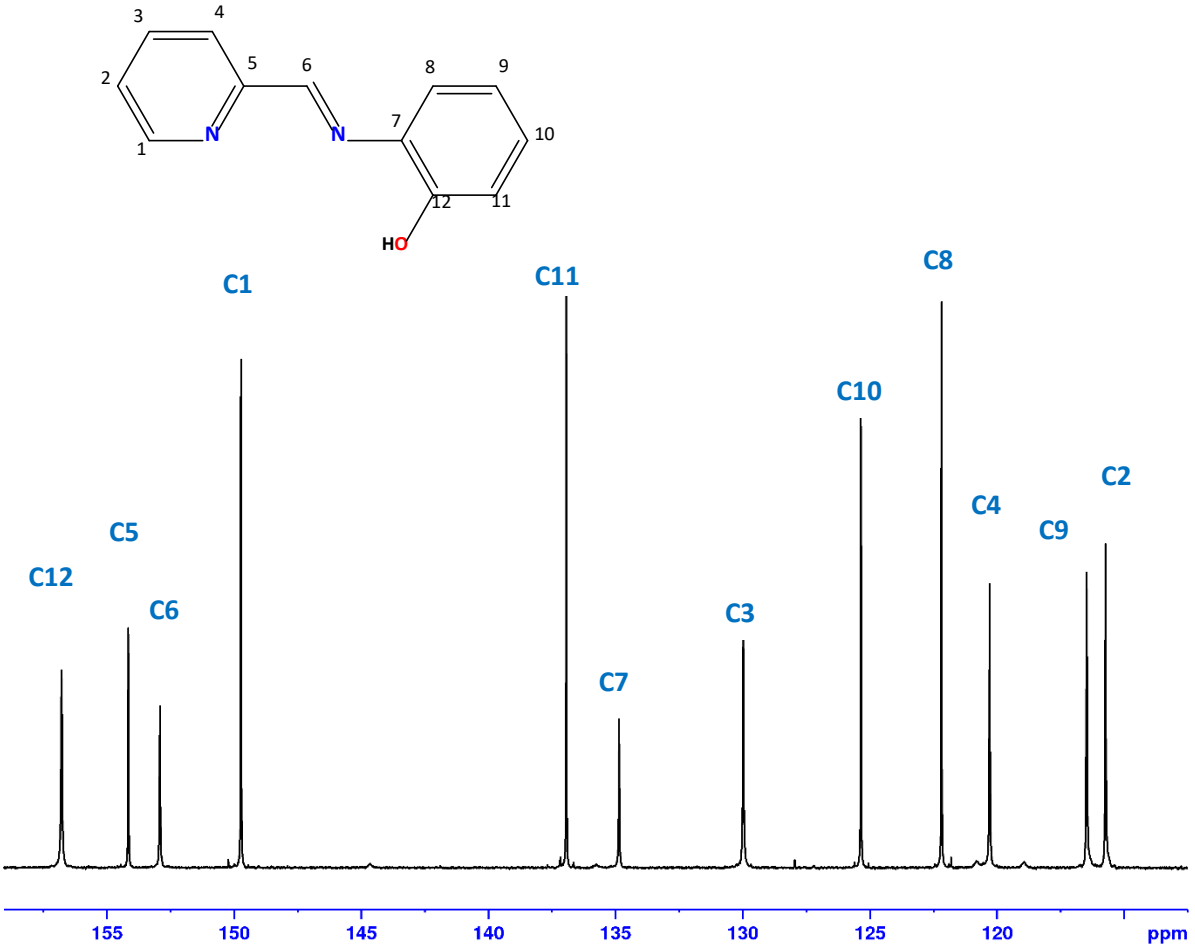

Figure 4.9: ^{13}C NMR spectra of the Schiff base ligand.

The ^{13}C NMR spectrum of HL (Figure 4.9) showed the hydroxyl carbon (C-12) at 159.32 ppm, pyridine carbon (C-5) at 154.15 ppm, imine carbon (C-6) at 152.91 ppm and aromatic carbons were found at 115.73-149.72 ppm.[20,21] The NMR spectral data of the ligands supports the conclusions drawn from the IR spectra.

4.4: UV/Visible spectroscopy

4.4.1: Introduction

The absorption of ultraviolet (UV) and visible radiation is associated with electron excitation, in both molecules and atoms, from lower to higher energy levels. Since the energy levels are quantized, only radiation with the precise amount of energy can cause electronic transitions from one energy level to another; these will be absorbed.[14,15] There are different electronic transition states possible as shown below (Figure 4.10).[15]

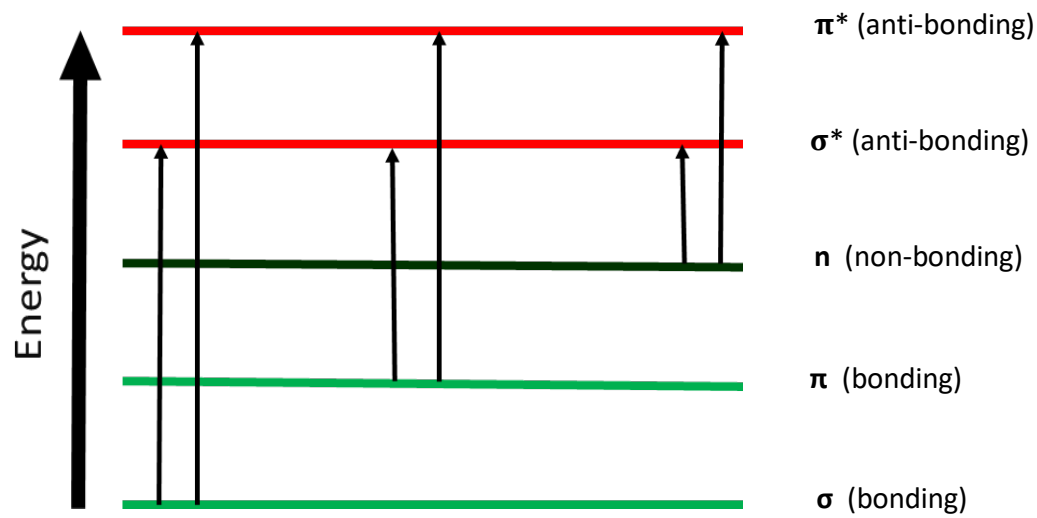

Figure 4.10: All possible electronic transitions.[15]

All molecules can undergo excitation following the absorption of light; however, for most molecules high energy radiation is required. As a result, only two transitions (Figure 4.11) take place upon the absorption of light in the UV-visible region. Therefore, the molecule should have either π bonds or atoms with non-bonding orbital in order to absorb light in this region (200-800 nm).[16]

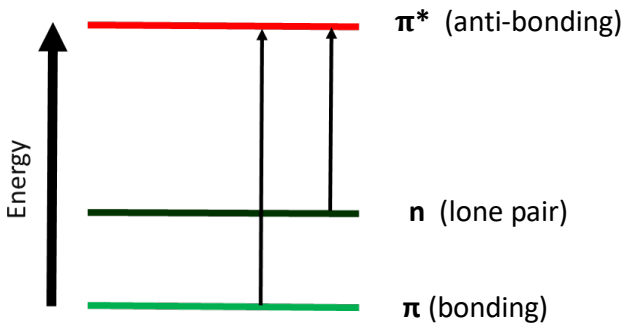

Figure 4.11: The only transitions that take place upon the absorption of light in the UV-visible region.[15,16]

The principles of UV spectroscopy are known to follow the Beer-Lambert Law. The law states that whenever monochromatic light passes through a sample with chromophores, the decreasing rate of radiation intensity along with the path length through the sample is proportional to the concentration of the solution. Hence UV/vis spectroscopy can be used to measure the concentration of a sample. Beer's Law can be expressed in an equation as follows:

A=εcL

Where, **A** is absorbance, **ε** is the extinction coefficient which is a constant for a particular substance at a particular wavelength ($dm^3\ mol^{-1}\ cm^{-1}$), **c** is the concentration of the solution (mol dm^{-3}) and **L** is the optical path length, which is the dimension of the cuvette or sample cell (cm).

In this study, UV/visible spectroscopy was used to determine the molar extinction coefficients of the absorption bands and to determine the types of electronic transitions occurring in the metal chelates and free ligands.

4.4.2 Results and Discussion

Absorption spectra of HL, $[Cu(L)(H_2O)_2]NO_3$, $[Cu(L)(phen\text{-}NH_2)]NO_3$ and $[Cu(L)(dppz)]NO_3$ were recorded in acetonitrile while $[Cu(L)(phen)]NO_3$ and $[Cu(phen\text{-}NH_2)_2(Cl)]Cl$ complexes were recorded in water. The spectral data is summarised in Table 4.3. UV/vis spectra were recorded for 3×10^{-3} M solutions in the range 200-700 nm. The UV/vis spectra of HL and all complexes are available in Appendix C. The spectrum of HL shows a band at 290 nm which is attributed to π-π* transitions of the aromatic ring (see Figure 4.12). A second band at 356 nm could be due to a lower energy n → π* electronic transition of the azomethine group in HL. The band at 283 nm underwent a bathochromic shift in the spectra of $[Cu(L)(H_2O)_2]NO_3$ to 303 nm, due to chelation with metal ions. The complex $[Cu(L)(H_2O)_2]NO_3$ also shows a less intense peak at 428 nm which is assigned as a metal-to-ligand charge transfer band (MLCT).19

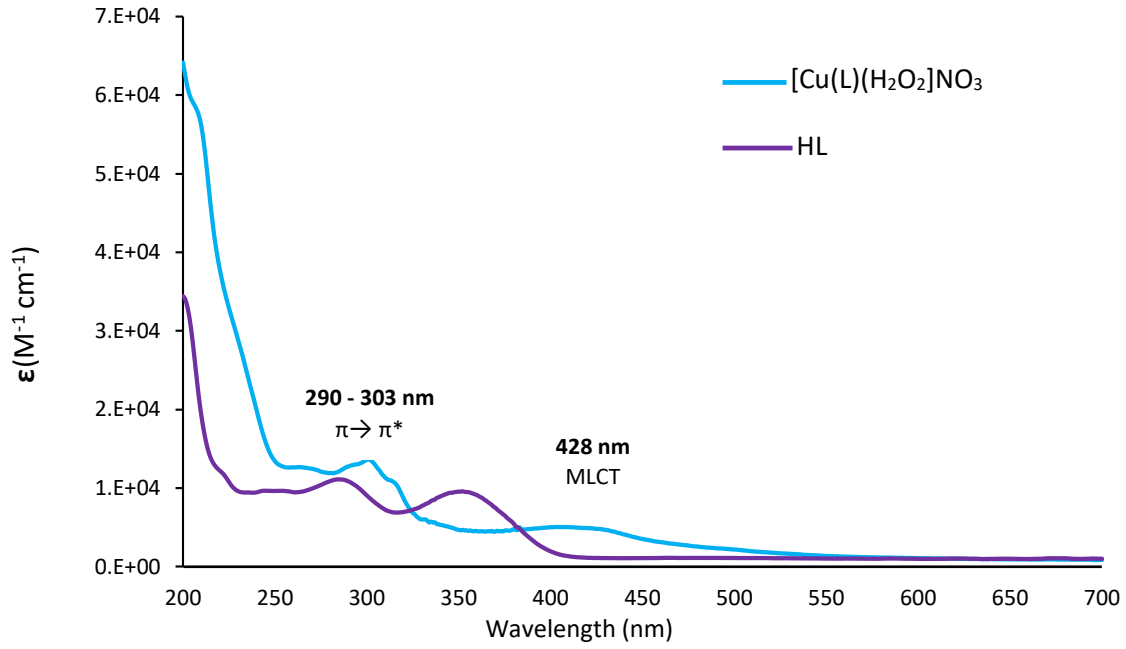

Figure 4.12: Overlay of the UV/visible spectra of $[Cu(L)(H_2O)_2]NO_3$ (Blue) and HL (purple) highlighting the bathochromic shift (290 nm to 303 nm) and the additional peak at 426 nm as a result of chelation.

The complex $[Cu(L)(phen)]NO_3$ shows a similar band to $[Cu(L)(H_2O)_2]NO_3$, an intense band at 226 nm due to a π-π* transition. However, there is an additional intense band at 265 nm as a result of another π → π* transition of the co-ligand 1,10-phenanthroline. The MLCT transition (nm) has shifted to 516 nm in the spectrum of $[Cu(L)(phen)]NO_3$, confirming the presence of both ligands coordinated to the metal centre.[17]

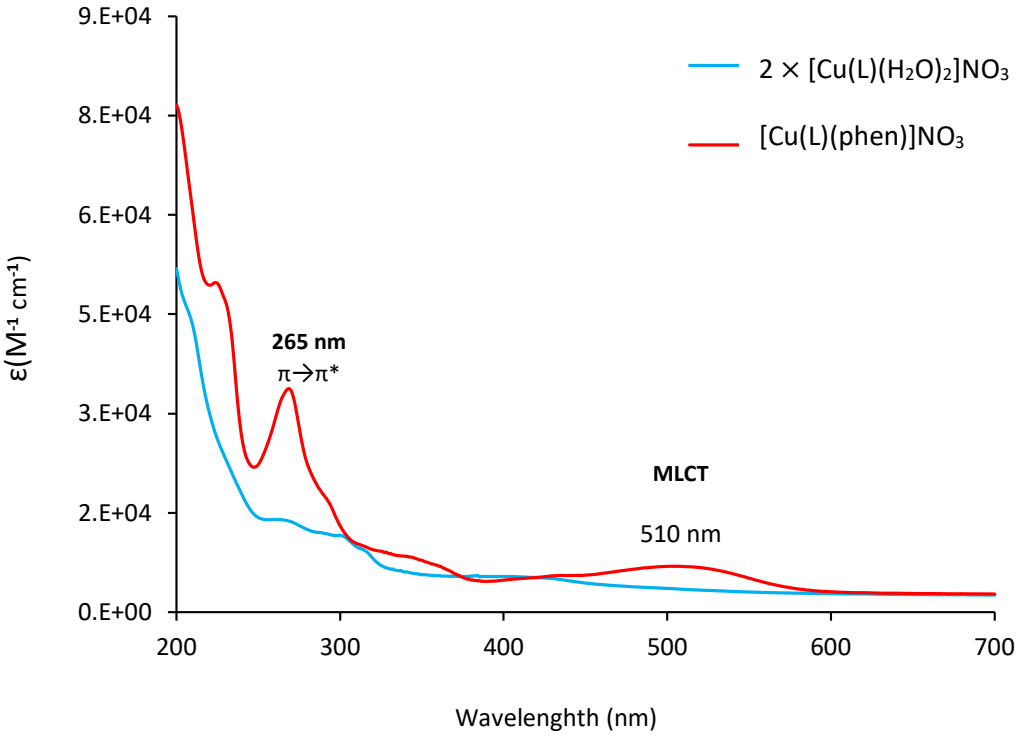

Figure 4.13: Overlay of the UV/visible spectra of $[Cu(L)(H_2O)_2]NO_3$ (blue) and $[Cu(L)(phen)]NO_3$ highlighting the bathochromic shift (290 nm to 303 nm) and the additional peak at 265 nm as a result of co-ligand chelation. The extinction coefficient of $[Cu(L)(H_2O)_2]NO_3$ was normalized by a factor of two to allow for better comparison with $[Cu(L)(phen)]NO_3$.

All the spectra of the copper complexes (Figure 4.14) show lower bands than 450 nm due to n → n* and π → π* transitions for the aromatic ring, these are of considerably lower intensity. The absorption bands at 435 nm and 455 nm are due to intraligand charge transfer transitions.[17,18]

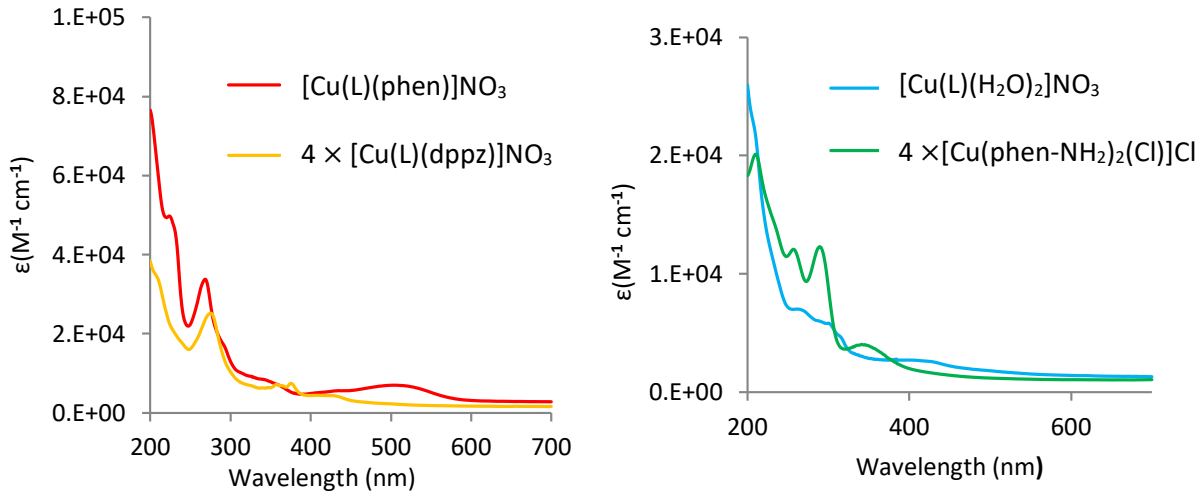

Figure 4.14: (Left) Overlay of the UV/vis spectra of [Cu(L)(phen)]NO_3 (red) and [Cu(L)(dppz)]NO_3 (orange) higlighting the more defined additional peaks at 272nm. (Right) Overlay spectra of [Cu(L)(H_2O)$_2$]NO_3 (blue) and [Cu(phen-NH_2)$_2$(Cl)]Cl. The extinction coefficient of [Cu(L)(dppz)]NO_3 and [Cu(phen-NH_2)$_2$(Cl)]Cl was normalized by a factor of four to allow for better comparison with [Cu(L)(phen)]NO_3 and [Cu(L)(H_2O)$_2$]NO_3, respectively.

The basic shape of the electronic spectrum of [Cu(L)(phen)]NO_3 and [Cu(L)(dppz)]NO_3 are similar. Both spectra contain a shoulder band at 209-216 nm and an intense band at about 280 nm, however, the spectra of complex [Cu(L)(dppz)]NO_3 (yellow) has more defined absorption peaks at 276-260 nm due to the extended conjugation and large aromatic chromophores of the dppz co-ligand. The homoleptic complex [Cu(phen-NH_2)$_2$(Cl)]Cl shows intense absorption peaks (Figure 4.14 (right)) due to increased aromaticity of the complex. Table 4.3 lists the values of λ_{max} for the complexes and their corresponding extinction coeffients.

Table 4.3: A summary of the λ_{max} and extinction coefficients for absorption bands of the copper(II) chelates.

Complex	Solvent	λ_{max}/nm (ε / M^{-1} cm^{-1})					
[Cu(L)(H_2O)$_2$]NO_3	CH_3CN	210 (14646)	266 (3235)	302 (3491)	315 (2743)	435 (1087)	
[Cu(L)(phen)]NO_3	H_2O	225 (41099)	270 (26561)	294 (13025)	345 (5417)	435 (2732)	510 (4146)
[Cu(L)(phen-NH_2)]NO_3	CH_3CN	204 (62431)	258 (22455)	289 (25799)	340 (10082)	450 (4764)	
[Cu(L)(dppz)]NO_3	CH_3CN	209 (6052	276 (5208)	359 (1260)	376 (1383)	431 (647)	
[Cu(phen-NH_2)$_2$(Cl)]Cl	H_2O	210 (3560)	258 (2167)	290 (2439)	343 (615)		

4.4.3: Solubility and analytical data of copper(II) complexes

Poorly soluble compounds carry a high risk of failure during drug discovery and development since the insufficient solubility may influence both phamacodynamic and pharmacokinetic properties of the compound. This in turn reduces target specificity, lowers bioavility in animal studies and precipitates during serial dilution in biochemical assays; cell-based assays and function assays.[8]

The solubility of the complexes were investigated in water, dimethylsulfoxide, *N,N*-dimethylformide, methanol, and other organic solvents by shaking a small amount (~2 g) of sample in a test tube with the respective solvents (3 mL).

Table 4.4: Solubility data of copper (II) chelates.

Complexes	Solvents						
	Water	DMSO	DMF	MeOH	Acetone	Toluene	DCM
$[Cu(L)(H_2O)_2]NO_3$	PS	S	S	S	S	IS	PS
$[Cu(L)(phen)]NO_3$	S	S	S	S	S	IS	S
$[Cu(L)(phen\text{-}NH_2)]NO_3$	S	S	S	S	S	IS	S
$[Cu(L)(dppz)]NO_3$	PS	S	S	S	S	IS	IS
$[Cu(phen\text{-}NH_2)_2(Cl)]Cl$	S	S	S	S	S	IS	PS

S= soluble; **PS**= partially soluble; **IS**=insoluble.

The data in Table 4.4 above show that the solubility of the complexes is good in a range of solvents. This simplifies the biological testing. The validity of biological testing is also highly reliant on the purity of the compounds. This was confirmed using elemental analysis. These composition data are summarised in Table 4.5.

Table 4.5: Elemental analysis data for the copper(II) chelates.

Chelates	Percentage C cal./found	Percentage N cal./found	Percentage C cal./found
$[Cu(L)(H_2O)_2]NO_3$	44.64/44.65	13.02/13.03	2.81/2.801
$[Cu(L)(phen)]NO_3$	57.29/57.38	13.93/13.84	3.41/3.45
$[Cu(L)(phen\text{-}NH_2)]NO_3$	55.63/55.61	16.23/16.33	3.50/3.54
$[Cu(L)(dppz)]NO_3$	59.53/59.56	16.21/16.47	3.17/3.43
$[Cu(phen\text{-}NH_2)_2(Cl)]Cl$	54.90/54.66	16.02/16.14	3.46/3.45

4.5 Electron Paramagnetic Resonance (EPR) Spectroscopy.

4.5.1 Introduction

EPR spectroscopy is a technique used to study structures and environments of species with unpaired electrons, such as free organic radicals and transition metals. Inorganic chemists are interested in the use of this technique to evaluate and understand the electronic structure of the complexes formed by paramagnetic metal ions. Generally, structural fixtures and a greater amount of information related to paramagnetic or nuclear sites in solid material can be obtained directly from measurements in single crystals. However, not all materials exist in the form of crystals, some materials are only available as powders, frozen solutions and amorphous material that can be studied by EPR spectroscopy. Although experiments on single crystals are more precise, they can be time-consuming and tedious when compared to the simplicity and speed with which data may be collected for solution and powdered samples.

The Cu(II) ion has one unpaired electron in its $3d^9$ configuration, hence it exhibits an electronic spin (S = 1/2) and nuclear spin (I = 3/2) that is expected to generate 4 hyperfine lines due to ^{63}Cu and ^{65}Cu copper isotopes. In this study, EPR spectroscopy was used to study and elucidate the geometry and the local environment around the metal centre.

4.5.2 Results and Discussion

The EPR spectra of the Cu(II) chelates in methanol were recorded at 298 K. The X-band EPR spectra for all complexes were recorded at a field of 3000 G and a frequency of 9.1 GHz. The spectrum can be described in terms of a spin-Hamiltonian containing only Zeeman and hyperfine terms of the following form (Equation 4.5.1):

$$H= [g_{//}B_zS_z + g_{\perp}(B_xS_x + B_yS_y)] + [A_{//}I_zS_z + A_{\perp}(I_yS_y + I_xS_x)] \quad .....4.5.1$$

where $g_z = g_{//}$ and $g_x = g_{\perp} = g_y$ are g-factors, β-Bohr magneton, B is the resonance magnetic field, I is the nucleus spin, S is the electron spin and $A_{//}$ and $A_{\perp}$ are the parallel and perpendicular components of the hyperfine tensor A. For the copper(II) chelates in this study, the Hamiltonian parameters are presented in Table 4.6. Due to spectral overlap; separately described parameters for ^{65}Cu and ^{63}Cu isotopes because of corresponding EPR lines covers each other.

The EPR spectrum of the $[Cu(phen\text{-}NH_2)_2(Cl)]Cl$ copper complex shows a completely different pattern from that of the $[Cu(L)(H_2O)_2]NO_3$, $[Cu(L)(phen\text{-}NH_2)]NO_3$, $[Cu(L)(dppz)]NO_3$ and $[Cu(L)(phen)]NO_3$, hence they are expected to have different geometries (see Figure 4.15). The spectral parameters for copper(II) complexes are summarised in Table 4.6. Five-coordinate copper(II) complexes may possess two geometries, i.e. square pyramidal and trigonal bipyramidal, which are characterized by a ground state dz^2 or $dx^2\text{-}y^2$ orbital, respectively.[9] The EPR spectra provide an excellent basis to distinguish between these two ground states.

The spectrum of complex $[Cu(L)(H_2O)_2]NO_3$ showed axial spectra with a well-defined $g_{\perp}$ (2.154) and $g_{//}$ (2.073) features together with hyperfine lines (Table 4.6). The value $g_{\perp} > g_{//}$ suggests a

trigonal bipyramidal geometry and rules out the possibility of a square pyramidal which would be expected to have $g_{\perp} < g_{//}$. The $g_{//}$ value is crucial for indicating the metal-ligand bond character, for ionic character $g_{//} > 2.3$ and for covalent $g_{//} < 2.3$. In the present complexes the $g_{//}$ values were less than 2.3, indicating a covalent character for the metal-ligand bond. The geometric parameter (G) which is the measure of the extent of exchange interaction can be expressed as:

$$G = \frac{g_{//}-2}{g_{\perp}-2} \qquad \text{.....4.5.2}$$

If the G value is greater than 4 the exchange interaction between the copper centres is negligible whereas if its value is less than 4, the exchange interaction is noticed. The calculated geometric parameters (G) for the complexes are less than 4 which indicates that the exchange coupling effects are operational in our complexes.

Table 4.6: Spectral parameters obtained for the five investigated copper(II) chelates at room temperature.

Complex	$g_{\perp}$	$g_{//}$	$A_{//}$ (10^{-4} cm^{-1})	G
$[Cu(L)(H_2O)_2]NO_3$	2.154	2.073	145	0.474
$[Cu(L)(phen)]NO_3$	2.143	2.071	141	0.496
$[Cu(L)(phen\text{-}NH_2)]NO_3$	2.104	2.050	130	0.481
$[Cu(L)(dppz)]NO_3$	2.144	2.069	138	0.479
$[Cu(phen\text{-}NH_2)_2(Cl)]Cl$	2.084	2.152	152	1.810

In all of the complexes analysed; no significant variations of $A_{//}$ values were observed for each of the co-ligand, which indicates that the electron density around the metal centre is not changed upon coordination of different coligands.[3] In square planar complexes, the g-tensor parameter with $g_{//} > g_{\perp} > 2.0023$, the unpaired electron lies in the d_z^2 orbital with $^2A_{1g}$ as the ground state. In the present study the observed measurements of the complex $[Cu(phen\text{-}NH_2)_2(Cl)]Cl$ is $g_{//}$ (2.152) > $g_{\perp}$ (2.084) > 2.0023 which indicates that the complex is axially symmetric and the copper sites has a $d_{x^2-y^2}$ ground state characteristic of a square planar geometry. The $g_{//}$ is less than 2.3, which indicates covalent character for the metal-ligand bond. The geometric parameter G-value for this complex is 1.810 which suggest no interaction between Cu(II) centres of the complex.[4,5]

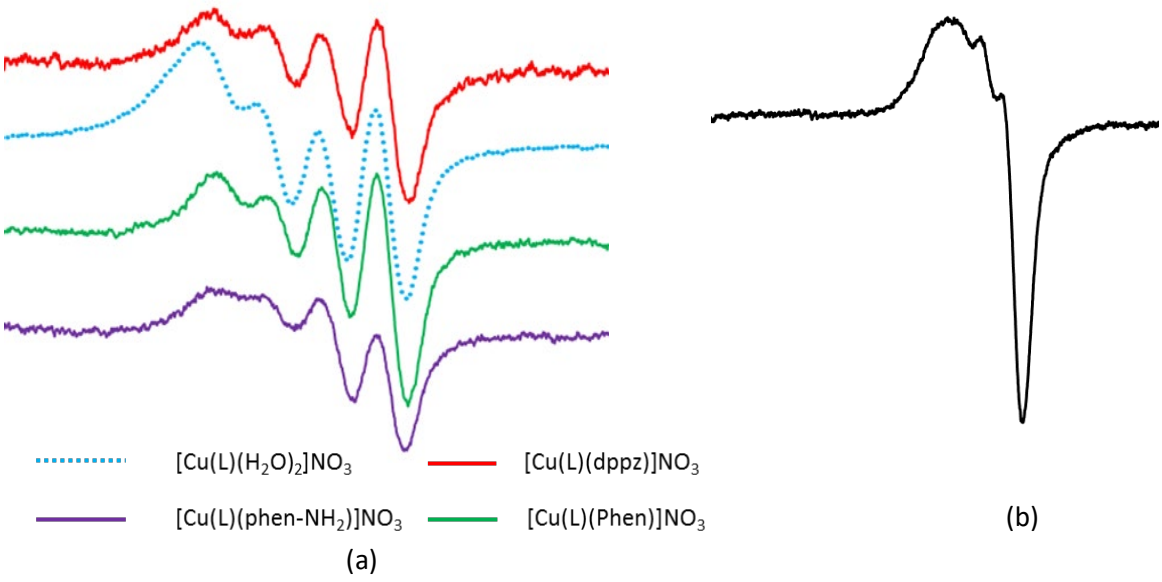

Figure 4.15: (Left) The EPR overlay spectrum of $[Cu(L)(H_2O)_2]NO_3$ (blue), $[Cu(L)(phen)]NO_3$ (green), $[Cu(L)(phen\text{-}NH_2)]NO_3$ (purple) and $Cu(L)(dppz)]NO_3$ (red). (Right) EPR spectrum of $[Cu(phen\text{-}NH_2)_2(Cl)]Cl$.

Considering the pattern of the EPR spectra of $[Cu(L)(H_2O)_2]NO_3$, $[Cu(L)(phen)]NO_3$, $[Cu(L)(phen\text{-}NH_2)]NO_3$ and $Cu(L)(dppz)]NO_3$ (Figure 4.15 a), it is quite logical to assume the same geometry for the present series of complexes, which is trigonal bipyramidal in solution at room temperature. The complex $[Cu(phen\text{-}NH_2)_2(Cl)]Cl$ (Figure 4.5 b) shows a different spectrum compared to the other complexes. This is due to the fact that it has a different coordination sphere (four N-coordinated) forming a square planar geometry.

4.6 Mass Spectrometry

4.6.1 Introduction

Mass spectrometry (MS) is an analytical technique used to identify unknown compounds, quantify known material within a sample, and to elucidate the structure of different molecules. The basic principle involves the fragmentation of a molecule into charged species, which are then accelerated, deflected, and finally focused on the detector based on their mass-to-charge (m/z) ratio.[6] The MS analyzers differentiates and resolves the ions based on their m/z ratio, this separation is driven by magnetic or electric fields.

Different types of analyzers may be used depending on the nature of the sample, this includes time of flight (TOF). They may vary in terms of mass range, resolution, dynamic range, sensitivity and performing tandem MS experiments. TOF analyzers consist of a flight tube of specific length placed in high vacuum and the m/z ratio of a molecule is deduced from its flight time through a tube.

In this study, the mass-to-charge ratio of the copper(II) complexes was investigated using TOF-MS. The TOF analyzers performance is known to be particularly good in terms of mass accuracy and resolution.[7]

4.6.2 Results and Discussion

The TOF-MS spectra of the copper(II) chelates have been studied. The TOF-MS studies of all complexes exhibit molecular ion peaks equivalent to their molecular weights along with other fragment ion peaks. Table 4.7 below shows the molecular ion peak and isotopic peaks for copper(II) complexes which are equivalent to their molecular weight. An interesting feature of the mass spectra of all the copper(II) chelates is the characteristic isotopic ratios. In the case of natural copper, there are two isotopes: ^{63}Cu and ^{65}Cu. These manifest as two adjacent peaks in the mass spectrum and are a useful tool for confirming copper ion chelation.

Table 4.7: The predicted and experimental high resolution m/z masses of copper(II) complexes.

Complex	Predicted (m/z)	Experimental (m/z) ^{63}Cu	Experimental (m/z) ^{65}Cu
$[Cu(L)(H_2O)_2]NO_3$	260.001	260.01	262.01
$[Cu(L)(phen)]NO_3$	440.069	440.11	442.11
$[Cu(L)(phen\text{-}NH_2)]NO_3$	455.080	455.13	457.12
$[Cu(L)(dppz)]NO_3$	542.091	542.07	544.07
$[Cu(phen\text{-}NH_2)_2(Cl)]Cl$	453.088	454.96	456.95

The experimental m/z values are in good agreement with the predicted values. It is interesting to note that the mass for the Schiff base copper(II) chelate shows that the water molecules are lost during the experiment. This shows they are weakly coordinated and could explain why they are easily displaced during the solid state reaction in which the co-ligand is added. The mass of the $[Cu(phen\text{-}NH_2)_2(Cl)]Cl$ complex appears as just the mass of the two bidentate ligands and copper(II) ion, suggesting a square planar configuration; this is in agreement with the EPR studies of the solution state complex.

4.7 References.

1. Lindon, J.C., Tranter, G.E. and Koppenaal, D 2016. *Encyclopedia of Spectroscopy and Spectrometry*, Academic Press, Oxford.
2. http://www.columbia.edu/~vjd1/electromag_spectrum.htm (The electromagnetic spectrum).
3. Rajarajeswari, C., Ganeshpandian, M., Palaniandavar, M., Riyasdeen, A. and Akbarsha, M.A., 2014. Mixed ligand copper (II) complexes of 1, 10-phenanthroline with tridentate phenolate/pyridyl/(benz) imidazolyl Schiff base ligands: Covalent vs non-covalent DNA

binding, DNA cleavage and cytotoxicity. *Journal of Inorganic Biochemistry*, *140*, pp.255-268.
4. Rout, K.C. and Mondal, B., 2015. Aromatic C-nitrosation by a copper (II)–nitrosyl complex. *Dalton Transactions*, *44*(4), pp.1829-1835.
5. Raj, K.M., Vivekanand, B., Nagesh, G.Y. and Mruthyunjayaswamy, B.H.M., 2014. Synthesis, spectroscopic characterization, electrochemistry and biological evaluation of some binuclear transition metal complexes of bicompartmental ONO donor ligands containing benzo [b] thiophene moiety. *Journal of Molecular Structure*, *1059*, pp.280-293.
6. Rajawat, J. and Jhingan, G., 2019. *Mass Spectroscopy*, Academic Press, New Delhi.
7. Domon, B. and Aebersold, R., 2006. Mass spectrometry and protein analysis. *Science*, *312*(5771), pp.212-217.
8. Savjani, K.T., Gajjar, A.K. and Savjani, J.K., 2012. Drug solubility: importance and enhancement techniques. *ISRN Pharmaceutics, 2012*, pp.1-8.
9. Uçar, İ., Bozkurt, E., Kazak, C. and Bulut, A., 2009. Structural characterization and EPR spectral studies on mononuclear copper (II) complex of saccharin with ethylnicotinate. *Spectrochimica Acta Part A: Molecular and Biomolecular Spectroscopy*, *72*(1), pp.11-16.
10. Theophanides, T 2012. *Introduction to infrared spectroscopy: Materials, Science, Engineering and Technology*, InTech, Rijeka.
11. https://www.chromacademy.com/lms/sco533/01-infrared-spectroscopy-introduction.html?fChannel=14&fCourse=77&fSco=533&fPath=sco533/01-infrared-spectroscopy-introduction.html (Infrared region).
12. Burns, B.L., 2014. 'Sparse Image Reconstruction and Artifact Correction of Multi-Dimensional Spectroscopic Imaging Data', PhD thesis, University of Califonia, Los Angeles.
13. https://pharmaxchange.info/2011/12/ultraviolet-visible-uv-vis-spectroscopy-principle/ (UV-vis spectroscopy).
14. Bruice, P. Y 2007. *Organic Chemistry*, 5th edn, Pearson International Edition, Lincon.
15. Bruice, P.Y 2016. *Essential Organic Chemistry*, 8th edn, Pearson Education Limited, Harlow.
16. Abd El-Halim, H.F., Mohamed, G.G., Anwar, N.A., 2017.Antimicrobial and anticancer activities of Schiff base ligand andits transition metal mixed ligand complexes with heterocyclic base*. Applied Organometallic Chemistry,32*(1), pp.4-9.
17. Golchoubian, H. and Fazilati, H., 2012. Synthesis and Spectral Studies on Heteroleptic Chelated Copper (II) Complexes of Diamine and Acetylacetonate. *Iranica Journal of Energy & Environment*, *3*(3), pp.264-269.
18. Molphy, Z., Prisecaru, A., Slator, C., Barron, N., McCann, M., Colleran, J., Chandran, D., Gathergood, N. and Kellett, A., 2014. Copper phenanthrene oxidative chemical nucleases. *Inorganic Chemistry*, *53*(10), pp.5392-5404.
19. Bhaumik, P.K., Jana, S. and Chattopadhyay, S., 2012. Synthesis and characterization of square planar and square pyramidal copper (II) compounds with tridentate Schiff bases: Formation of a molecular zipper via H-bonding interaction. *Inorganica Chimica Acta*, *390*, pp.167-177.
20. Chatturgoon, T 2016, 'Synthesis, Characterisation and Biological Activity of a Series of Single-Ligand and Heteroleptic Copper(II) Schiff Base Complexes: Potential Chemotherapeutic Agents'. Master's Thesis, University of KwaZulu-Natal, Pietermaritzburg.

CHAPTER 5: X-RAY CRYSTALLOGRAPHY

5.1 Introduction

The main objective of the single crystal X-ray diffraction experiments was to determine the solid state structures of the copper(II) chelates synthesized in this study. These experiments would provide information on the solid state interactions of the chelates and would therefore give an insight on whether or not these chelates would effectively interact with DNA. Similar structures to those synthesised in this work were found by a search of the Cambridge Structural Database[1] (CSD) and are reviewed as an introduction to this chapter.

5.1.1 Previously Reported Copper Chelates

In this study a total of six heteroleptic copper(II) chelates were synthesized. From the synthesized complexes, three crystal structures were obtained. A search of the CSD showed many metal chelates that are structurally comparable to those of this study. Table 5.1 summarizes the CSD data of the relevant metal chelates. The crystal structures are displayed in Figure 5.1.

Table 5.1: Previously reported X-ray crystal structure of related metal chelates.

CSD Ref. Code	Compound name	Lit. References
QAZBUQ	Diaqua-(2-(((pyridin-2-yl)methylene)amino)phenolato)-copper(ii) nitrate	2
BEYMAU	Chloro-bis(1,10-phenanthroline)-copper(ii) tetrafluoroborate	3
PUWQII	Diaqua-(2-methoxy-6-(((quinolin-8-yl)imino)methyl)phenolato)-copper(ii) perchlorate	4

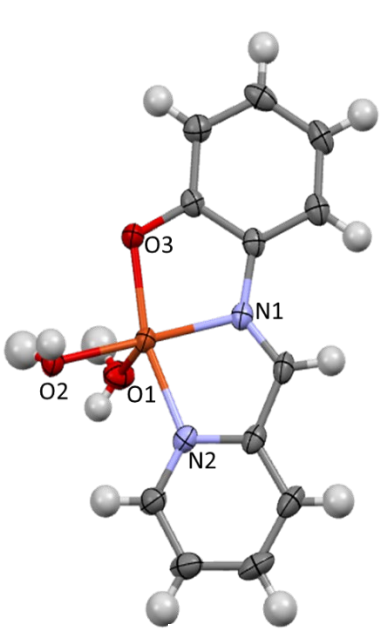

(a)

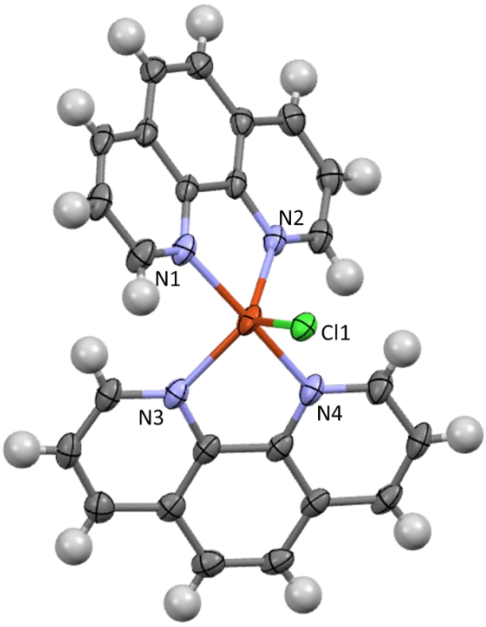

(b)

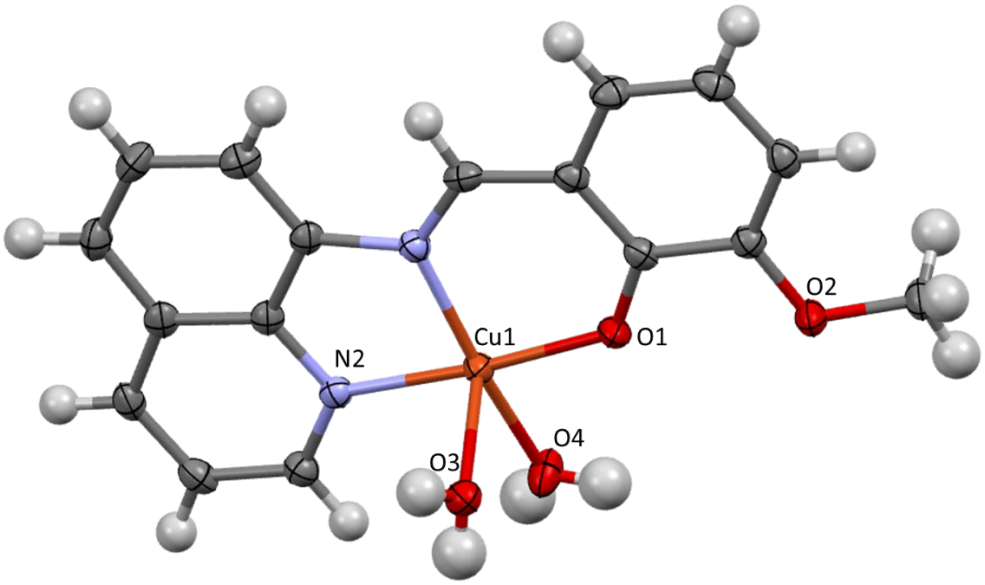

(c)

Figure 5.1: X-ray crystal structures of (a) QAZBUQ, (b) BEYMAU and (c) PUWQII. Counter anions have been omitted for clarity.

The chelate QAZBUQ is the same as the single-ligand complex $[Cu(L)(H_2O)_2]NO_3$, however the data collected in the present study is of significantly higher quality being recorded at 100 K and having a higher C-C bond precision. The ligand has coordinated to copper(II) through two neutral nitrogen atoms (imine N and pyridine N) and one phenolate oxygen atom forming the five-membered chelate rings. The chelate bite angles for the five-membered rings resulting from chelation of the Schiff base ligand are in the range of 80.85-83.73°. The two remaining bonding sites are occupied by two water molecules resulting in a square pyramidal geometry. The chelate BEYMAU is penta-coordinated by one chlorine ligand and four N atoms of two 1,10-phenantroline ligands. The geometry of the chelate may be described as a near regular trigonal bipyramidal, in which N1 and N4 atoms are axially coordinated while the trigonal plane, is comprised of the N2, N3 and Cl1 atoms. In compound PUWQII, the copper(II) center is also five-coordinate, with a tridentate ligand coordinated to the Cu(II) metal ion through its NNO donor atoms in meridional fashion. The other two coordination sites are occupied by two water molecules which are *cis*-coordinated to the copper(II) ion, resulting in a square-pyramidal geometry. The average bond angles and bond lengths of these complexes are summarised in Table 5.2

Table 5.2: Avarage bond lengths and bond angles for previously reported metal chelates.

	QAZBUQ	PUWQII	BEYMAU
Bond Length (Å)			
N1-Cu	1.95(3)	1.95(2)	1.99
N2-Cu	2.02(4)	1.99(2)	2.10
C=N$_{imine}$	1.28(7)	1.31(3)	
O1-Cu	2.26(5)	1.90(1)	
O2-Cu	1.96(3)		

O3-Cu	1.95(4)	2.36(2)	
O4-Cu		1.98(2)	
Cl1-Cu			2.35
N4-Cu			2.00
N3-Cu			2.10
Bond angles (°)			
N1-Cu-N2	80.85(1)	83.35(7)	81.29
N1-Cu-O1	103.15(2)	93.71(7)	
N1-Cu-Cl1			92.08
N3-Cu-Cl1			119.52
O4-Cu-O3		87.75(7)	
01-Cu-O3	96.39(2)		

The metal complex QAZBUQ and PUWQII share numerous similarities; same metal centre and similar ligand (with same donor atoms) and forming similar geometry, as a result they possess similar bond lengths and angles for comparable bonds. The $C=N_{imine}$ bonds of these complexes are comparable, with QAZBUQ having slightly longer bond, both Cu-N1 and Cu-N2 bonds are approximately equal in length. The bond angles for N1-Cu-N2 are within a reasonable range for both complexes. However, the bond angle for N1-Cu-O1 of PUWQII is larger by 10° compared to the corresponding N1-Cu-O1 angle of QAZBUQ. This can be attributed to the complex PUWQII forming a six-membered chelation ring as opposed to the five membered rings formed by QAZBUQ.

The mean planes of these complexes were calculated using all non-hydrogen atoms and are represented in Figure 5.2. The dihedral angles subtended by the ligands were also measured. This illustrates the planarity of the ligands within the complex, which is a useful indicator to determine whether these copper(II) chelates are likely to be affective DNA binding agents. In the study of DNA binding, the angle between two planes of ligands is crucial since only one ligand interacts directly with the DNA helix. The closer the dihedral angle is to 90^{o} the better the intercalation properties.[2] The angles are summarized in Table 5.3.

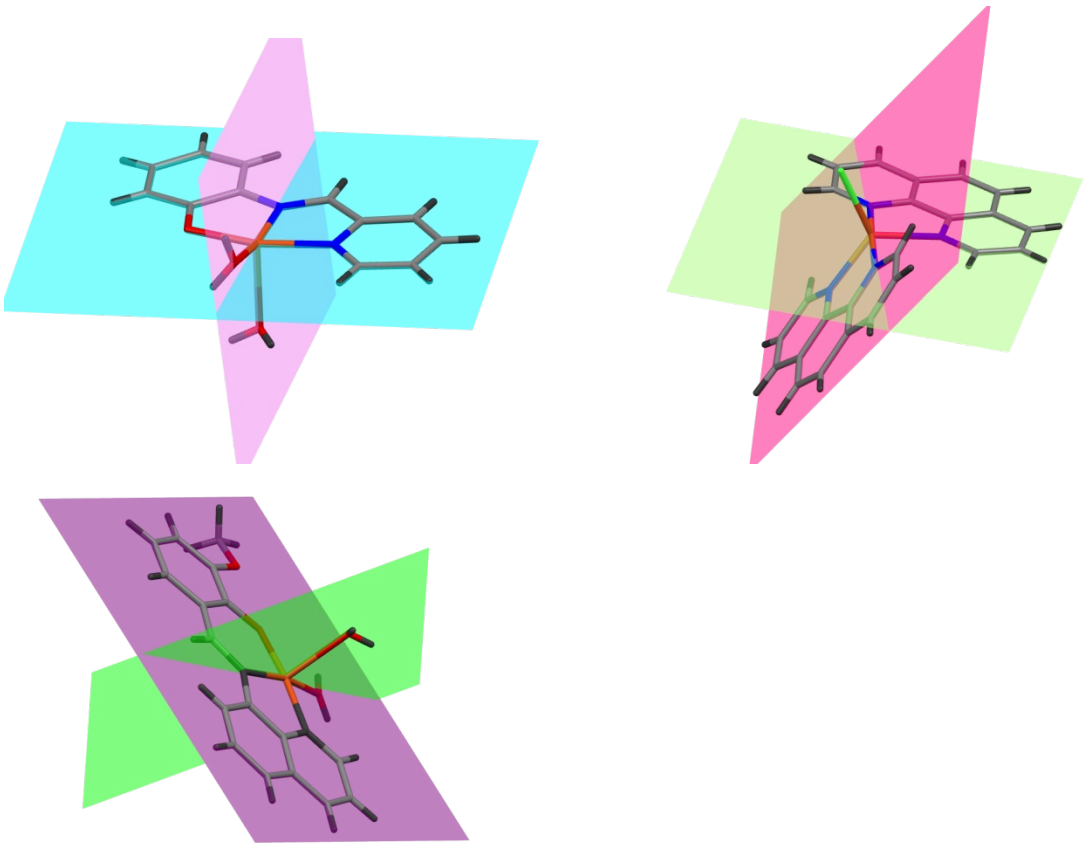

Figure 5.2: The two planes illustrating the relative positions of the coordinated ligands for the copper(II) complexes: (a) QAZBUQ, (b) BEYMAU and (c) PUWQII.

Table 5.3: The measured dihedral angles between the two planes of the ligands of the reported chelates.

CSD Ref. Code	Dihedral angle between planes (°)
QAZBUQ	86.98
BEYMAU	59.45
PUWQII	89.79

The dihedral angle of QAZBUQ and PUWQII show the tridentate ligand are nominally perpendicular to the plane of the water ligands. The angle for BEYMAU shows that the phenanthroline ligands are out-of-plane. The main factor is likely to be steric hindrance between the two phenanthroline ligands. The chelates will adapt an orientation which minimises any non-bonded repulsion between these two ligands.

5.2 Experimental

The X-ray data were recorded on a Bruker Apex Duo diffractometer equipped with an Oxford Instruments Cryojet operating at 100(2) K and an Incoatec microsource operating at 30 W power. For all structures the data were collected with Mo *K*α (λ = 0.71073 Å) radiation at a crystal-to-detector distance of 50 mm. The data collections were performed using omega and phi scans with exposures taken at 30 W X-ray power and 0.50° frame widths using APEX2.[3]

The data were reduced with the program SAINT using outlier rejection, scan speed scaling, as well as standard Lorentz and polarisation correction factors.[5] A SADABS semi-empirical multiscan absorption correction was applied to the data.[5] Direct methods, SHELX and WINGX were used to solve all structures. All non-hydrogen atoms were located in the difference density map and refined anisotropically with SHELX.[6] The hydrogen atoms of all NH and OH groups were located in the density map and allowed to refine isotropically. All diagrams were rendered using Mercury 3.3.[6,7] Table 5.4 provides summarized crystallographic data for the copper(II) chelates studied by single crystal X-ray crystallography in this work.

Table 5.4: Summary of crystallographic data and structure refinement details for the copper(II) chelates.

	$[Cu(L)(H_2O)_2]NO_3$	**$[Cu(L1)(H_2O)_2]NO_3$**	**$[Cu(phen\text{-}NH_2)_2(Cl)]Cl$**
Formular	$C_{12}H_{13}CuN_3O_6$	$C_{16}H_{15}CuN_3O_6$	$C_{24}H_{18}Cl_1Cu_1N_6$
Space group	$P\bar{1}$	$P\bar{1}$	$P\bar{1}$
Temperature (K)	100	100	100
a/Å	7.6666(4)	7.3221(2)	13.582(6)
b/ Å	8.8626(5)	13.3193(5)	14.014(6)
c/ Å	11.0903(6)	16.8536(6)	14.481(6)
α/ °	102.003(3)	105.054(2)	78.02(2)
β/ °	103.996(3)	93.318(2)	80.00(2)
γ / °	103.547(3)	100.653(2)	64.315(18)
Z	2	2	4
Bond precision: C-C(Å) and Wavelength	0.0045, 0.71073	0.0030, 0.71073	0.0193, 0.71073
Theta (max)	26.033	29.913	26.375
Radiation type	M_oK_α		
V(Å^3)	682.288	1550.15	2418.9
F(000)	366.0	816.0	1043.0
μ (mm-1)	1.636	1.448	1.120
Diffractometer	Bruker APEX-II CCD		
Absorption correction	Multi-scan SADABS, Bruker 2012		
R(reflection), *S*	0.0328 (2401), 1.104	0.0351 (7030), 1.025	0.1291 (4862), 1.1279
wR_2(reflections)	0.0891 (2642)	0.0885 (8757)	0.3970 (9198)
No. of reflections	2692	8964	9898
No. of parameters	201	478	613
No. of restraints	0	0	0
h, k, l (max)	9, 10, 13	10, 18, 23	16, 17, 18
Density (g cm^{-3})	1.747	1.713	1.411

5.3 Results and Discussion

5.3.1 X-ray crystallography of $[Cu(L)(H_2O)_2]NO_3$

The chelate $[Cu(L)(H_2O)_2]NO_3$ crystallized in the space $P\bar{1}$ with one complex molecule and one nitrate counter ion in the asymmetric unit (Z=2) . A thermal displacement plot of the discrete mononuclear unit of this chelate with key non-hydrogen atoms labelled and unit cell are shown in Figure 5.3 (a) and (b). The complex shows the Schiff base ligand coordinates to the copper(II) ion *via* the imine N, pyridine N and phenolate O atom forming two five-membered rings. Two aqua ligands coordinate to the copper(II) ion completing a square pyramidal geometry. This was confirmed by a geometry index τ= 0.0332 (τ = (β-α)/60°), where α and β are the bond angles subtended by the *trans* donor atoms in the basal plane and are the greatest valence angle of the coordination centre. The τ value indicates how closely the coordination geometry approaches ideality, in this case square pyramidal.[4,8] The basal plane of this structure is completed by two nitrogen and one oxygen donor atoms N1, N2 and O1 of the tridentate ligand and the O5 oxygen atom of one of the coordinated aqua ligands, the O6 of the second water molecule occupies the apical position. The Schiff base ligand forms a five-membered ring with the metal centre and the chelate bite angles are in the range 80.92- 83.85°.

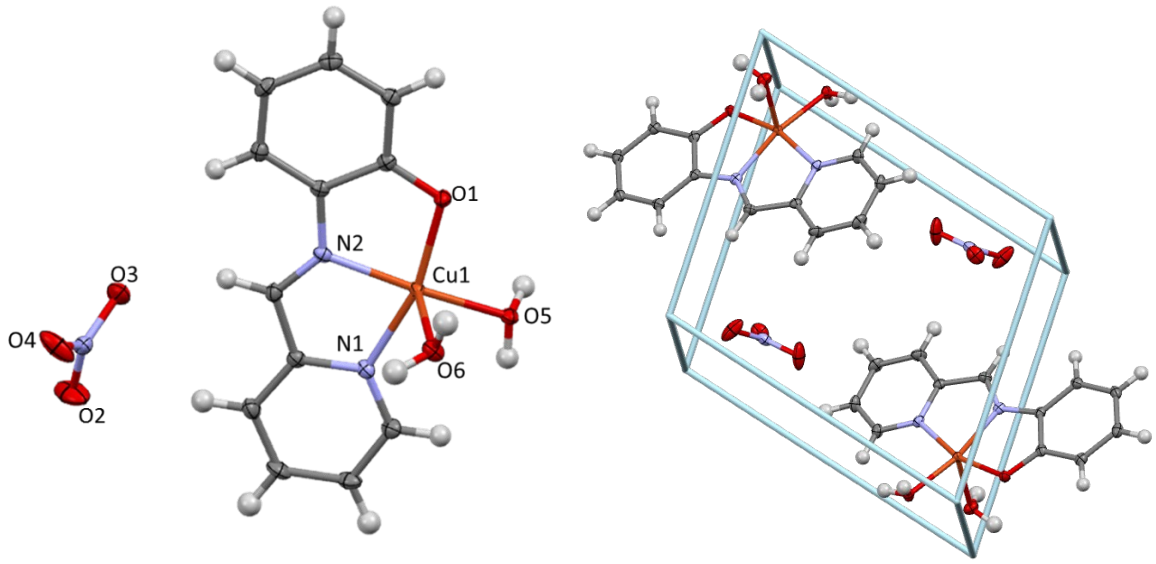

Figure 5.3: (a) The asymmetric unit of $[Cu(L)(H_2O)_2]NO_3$ with thermal ellipsoids drawn at the 50% probability level. (b) Packing within the unit cell. Hydrogen and carbon atoms are not numbered for clarity. Hydrogen atoms are shown as spheres of arbitrary radius.

The crystal structure of $[Cu(L)(H_2O)_2]NO_3$ has been crystallised by Bhaumik *et al.* and the bond lengths and angles are comparable with those reported.[4] The comparison of selected bond lengths and angles for $[Cu(L)(H_2O)_2]NO_3$ and QAZBUQ are summarised in Table 5.5.

Table 5.5: The summary of the bond lengths and bond angles between $[Cu(L)(H_2O)_2]NO_3$ and the previously reported QAZBUQ.

	$[Cu(L)(H_2O)_2]NO_3$	**QAZBUQ**
	Bond Length (Å)	
Cu-N_{imine}	1.945(2)	1.95(3)

Cu-$N_{pyridine}$	2.012(3)	2.02(4)
C=N_{imine}	1.284(4)	1.28(7)
Cu-$O_{phenolate}$	1.957(2)	1.95(4)
Cu-O_{H20}	2.246(3)	2.26(5)
Cu-O_{H20}	1.962(2)	1.96(3)
	Bond angles	
$N_{pyridine}$-Cu-N_{imine}	80.92(1)	80.85(1)
$O_{phenolate}$-Cu-N_{imine}	83.85(9)	83.73(1)
O_{H20}-Cu-O_{H20}	90.20(9)	91.30(2)

The compound $[Cu(L)(H_2O)_2]NO_3$ crystallised in the triclinic space group $P\bar{1}$ with a single molecule in the unit cell. The nitrate ion is confirmed to be outside the coordination sphere. The nitrate ions are hydrogen bonded to the coordinated aqua ligands, this leads to a hydrogen-bonded dimer structure comprising two chelate molecules and two nitrate molecules. The dimeric structure is shown below in Figure 5.4. The nitrate-bridged dimeric structure is an inversion dimer, with only two unique hydrogen bonds. The hydrogen bond parameters are summarised in Table 5.6.

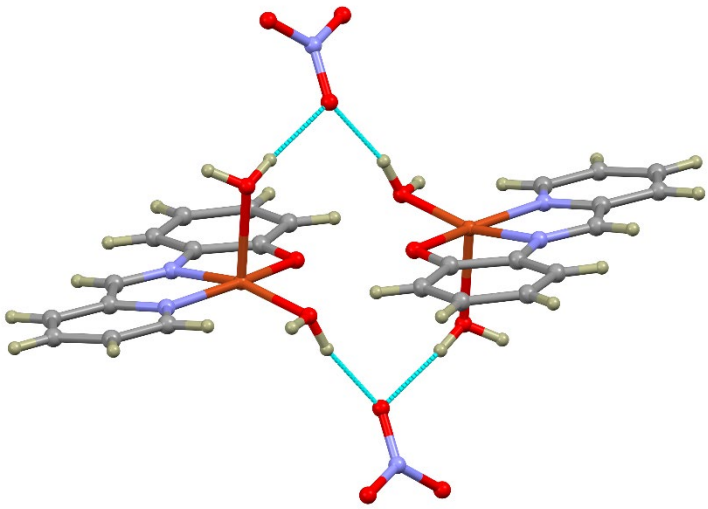

Figure 5.4: Dimeric structure of $[Cu(L)(H_2O)_2]NO_3$ showing the bridging nitrate ions. A single nitrate oxygen atom acts as a hydrogen bond acceptor for two hydrogen bonds to adjacent chelate molecules.

Table 5.6: Hydrogen bond parameters for $[Cu(L)(H_2O)_2]NO_3$.

Bond	D–H	H···A	D···A	D–H···A
O6–H6B···O4 $^{x, y, -1+z}$	0.871	1.875	2.735(4)	169.1
O5–H5A···O4 $^{1-x, 2-y, 1-z}$	0.871	1.800	2.656(3)	166.8

The data in Table 5.6 above show that the hydrogen bond lengths are significantly shorter than the sum of the van der Waals radii, on average 0.88 Å shorter. This short bond length coupled with the near ideal (180°) bond angles suggests that these intermolecular interactions are likely to be moderately strong. The dimeric structures are linked by weak π··π interactions and weak C–H···O interactions to form an extended three-dimensional supramolecular structure. The interplanar spacing between 16 atom mean planes comprising the aromatic Schiff base ligand and copper(II) ion measures 3.259 Å, this is shorter than the interplanar spacing in graphite which measure 3.35 Å. This suggests that these are genuine stabilising interactions. The π···π interactions are indicted below in Figure 5.5.

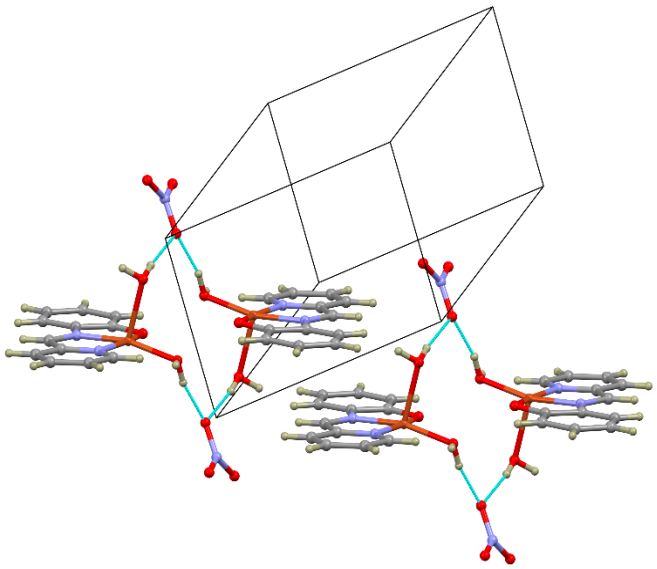

Figure 5.5: π-stacking between two adjacent aromatic ligands which link the dimeric structures.

5.3.2 X-ray crystallography of $[Cu(L1)(H_2O)_2]NO_3$

The complex $[Cu(L1)(H_2O)_2]NO_3$ was synthesized, however co-ligands were not successfully coordinated to form heteroleptic complexes and hence no further development or testing was completed. The X-ray structure for this precursor compound was, however, elucidated and is discussed here. The single crystal X-ray diffraction analysis showed that the copper(II) complex $[Cu(L1)(H_2O)_2]NO_3$ belongs to the space group $P\bar{1}$ and triclinic crystal system. The crystal structure of this complex with labels is shown in Figure 5.6. The unit cell of the complex $[Cu(L1)(H_2O)_2]NO_3$ contains two different molecules, both contain the copper(II) centre which is penta-coordinated by one deprotonated L1 ligand and one water molecule. The remaining coordination site is occupied by one nitrate anion for the first complex and one aqua ligand in the second complex of the asymmetric unit. For clarity, our discussion focused on the first complex, with the nitrate anion illustrated in Figure 5.6 (b). The coordination geometry of this complex is square pyramidal in which the O1, N1 and N2 atoms of the tridentate HL1 ligand and the O2 atom of the aqua ligand form the planar quadrilateral of the tetragonal pyramid, and one oxygen atom of the nitrate anion occupies the axial position.

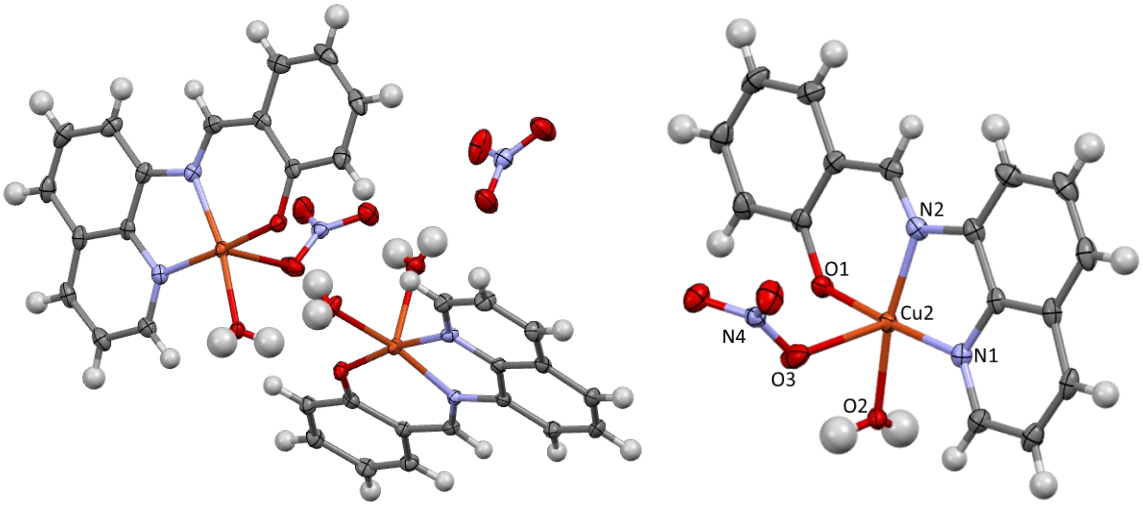

(a) (b)

Figure 5.6: (a) The asymmetric unit of $[Cu(L1)(H_2O)_2]NO_3$ with displacement ellipsoids shown at the 50% probability level. (b) The partially labelled solid state structure showing one of two molecules in the unit cell.

The Cu-N and Cu-O bond lengths are in the range 1.956-1.980 and 1.897-2.383 Å, respectively, which fall within the normal range.[10] The bond lengths of the $C=N_{imine}$ measures 1.300 Å and again compares favourably to previously related structures within the range of 1.274-1.366 Å.[10] The length is slightly longer than a formal C=N double bond (*ca.* 1.280 Å) this indicates some delocalisation of the electrons over the phenyl and quinolyl rings and subsequent lowering of the bond order. The selected bond lengths and angles are summarized in Table 5.7. The bond angles deviate from the ideal values of square pyramidal which should be 90° and 180°, the largest deviation occurs at O3-Cu2-O2 and O3-Cu2-N2 which measure 83.67° and 104.90°, respectively. The O1-Cu2-O3 bond angle (90.91°) is closest to the ideal 90°. This is likely because the monodentate aqua ligand has more degrees of freedom and hence a bond angle closer to ideality is possible. Also, the coordinated water molecule is displaced from the square plane N1-N2-Cu2-O1-O2 by 0.234 Å.

The bond angles, N2-Cu2-N1 and N2-Cu2-O1, measuring 83.41° and 94.31°, respectively are comparable to related structures.[7] The difference between the two angles is due to the differing bite of the ligand chelating atoms; the six-membered ring C1-O1-Cu2-N2-C7-C6 having a larger angle than the five-membered C16-N1-Cu2-N2-C8 chelate rings. The summary of selected bond lengths and bond angles describing the coordination sphere is shown in Table 5.7.

Table 5.7: Summary of selected bond lengths (Å) and bond angles (°) for $[Cu(L1)(H_2O)_2]NO_3$.

	Bond Length
Cu2-O1	1.897(1)
Cu2-O2	1.962(2)
Cu2-O3	2.383(2)
Cu2-N1	1.980(2)
Cu2-N2	1.956(2)
C7-N2	1.300(3)

	Bond angle
O1-Cu2-O3	90.91(6)
O3-Cu2-N2	104.91(6)
O3-Cu2-N1	92.37(6)
O3-Cu2-O2	83.67(6)
O1-Cu2-O2	91.12(6)
O2-Cu2-N1	90.72(7)
N1-Cu2-N2	83.41(7)
N2-Cu2-O1	94.31(7)

The molecules within the unit cell are consolidated by intermolecular hydrogen bonding, forming a supramolecular structure. The hydrogens H(O2) and H(O9) from coordinated aqua ligands are involved in hydrogen bonding with symmetry-related phenoxo oxygen atoms O8 and O1, respectively. Similarly, the nitrate oxygen atoms O12 and O4 are involved in hydrogen bonding interactions with the symmetry-related hydrogen atoms H14 and H15, respectively. There is also an existing hydrogen bonding interaction between the two complexes as a result of the coordinated aqua ligands. The details of the hydrogen bonding are summarized in Table 5.8.

Table 5.8: Hydrogen bond distances (Å) of $[Cu(L1)(H_2O)_2]NO_3$.

	Bond distance
O-H···O1	2.628(2)
O-H···N4	2.905(2)
O-H···O2	3.022(2)

In the three-dimensional supramolecular structure of $[Cu(L1)(H_2O)_2]NO_3$, the polymeric chains of the complex self-assemble by not only hydrogen bonds, but also by means of the π-π stacking of the pi-system of the tridentate Schiff base. The combination of both the hydrogen bonding interactions and the π-π interactions form a supramolecular structure as shown in Figure 5.7.

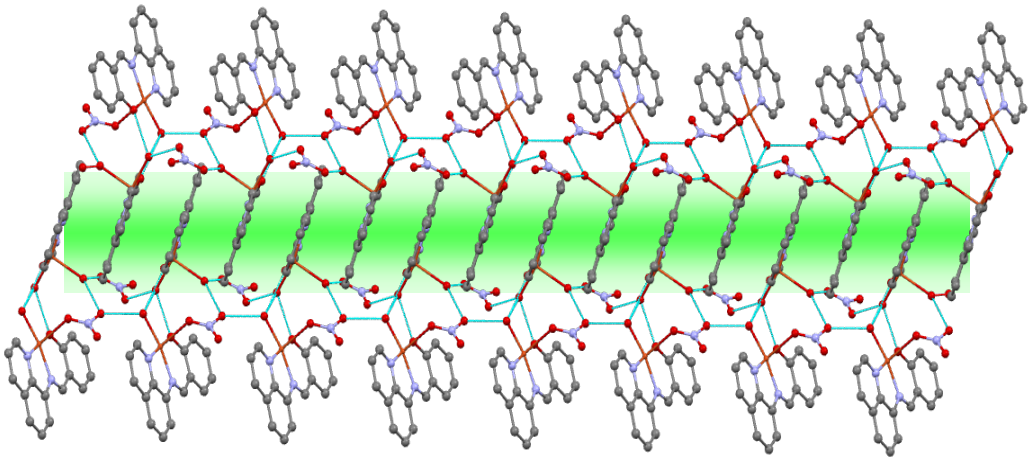

Figure 5.7: Repeating units of the polymeric chain of the complex showing the hydrogen bonding and (highlighted light green region) extended π-π system of the tridentate ligand.

5.3.3 Low resolution structure of $[Cu(phen\text{-}NH_2)_2(Cl)]Cl$

A low resolution X-ray structure of the compound [Cu(Phen-NH_2)$_2$(Cl)]Cl was elucidated. The low resolution data does not allow for precise bond measurements, but does provide some important insights into the structure of this complex. The structure shows that the copper(II) ion is coordinated by two bidentate ligands and a monodentate chloride ligand (Figure 5.8). It is interesting to note that the asymmetric unit contains two independent molecules, each with the same ligand set, but a different coordination geometry. The compound crystallises in the triclinic space group $P\bar{1}$ with $Z = 4$.

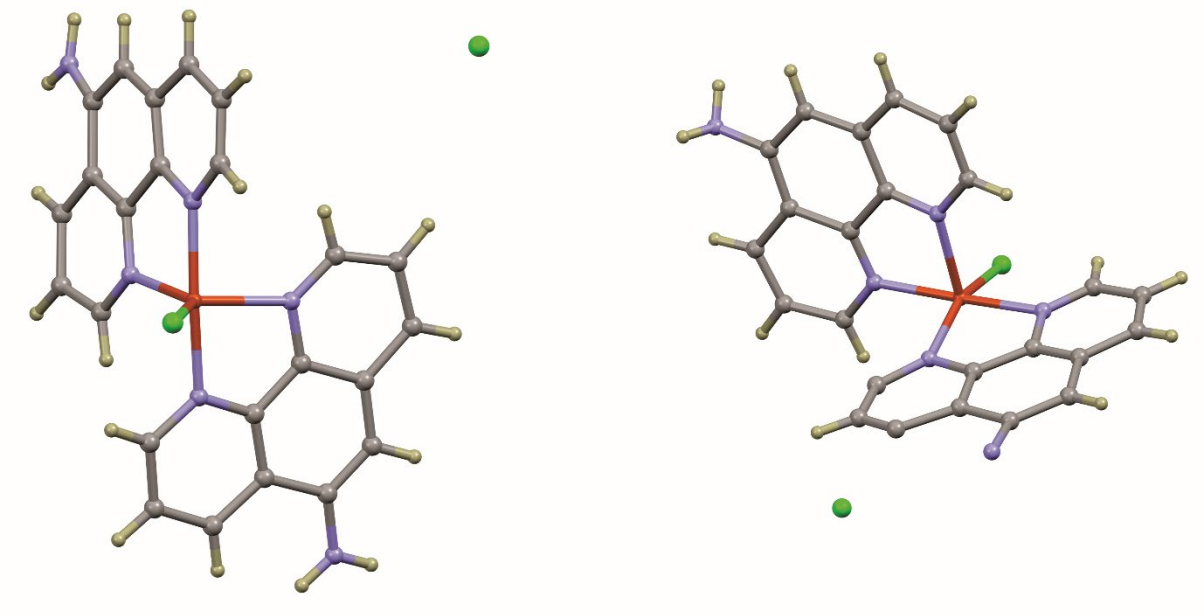

Figure 5.8: The two molecules from the asymmetric unit of [Cu(Phen-NH_2)$_2$(Cl)]Cl showing the different coordination geometries, despite the same atom donor sets. (Left) The trigonal bipyramidal metal centre. (Right) The square pyramidal metal centre. The disordered atoms have been omitted for clarity.

The structure shows a positional disorder with respect to the amine group of the phen-NH_2 ligand. The ratio of the two positions is 75:25. The energy barrier between the two geometries is generally low and structures with both coordination geometries in the same asymmetric unit are known in the literature.[9]

With the abundance of both hydrogen bond donors and acceptor groups in the metal chelates, the compound forms numerous hydrogen bonds in the solid state. The hydrogen bonds are mostly between the NH_2 groups (hydrogen bond donor) and the chloride ligands and counter anions. This extensive hydrogen bonding array leads to a three-dimensional supramolecular structure as shown in Figure 5.9 below. The three-dimensional arrangement leads to solvent accessible voids in the lattice which are occupied by numerous disordered solvent molecules. The voids comprise a total volume of 260.5 Å^3, i.e. 10.8% of the unit cell volume (these were calculated using a 1.2 Å probe radius). It is possible that these large voids and associated disordered solvent are responsible for the weak diffraction of the crystal samples.

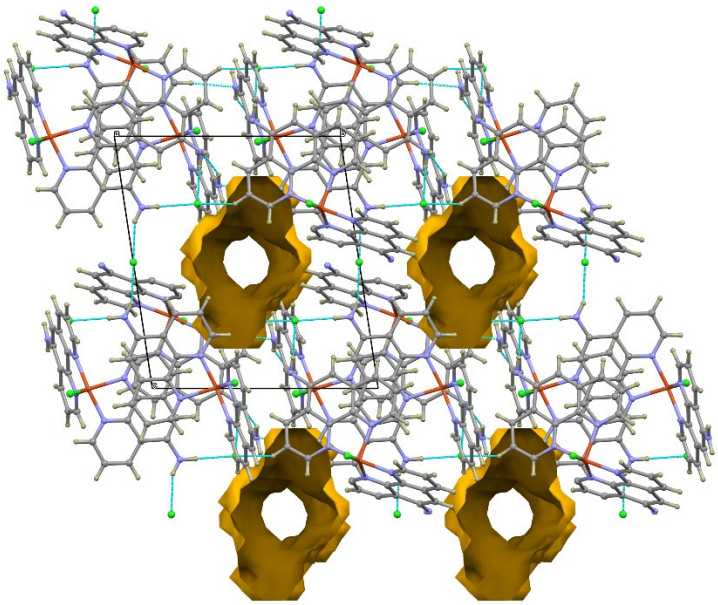

Figure 5.9: Three-dimensional hydrogen-bonded supramolecular structure of [Cu(Phen-NH_2)$_2$(Cl)]Cl showing the extensive hydrogen bonding network stabilising the structure. Voids are shown as yellow surfaces and were calculated using a probe radius of 1.2 Å.

5.4 Conclusion

The solid state structures of three copper(II) chelates [Cu(L)(H_2O)$_2$]NO_3, [Cu(phen-NH_2)$_2$(Cl)]Cl and [Cu(L1)(H_2O)$_2$]NO_3 were determined. These copper(II) chelates exhibit square pyramidal and trigonal pyramidal geometries around the metal centre which is in keeping with the previously reported chelates of this class. The bond angles and bond distances were comparable with those in the literature. The copper(II) ion coordinated as would be expected, to the tridentate Schiff base ligand and has a nearly ideal square pyramidal coordination sphere, where the coordinated Schiff base ligands are approaching planarity. The planar aromatic regions of the Schiff base ligand have the potential to enhance the intercalation of the complex between the DNA base pairs. The solid state structure of [Cu(phen-NH_2)$_2$(Cl)]Cl and [Cu(L1)(H_2O)$_2$]NO_3 have been shown to form π-π interaction, which is important as these interactions will stabilize the DNA-drug conjugate in a cellular environment.

5.5 References

1. Groom, C.R., Bruno, I.J., Lightfoot, M.P. and Ward, S.C., 2016. The Cambridge structural database. *Acta Crystallographica Section B: Structural Science, Crystal Engineering and Materials*, *72*(2), pp.171-179.
2. Bhaumik, P.K., Jana, S. and Chattopadhyay, S., 2012. Synthesis and characterization of square planar and square pyramidal copper (II) compounds with tridentate Schiff bases: Formation of a molecular zipper via H-bonding interaction. *Inorganica Chimica Acta*, *390*, pp.167-177.
3. Yanick Gaelle, D.S., Ondoh Agwara, M., Yufanyi, D.M., Nenwa, J. and Jagan, R., 2017. Crystal structure and antimicrobial properties of a copper (II) complex with 1, 10-

phenanthroline and azide co-ligand. *Inorganic and Nano-Metal Chemistry*, *47*(4), pp.618-625.
4. Bhaumik, P.K., Bauzá, A., Drew, M.G., Frontera, A. and Chattopadhyay, S., 2015. Syntheses, crystal structures and density functional theory investigations of copper (ii) complexes bearing tridentate Schiff base ligands derived from 8-aminoquinoline. *Crystal Engineering Communication*, *17*(30), pp.5664-5671.
5. Inc, B.A, *Bruker APEX2, SAINT and SADABS*, Wisconsin, USA, 2012.
6. Farrugia, L.J., 1999. WinGX suite for small-molecule single-crystal crystallography. *Journal of Applied Crystallography*, *32*(4), pp.837-838.
7. Spek, A.L., 2015. PLATON SQUEEZE: a tool for the calculation of the disordered solvent contribution to the calculated structure factors. *Acta Crystallographica Section C: Structural Chemistry*, *71*(1), pp.9-18.
8. Baul, T.S.B., Kundu, S., Singh, P. and da Silva, M.F.C.G., 2015. Insight into inhibition of the human amyloid beta protein precursor (APP: PDB ID 3UMI) using (E)-N-(pyridin-2-ylmethylene) arylamine (LR) models: structure elucidation of a family of ZnX 2-LR complexes. *Dalton Transactions*, *44*(5), pp.2359-2369.
9. Raymond, K.N., Corfield, P.W.R. and Ibers, J.A., 1968. Structure of tris (ethylenediamine) chromium (III) pentacyanonickelate (II) sesquihydrate, $[Cr(NH_2CH_2CH_2NH_2)_3][Ni(CN)_5]$. 1. $5H_2O$. *Inorganic Chemistry*, *7*(7), pp.1362-1372.
10. Qin, Q.P., Li, Y.L., Liu, Y.C. and Chen, Z.F., 2014. Synthesis, crystal structure, cytotoxicity and cell apoptosis induction of a copper (II)-based Schiff base complex. *Inorganica Chimica Acta*, *421*, pp.260-266.

CHAPTER 6: BIOLOGICAL STUDIES

6.1 DNA Binding Studies

6.1.1 Introduction

Deoxyribonucleic Acid (DNA) is an important genetic biomolecule that carries the hereditary codes required for the synthesis of all enzymes and proteins. DNA is the pharmacological target for various therapeutically important small molecules that belong to different classes of drugs, ranging from antibiotics to anticancer drugs.[1] The understanding of drug-DNA interactions plays a vital role in pharmacology and is of great significance for the design and synthesis of novel drugs

targeted to DNA. Also, their effectiveness highly depends on the mode and affinity of the binding to DNA.[1,2] The interaction of metal complexes with DNA has been a subject of interest since the discovery of cisplatin and its therapeutic activity. In search of new metallodrugs, it is anticipated that a drug based on essential metal ions may be less toxic, this has led to the studying of copper-based drugs. Copper is a physiologically important element that plays a vital role in endogenous oxidative DNA damage associated with aging and cancer.[2] Copper complexes in this study are expected to exert their cytotoxicity through DNA binding and through hydroxyl radical-induced DNA cleavage. This class of complexes has been reported to bind to DNA through hydrophobic interactions in DNA's minor groove and by the partial intercalation of the co-ligand into the major groove.[3]

The number and variety of techniques used to determine drug-DNA interaction is continuously growing.[4] Experimental techniques include emission and absorption spectroscopies, NMR or atomic force microscopy.[5] In this research study, two methods (direct binding and competitive binding) were employed to determine the binding affinity of the copper(II) chelates using ethidium bromide (EB) as the intercalating compound. Small molecules such as ethidium bromide are known to bind to DNA and other polynucleotides, and such chemical interactions may be responsible for their biological activities.[6]

The direct binding method involves the monitoring of the absorption spectrum of EB as a function of the increasing concentration of ctDNA. During the DNA titration, EB intercalates between the base pairs of the DNA double helix, lowering the effective concentration of EB leading to both hypochroism and a bathochromic shift. In a competitive binding method, the metal chelate is introduced to a ctDNA-EB adduct, EB is displaced by the metal chelate thus quenching the florescence emission of ctDNA intercalated by EB.[7] The binding constant can be determined by monitoring the decrease in emission of EB as a function of metal chelate concentration. Copper(II) chelates with an apparent binding constant (K_{app}) higher than that of EB would be regarded as highly effective DNA intercalators.

6.1.2 Experimental

DNA-binding experiments were performed by UV/vis and emission spectroscopy using a 25mM Tris-HCl buffer at 37 °C to mimic the cellular environment of a human. The buffer was prepared with ultrapure water and adjusted to pH using 1M HCl. The DNA solution was prepared by dissolving the ctDNA purchased from Sigma Aldrich in the buffer solution; the mixture was stired overnight and filtered to remove any large suspended DNA particulates. The ctDNA stock solution was stored at 4 °C and used over no more than 2 days after which the solution quality began to deteriorate.

The EB solution used had a concentration of 3.0 mM in Tris-HCl buffer solution (pH 7.0) in a 1.0 cm path quartz cuvette at 25 °C. The ctDNA solution was added to the solution of EB in small

incremental aliquots over intervals of ten minutes per addition. This incubation period ensures that the intercalation process went to completion and the equilibrium was re-established before spectra were recorded. The spectra were recorded in the range of 200-700 nm. To determine the DNA binding constant of EB, equation 6.1 below was used. The binding affinity of ethidium bromide under the same conditions as those used for the competitive binding must be measured. The binding affinity is dependent on temperature and the solvent system in use. The EB binding affinity is required to calculate the apparent binding constant of the metal chelate which displaces the EB in the competitive emission binding studies.

$$\frac{\varepsilon_a - \varepsilon_f}{\varepsilon_b - \varepsilon_f} = \frac{\left[b - \left(\frac{b^2 - 2K_b^2 C_t[\mathrm{DNA}]}{s}\right)^{\frac{1}{2}}\right]}{2K_b C_t} \quad \text{..... 6.1}$$

Where;

$$b = 1 + K_b C_t + \frac{K_b[\mathrm{DNA}]}{2s}$$

ε_a = Extinction coefficient of EB band at a given [ctDNA]

ε_b = Extinction coefficient of fully intercalated EB

ε_f = Extinction coefficient of free EB

K_b = Equilibrium constant in M^{-1}

C_t = Total concentration of ctDNA

s = Binding site size

For the competitive binding studies of the copper(II) chelates, stock solutions were prepared in ultrapure water and acetonitrile (3×10^{-3} M concentration). Aliquots of each metal complex were added to a solution containing 15 µM of ctDNA and 15 µM EB in a buffer solution. After each addition there was an incubation period of ten minutes to allow an equilibrium to establish before the emission spectra of the solution were recorded between 540-800 nm. The wavelength of 530 nm was used for the excitation. Equation 6.2 was used to calculate the apparent binding constant K_{app} for metal chelates.

$$K_{app}[Complex] = K_{EB}[EB] \quad \text{..... 6.2}$$

Where;

K_{app} = Apparent binding constant of the metal chelate

K_{EB} = ctDNA binding constant of EB

[EB] = EB molar concentration

[Complex] = Molar concentration of copper(II) chelate that caused the 50% quenching of the initial fluorescence intensity (C_{50}).

To confirm the quenching of EB-ctDNA fluorescence, a Stern-Volmer equation is used (equation 6.3:

$$\frac{I_O}{I} = 1 + kr \quad \text{..... 6.3}$$

Where;

I_o = Initial fluorescence intensity of EB-ctDNA complex

I = Intensity of the quenching EB-ctDNA complex

r = Ratio between total concentration of the metal complex and DNA concentration

k = Stern Volmer constant.

6.1.3 Results and Discussion

The UV/vis spectrum of ct-DNA shows a strong band (200-350 nm) with the maximum absorption at 260 nm. This absorption is a result of the chromophoric groups in pyrimidine (thymine and cytosine) and purine (guanine and adenine) moieties responsible for the electronic transition.[8,9] The probability of these transitions is high, hence the extinction coefficient (ε) is of order 10^4 M^{-1} cm^{-1}. By measuring the absorbance value at 260nm, the molar concentration of ctDNA can be determined using the Beer-Lambert Law and the extinction coefficient of 13200 m^{-1} cm^{-1}. The extinction coefficient measures how strongly the absorbing bases reduce the intensity of the UV light from incidence to transmission. Since the absorbance of each base is different, base composition, base order, and sequence length will influence the final absorbance of the particular nucleic acid undergoing quantification. Therefore, the greatest accuracy is achieved when the extinction coefficient is calculated for each oligonucleotide.[19]

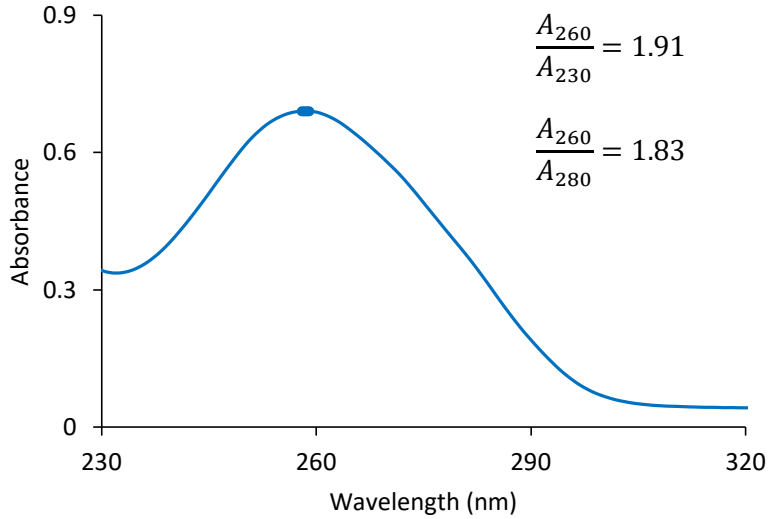

Figure 6.1: The absorption spectra of a ctDNA solution 230-320 nm.

To determine the purity of the DNA (to ensure it is free from protein contaminants), the absorbance ratios (A_{260}/A_{230} and A_{260}/A_{280}) are measured. These ratios should be within the range 1.8-1.9 to ensure that the DNA is sufficiently free of protein.[8] The DNA solution was found to be free of protein (ratio 1.91 and 1.83, respectively (Figure 6.1)) with the molar concentration of 6.57 mM.

To determine the binding constant of EB (K_{EB}) to ctDNA, a direct DNA titration was conducted. EB is said to have a high affinity for DNA, hence a large binding constant is expected. The high value of the binding constant ($K_{EB} = 4.36 \times 10^6\ M^{-1}$), illustrates that there is high affinity of EB for DNA. The addition of increasing amounts of DNA to EB shifts the visible absorption maximum of EB from 480 nm to 520 nm. This shift and the existence of a well-defined isobestic point at 520 nm is an indication of the formation of the EB-ctDNA complex and binding to both primary and secondary sites of EB to ctDNA.[9] The observed spectroscopic changes also indicate the intercalative mode of binding that involves a stacking interaction between aromatic chromophores of EB and the base pairs of DNA. In general, during a direct DNA binding experiment a bathochromic shift is indicative of intercalation while a hypsochromic shift suggests groove binding. The π* orbital of the intercalated EB can couple with the π orbital of base pairs, consequently decreasing the $\pi \rightarrow \pi^*$ transition energy and results in bathochromism.[10] The UV/vis spectrum of EB with increasing concentration of ctDNA is shown below (Figure 6.2a). Using the non-linear plot of the EB titration at 480 nm K_{EB} was calculated to be $4.36 \times 10^6\ M^{-1}$ using equation 6.1 (Figure 6.2(b)).

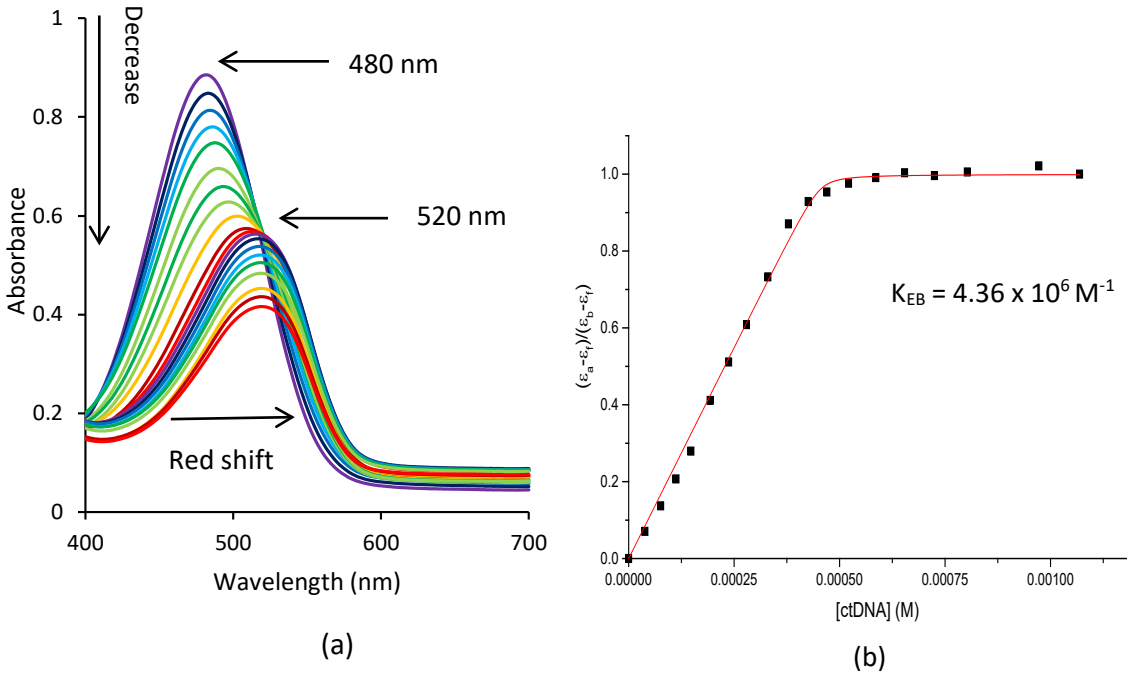

Figure 6.2: (a) The UV/vis spectrum showing the absorbance titration of EB with increasing concentration of ctDNA. (b) Non-linear fit for EB titration with ctDNA at 480 nm.

The fluorescence competitive binding DNA titrations were conducted to determine the binding affinity of the copper(II) complexes for ctDNA. This was determined by the addition of increasing aliquots of the complex to the solution of ctDNA and EB under specific conditions of the experiment (5% DMSO, TRIS buffer, pH= 7.0, 25 °C). When EB is intercalated into the base pairs of ctDNA it gives a significant fluorescence emission intensity. The fluorescence quenching curve of the EB-ctDNA conjugate by metal chelate [Cu(L)(phen-NH_2)]NO_3 is presented in Figure 6.3 below.

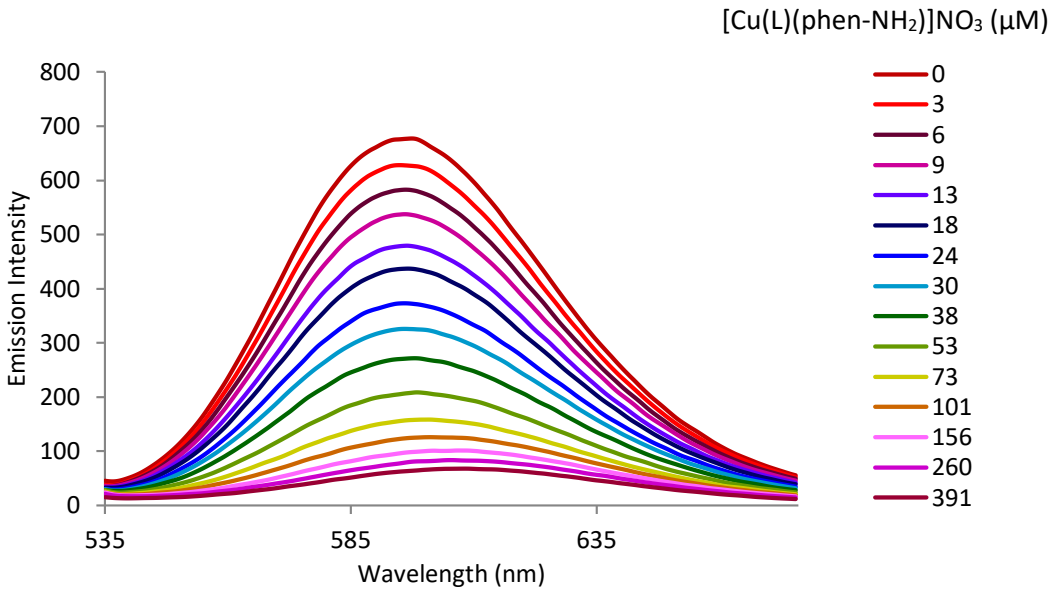

Figure 6.3: The fluorescence quenching curve of EB bound to ctDNA showing displacement of ct-DNA intercalated EB by [Cu(L)(phen-NH_2)]NO_3.The emission spectra were corrected for dilution effects.

The additions of the metal complex solution quench the emission intensity of the EB-DNA conjugate as the metal complex out-competes and displaces EB from the DNA. Free EB is non-emissive. All complexes show similar fluorescence; quenching which indicates that the complexes displace the strongly intercalated EB and bind to the DNA. The apparent binding constant (K_{app}) of the complexes were determined using Equation 6.2 and are listed (Table 6.1). The equation requires the concentration of the complex at which 50% reduction of the fluorescence intensity of ctDNA-EB conjugate occurred. This was determined from the non-linear fit of the change in emission intensity at 594 nm as a function of the increasing chelate concentration. The quenching efficiency for all complexes was evaluated by a Stern-Volmer plot. Figure 6.4 shows both the non-linear fit and Stern-Volmer plot. It is important to note that this experiment does not predict a DNA binding mode, i.e. groove binding versus intercalation, but does show the affinity of the complex for DNA.

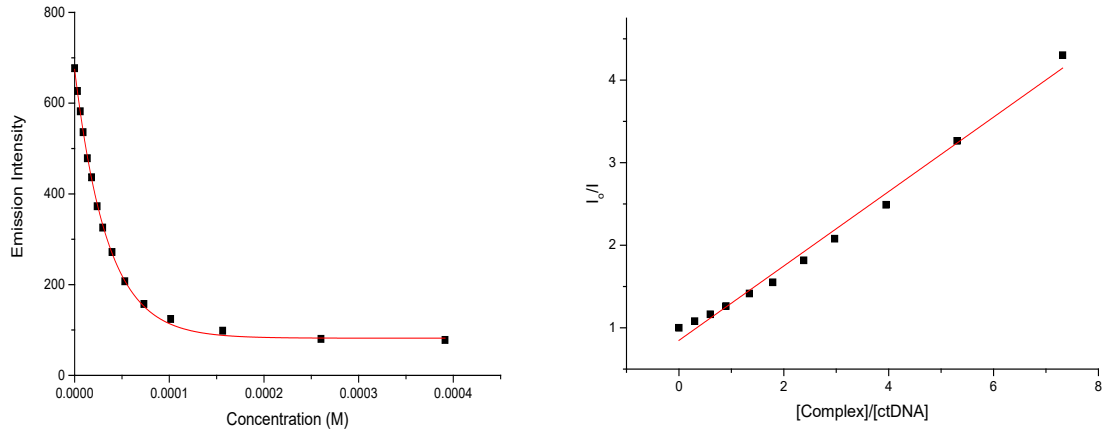

Figure 6.4: The least-squares fit of the change in ctDNA-EB emission at 595 nm with the increasing concentration of the metal chelate (left). Stern-Volmer plot for [Cu(L)(phen-NH_2)]NO_3 (right).

The linear Stern-Volmer plot illustrates the quenching of emission of the EB-ctDNA conjugate by the complex indicating that the complexes bind to DNA. The quenching constant K_{sq} is obtained as the ratio of the slope to intercept. The K_{sq} values for the complexes suggest a strong interaction of the complexes with DNA.[10] The K_{app} of the complexes ranges from 2.79×10^5 M^{-1} for $[Cu(L)(H_2O)_2]NO_3$ to 5.31×10^6 M^{-1} for $[Cu(phen\text{-}NH_2)_2(Cl)]Cl$. Apparent binding constants of this order of magnitude show the complexes in this study have a high ct-DNA binding affinity. The summary of K_{app} for all the complexes is presented in Table 6.1.

Table 6.1: A summary of the apparent binding constant (K_{app}) of copper(II) complexes to ctDNA.

Complex	**K_{app}(M^{-1})**
$[Cu(L)(H_2O)_2]NO_3$	2.79×10^5
$[Cu(L)(phen)]NO_3$	4.38×10^5
$[Cu(L)(phen\text{-}NH_2)]NO_3$	3.76×10^6
$[Cu(L)(dppz)]NO_3$	1.27×10^6
$[Cu(phen\text{-}NH_2)_2(Cl)]Cl$	5.30×10^6

The Cu-bis-phenantroline complex $[Cu(phen)_2(Cl)]Cl$ ($K_{app} = 6.67 \times 10^5$) is known to induce oxidative damage in the presence of a reductant and oxidant, e.g O_2 through the free radical oxidation of DNA.[11] However, this complex binds without specificity to a number of different biomolecules not only DNA but also protein. In an effort to enhance DNA binding, the complex $[Cu(phen\text{-}NH_2)_2(Cl)]Cl$ was synthesised, and found to have a K_{app} value of 5.31×10^6, greater than that of $[Cu(phen)_2(Cl)]Cl$. This is likely due to the amine group which favours stronger interactions with DNA due to the hydrogen bonding ability of the amine group which stabilises the DNA/drug conjugate. Hydrogen bonding of the coordinated ligand with polynucleotides are known, in particular with phosphate oxygen atoms on the backbone of DNA and stabilises the ctDNA-$[Cu(phen\text{-}NH_2)_2(Cl)]Cl$ conjugate.

Ude *et al*. reports that by systematically extending the phenazine ligand of $[Cu(Phen)_2(Cl)]Cl$ from phen to dppz, the resulting complexes enhance oxidative DNA degradation and therefore cell apoptosis. The ctDNA binding constants (~10^7 M^{-1}) for these complexes are among the highest reported for Cu-phenanthroline-based systems.[11] The competitive binding fluorescence were also done for Ru(dppz) complexes, for this study the binding constants were found to be in the range (10^6-10^7), indicating a strong interaction with DNA.[12] As the binding constant (K_{app}) for the copper(II) chelates presented in this study are similar to those previously reported, it indicates that the complexes have a high affinity for ctDNA.

The binding constant of the Schiff base complex of chromium(III) $[Cr(salen)(H_2O)_2]^+$ (where salen =1,2-bis(salicylideneamino)ethane) was reported to be 2.5×10^3 M^{-1}.[13] This K_b value is lower than that of $[Cu(L)(H_2O)_2]NO_3$ (2.79×10^5 M^{-1}), this indicates a strong affinity of $[Cu(L)(H_2O)_2]NO_3$ for DNA relative to the chromium complex with a similar ligand. This could be due to the octahedral nature of the metal chelate hindering the penetration of the complex into the DNA, hence poor binding. In comparison, $[Cu(L)(H_2O)_2]NO_3$ has a tridentate Schiff base that is small, planar and the overall chelate is square pyramidal as opposed to octahedral, which enables the complex to interact and stack more effectively with the DNA base pairs. A comparison of the structures of the copper(II) chelate from this work and that of the previously reported chromium complex is presented in Figure 6.5.

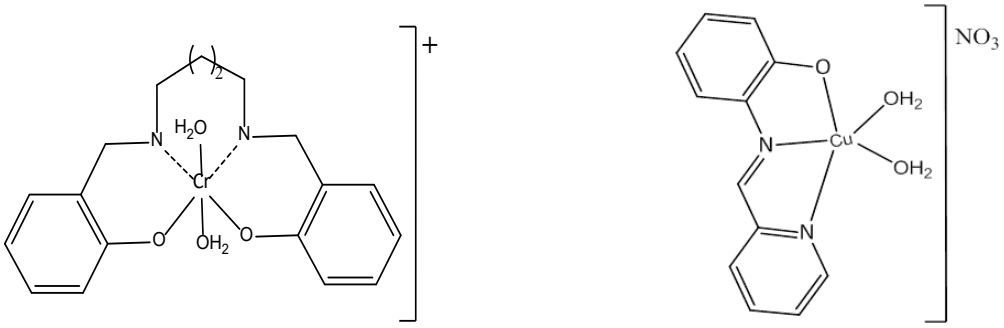

Figure 6.5: Structure of $[Cr(salen)(H_2O)_2]^+$ (left) and $[Cu(L)(H_2O)_2]NO_3$ (right).[13]

The strong affinity of $[Cu(L)(dppz)]NO_3$ relative to $[Cu(L)(phen)]NO_3$ is related to the presence of the dppz ligand which possesses a greater planar area and an extended π system compared to the phen co-ligand. The greater the extended aromaticity, the more efficiently a complex interacts with the aromatic base pairs of the DNA helix. This extended aromaticity increases the stability of the DNA-drug conjugate, and hence a higher DNA binding constant is noted.

The binding constant of $[Cu(L)(phen\text{-}NH_2]NO_3$ and $[Cu(L)(phen)]NO_3$ are significantly different, showing the effect in DNA interaction caused by the addition of the NH_2 group. This is due to the additional hydrogen bonding ability of the NH_2 group which further stabilises the DNA/drug conjugate. The K_{app} value of $[Cu(L)(phen\text{-}NH_2)]NO_3$ is the second highest of all complexes, higher than that of $[Cu(L)(dppz)]NO_3$ suggesting that the addition of hydrogen bonding has a greater effect than extending the aromaticity in stabilising the DNA-drug conjugate.

The $[Cu(phen\text{-}NH_2)_2(Cl)]Cl$ complex has a square planar geometry (in solution), containing *N,N* donor atom sets and has the highest binding constant. This geometry increases the planarity of the complex thus increasing the ability to effectively interact with the DNA helix. Also, the presence of hydrogen bonding sites on both ligands further stabilises the DNA-drug conjugate, resulting in a greater DNA binding constant. In this study, the hydrogen bonding ability and the planarity of the complexes have proven to have a significant effect on DNA-drug interactions. However, it is important to note that DNA binding is more complex than these two aforementioned factors. The stability of a DNA-drug conjugate can also be enhanced by electrostatic interaction between the drug candidate and DNA helix. Complexes in this study possess an overall positive charge, which stabilises the DNA-drug conjugate through interaction with the negatively charged phosphate backbone of the DNA helix.

6.2 Cytotoxicity

6.2.1 Introduction

Breast cancer is the most common cancer worldwide, with increasing incident cases from 1.7 million in 2005 to 2.4 million in 2015.[14] According to GLOBACAN, an estimated 94 378 new cases of breast cancer are diagnosed annually in sub-Saharan Africa alone. The National Cancer Registry (NCR) 2014 reported that breast, cervical, colorectal, uterine and lung cancer are the top five cancers affecting South African women, with both breast and cervical cancer identified as a national priority.[15] With these statistics, MDA-MB (Triple negative breast cancer cells) cell line screening will be discussed in detail in this section. The triple-negative breast cancer cell line is particularly relevant for cancer research in Africa as it is a particularly aggressive tumour with a high mortality rate and it has a higher prevalence in women of African descent.

In general, breast cancer tends to be classed as a single disease, however there are several different types of breast cancers. Breast cancer is a heterogenenous disease comprising of molecularly and clinically distinct subtypes. The triple negative breast cancer (TNBC) represents between 10-15% of all breast cancer cases reported and it is defined by the lack of expression of progesterone and oestrogen receptors, and the lack overexpression of the human epithelial receptor 2 (Her2 gene). Since TNBC does not have progesterone, oestrogen or HER2 receptors, anti-HER2 target therapies and hormone therapies are less effective. Patients suffering from TNBC tend to experience unfavourable prognosis, particularly when they respond poorly to anthracylinetaxane chemotherapy. Since there are limited treatment options for TNBC patients besides classical chemotherapy, the development of novel chemotherapeutic agents are urgently needed in order to improve the prognosis of patients with TNBC.[17]

6.2.2 Experimental

The cytoxocity assay was conducted as per a standard method described previously.[16] Briefly, 96-well microtiter plates were seeded with cell lines (HEK293, MDA-MB, HELA or SHSY5Y) at a concentration of 2×10^5 cells/mL and allowed to stabilize for 4 hours at 37°C and 5% CO_2. Thereafter, either the copper(II) compounds or cisplatin (as a reference compound) were added to the plate through two-fold serial dilution to allow for eight final compound concentrations ranging from 100 to 0.781 µM in a total volume of 200 µL / well. The plate was then incubated for 96 hours at 37°C and 5% CO_2. To each well, 20 µL Cell Titer 96 AQueous One Solution (Promega, Madison, WI, USA) was added and the plates were incubated for 4 hours as previously described. Thereafter, the absorbance was read at 490 nm on a multiplate reader (Molecular Devices, San Jose, CA, USA). EC_{50} values were determined as the concentration of each compound required to reduce cell viability by 50% and were calculated using OriginPro 8.0 software (Origin Lab Corporation, Northampton, MA, USA). The values are presented as averages of at least three separate experiments.

The synthesized copper(II) complexes were designed to be used as chemotherapeutic agents and exert their cytotoxicity through DNA intercalation and the catalysis of ROS. DNA binding studies have shown that these complexes have the potential to act as chemotherapeutic agents as they are shown to have high DNA binding affinity. The cytotoxicity of the copper(II) complexes was determined by *in vitro* testing against four mammalian cell lines. The cell lines include HEK293 (healthy embryonic kidney cells), MDA-MB (triple negative cancer cells), HELA (cervical cancer cells) as well as SHSY5Y (human neuroblastoma cells). These screens gave the EC_{50} values, that are summarised in Table 6.2. The EC_{50} value is fundamental in pharmacology and is defined as the concentration of inhibitor at which the total growth is inhibited. It measures the effectiveness of a substance in inhibiting a specific biochemical or biological function. The lower the EC_{50} value, the more potent the inhibitor (compound) is. The IC_{50} value of the well-known chemotherapeutic drug, cisplatin is depicted on the dose response curve (Figure 6.6).

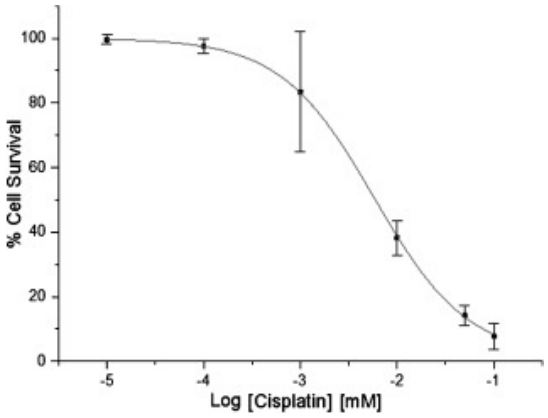

Figure 6.6: An IC_{50} curve for MCF7 cells (breast cancer cell line) treated with cisplatin. The percentage cell survival is plotted against the logarithm of treatment concentration.[18]

The IC_{50} value of cisplatin (5.75 ± 0.07 µM) against MCF7 cells show great cytotoxicity. The percentage cell survival is a measure of the fraction of cells retaining their productive integrity. The data obtained from such curves allows statistical comparison of the activity profile of a novel compound (with unknown mode of action) with the activity profile of known compounds with known mode of action. This is crucial in the process of drug discovery as it reduces the time taken to determine the mechanism of action.

Table 6.2: Tumour cell screening results for the copper(II) chelates for application as theranostic agents.

Compounds	Cell line	HEK293	MDA-MB	HELA	SHSY5Y
	Cisplatin	14.2 ± 3.8	>50	22.68± 4.89	Not Done
	$[Cu(L)(H_2O)_2]NO_3$	56.1 ± 5.2	39.71± 21.42	13.19± 4.23	14.93± 5.04
	$[Cu(L)(phen\text{-}NH_2)]NO_3$	4.8± 2.5	2.95± 0.70	2.72± 0.10	7.14± 1.75
	$[Cu(L)(phen)]NO_3$	5.5 ± 1.2	1.69 ± 0.07	2.71 ± 1.31	4.75 ± 2.75
	$[Cu(L)(dppz)]NO_3$	<1.56	2.92± 0.65	2.08± 1.00	3.53± 1.85
	$[Cu(phen\text{-}NH_2)_2(Cl)]Cl$	2.6± 0.2	0.56 ± 0.08	4.92 ± 1.52	6.59 ± 1.74

Table 6.2 shows the cytotoxicity of the copper(II) chelates against different cell lines. High EC_{50} values represent a compound that is less effective in lowering the growth of that cell line. Low EC_{50} values, on the other hand, indicate that the compound is effective in inhibiting the growth of that cell line. As discussed in Chapter One, cisplatin is one of the most used inorganic chemeotherapeutic agents worldwide. Hence a comparison of the efficiency of cisplatin with our complexes against three cancer cell lines and one healthy cell line is of particular interest. The data in Table 6.2 show that some of the complexes compare favourably with the commercial chemotherapeutic agent cisplatin and are in several respects more effective. The EC_{50} value for all the copper(II) complexes are lower than the EC_{50} value of cisplatin for all cell lines tested.

The data in Table 6.2 illustrate that each cell line responds differently to the different drugs. This implies that each of the complexes in this study have a unique cytotoxicity profile. The HEK293 cell line is a healthy embryonic kidney cell and was used as a control. The lack of cytotoxic activity of $[Cu(L)(H_2O)_2]NO_3$ chelate towards this cell line illustrates the enhanced selectivity of the copper(II) chelates towards neoplastic tissue, showing higher cytotoxicity towards all tumour cell lines compared to cisplatin. The selectivity of the copper(II) chelates varies depending on the specific tumour cell line. $[Cu(L)(dppz)]NO_3$ show less selectivity towards tumor cells as it is more toxic to healthy cells than tumour cells. The reason for this high cytotoxity could be related to the increased aromaticity and the increased DNA binding affinity. To improve the selectivity of the copper(II) chelates even further, a biotin based ligand could be incorporated into the structure of the drug, this will ensure higher uptake of the drug in neoplastic over healthy cells.

The complexes $[Cu(L)(phen)]NO_3$, $[Cu(L)(phen\text{-}NH_2)]NO_3$ and $[Cu(phen\text{-}NH_2)_2(Cl)]Cl$, significantly, show good cytotoxicity towards the triple negative breast cancer cells (MDA-MB). This suggests that these compounds could be suitable for the treatment of triple negative breast cancer. The $[Cu(L)(phen)]NO_3$ and $[Cu(L)(phen\text{-}NH_2)]NO_3$ similarly show great cytotoxicity toward cervical cancer cells, hence it would be pertinent to test these compounds against a wider range of cervical cancer cells for the development of the next generation cervical cancer drugs.

The complexes in this study seem to selectively target certain cells; $[Cu(L)(phen)]NO_3$, $[Cu(L)(phen\text{-}NH_2)]NO_3$ and $[Cu(phen\text{-}NH_2)_2(Cl)]Cl$ are all highly active against MDA-MB and HELA cell lines, but are significantly less active against SHSY5Y cell lines. $[Cu(L)(phen)]NO_3$ and

[Cu(L)(phen-NH_2)NO_3 have very similar structures, however the latter is more active than the former against the MDA-MB cell line. In addition, [Cu(L)(phen-NH_2)]NO_3 does show slightly less selectivity as it inhibits SHSY5Y cells at a EC_{50} value of 7.14 µM while the EC_{50} value for healthy embroyic kidney cells is 4.8 µM. This is a clear illustration of the fact that small structural modifications (such as addition of the NH_2 groups on the phen co-ligand) of a complex can result in significant changes to the efficacy (selectivity and activity) of the complex towards a specific cell line. [Cu(phen-NH_2)$_2$(Cl)]Cl is largely effective against the MDA-MB cell line while it is ineffective against HELA and SHSY5Y cell lines. This is important as it show that this complex exhibits inherent specificity toward specific cancer cells, it is therefore expected to have lower unspecific toxicity and hopefully fewer side effects. [Cu(L)(H_2O)$_2$]NO_3 is the least active of all copper(II) chelates in the study, but still retains the high selectivity.

The data in Table 6.2 is counterintuitive, thus it is represented as –logEC_{50} values in Figure 6.7. The higher the EC_{50} value of the complexes, the lower its –logEC_{50} value. This allows clear graphical representation and clear data analysis. A higher –logEC_{50} value indicates that the compound is more effective against that particular cell line.

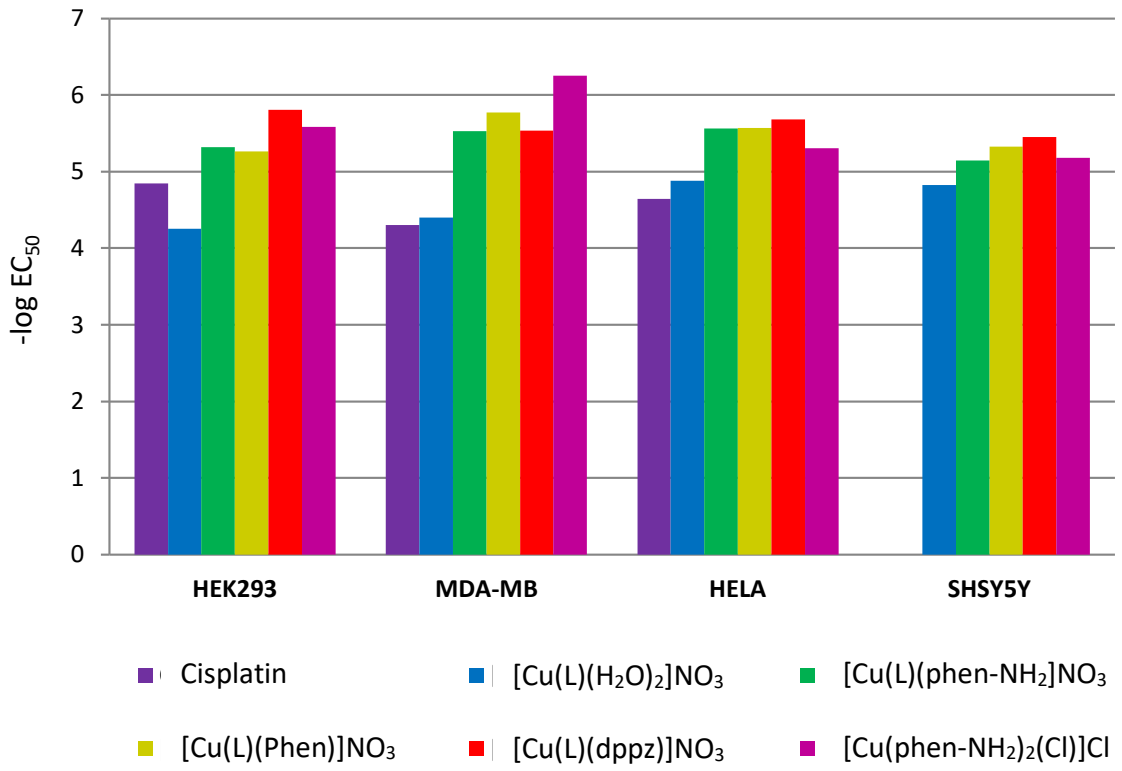

Figure 6.7: The –logEC_{50} values for cisplatin and copper(II) chelates against four cell lines and their mean cytotoxicity.

The addition of a co-ligand to [Cu(L)(H_2O)$_2$]NO_3 seems to increase the cytotoxicity and could lead to a potent chemotherapeutic. This is noted with the addition of the phen co-ligand to form [Cu(L)(phen)]NO_3; the cytotoxicity is largely enhanced. In addition, the mean cytotoxicity of all

complexes with co-ligands is greater than that of cisplatin. Although the coordination of a co-ligand improves the cytotoxicity, forming a complex with only co-ligands reduces the selectivity as it can be seen between $[Cu(phen\text{-}NH_2)_2(Cl)]Cl$ and $[Cu(L)(phen\text{-}NH_2)]NO_3$. This is a good illustration of the importance of the role played by the Schiff base ligand. The combination of the Schiff base ligand and the phenanthroline-based co-ligand leads to a more cytotoxic and selective chemotherapeutic agent than either ligand independently.

There is no clear correlation between the binding affinity of a copper(II) complex and their EC_{50} values, see Table 6.3. For all cell lines, the compound with the lowest binding constant, $[Cu(L)(H_2O)_2]NO_3$ (2.79×10^5 M^{-1}), results in higher EC_{50} value, possibly indicating that the DNA interaction might be significant for the efficacy of copper(II) Schiff base single-ligand complexes. However, for all other complexes there is little relationship. This shows that the mechanism of action for these copper(II) chelates is more complex than DNA binding alone. The redox activities of copper(II)/(I) is likely to be a main factor in the cytotoxicity. The co-ligand such as phen or phen-NH_2 is possibly more effective at stabilizing the chelate for a transition of copper(II) to copper(I) in the biological environment, increasing the production of ROS, inducing apoptosis and ultimately increasing the cytotoxicity.

Table 6.3: The relationship between the competitive binding affinities and cytototoxicity of copper(II) chelates.

Most Effective				**Least Effective**
Cytotoxicity: *in vitro* cell screening				
$Cu(L)(dppz)]NO_3$	$[Cu(phen\text{-}NH_2)_2(Cl)]Cl$	$[Cu(L)(phen)NO_3]$	$[Cu(L)(phen\text{-}NH_2]NO_3$	$[Cu(L)(H_2O)_2]NO_3$
Competitive binding Constants				
$[Cu(phen\text{-}NH_2)_2(Cl)]Cl$	$[Cu(L)(phen\text{-}NH_2)]NO_3$	$[Cu(L)(dppz)]NO_3$	$[Cu(L)(phen)]NO_3$	$[Cu(L)(H_2O)_2]NO_3$

In terms of cytotoxicity, and more importantly selectivity, the copper(II) chelates described in this study have a great potential as chemotherapeutics.

6.3 Conclusions

Heteroleptic copper(II) chelates were screened against four cell lines. The cell lines are as follows: HEK293 are Human Embryonic Kidney cells (i.e. a healthy cell line used to represent the toxicity to healthy human cells); the MDA-MB231 are triple-negative breast cancer cells, the HELA are cervical cancer cells and SH-SY5Y is a human neuroblastoma cell line. The triple-negative breast cancer cell line is particularly relevant for cancer research in Africa as it is a particularly aggressive tumour with a high mortality rate and it has a higher occurrence in women of African descent.

The cytotoxicity data show a few key points, firstly, the compounds are more cytotoxic towards these tumour cell lines than the current industry standard: cisplatin. Secondly, the cells are more toxic towards tumour cells than healthy cells. Lastly, the addition of the co-ligand has increased the tumour cell specificity as well as cytotoxicity. This was one of the key postulates of the initial project proposal.

The most cytotoxic compound was found to be $[Cu(L)(dppz)]NO_3$ while $[Cu(L)(H_2O)_2]NO_3$ was the least cytotoxic compound. Four of the five copper(II) chelates have greater cytotoxicity than cisplatin and the cytotoxicity varies between cell lines, this indicates that the compounds have chemotherapeutic potential against different types of cancers. There is little correlation between the cytotoxicity and DNA binding affinities. This suggests a more complex mechanism of action than just binding to DNA. The redox activity of copper and the catalytic production of ROS could be a key aspect in the mechanism of action.

6.4 References.

1. Rehman, S.U., Sarwar, T., Husain, M.A., Ishqi, H.M. and Tabish, M., 2015. Studying non-covalent drug–DNA interactions. *Archives of Biochemistry and Biophysics*, *576*, pp.49-60.

2. Shahabadi, N. and Fatahi, P., 2012. DNA Interaction Studies of a Copper (II) Complex Containing an Antiviral Drug, Valacyclovir: The Effect of Metal Center on the Mode of Binding. *DNA and Cell Biology*, *31*(7), pp.1328-1334.
3. Zeglis, B.M., Pierre, V.C. and Barton, J.K., 2007. Metallo-intercalators and metallo-insertors. *Chemical Communications*, (44), pp.4565-4579.
4. González-Ruiz, V., Olives, A.I., Martín, M.A., Ribelles, P., Ramos, M.T. and Menéndez, J.C 2011. *Biomedical Engineering, Trends, Research and Technologies,* IntechOpen, Rijeka.
5. Misiak, M., Mantegazza, F. and L Beretta, G., 2016. Methods for elucidation of DNA-anticancer drug interactions and their applications in the development of new drugs. *Current Pharmaceutical Design*, *22*(44), pp.6596-6611.
6. Greenstock, C.L. and Ruddock, G.W., 1975. Interaction of ethidium bromide with DNA as studied by kinetic spectrophotometry. *Chemico-Biological Interactions*, *11*(5), pp.441-447.
7. LV, Y., Li, P., Jiao, M.L., Liu, B.S. and Yang, C., 2014. Fluorescence quenching study of moxifloxacin interaction with calf thymus DNA. *Turkish Journal of Chemistry*, *38*(2), pp.202-209.
8. Sirajuddin, M., Ali, S. and Badshah, A., 2013. Drug–DNA interactions and their study by UV–Visible, fluorescence spectroscopies and cyclic voltametry. *Journal of Photochemistry and Photobiology B: Biology*, *124*, pp.1-19.
9. Talavera, E.M., Guerrero, P., Ocana, F. and Alvarez-Pez, J.M., 2002. Photophysical and direct determination of binding constants of ethidium bromide complexed to E. coli DNA. *Applied Spectroscopy*, *56*(3), pp.362-369.
10. Reddy, P.R. and Shilpa, A., 2012. 2-Hydroxynaphthalene-1-carbaldehyde-and 2-(Aminomethyl) pyridine-Based Schiff Base CuII Complexes for DNA Binding and Cleavage. *Chemistry & Biodiversity*, *9*(10), pp.2262-2281.
11. Ude, Z., Kavanagh, K., Twamley, B., Pour, M., Gathergood, N., Kellett, A. and Marmion, C.J., 2019. A new class of prophylactic metallo-antibiotic possessing potent anti-cancer and anti-microbial properties. *Dalton Transactions*, *48*(24), pp.1-10.
12. Liu, J.G., Zhang, Q.L., Shi, X.F. and Ji, L.N., 2001. Interaction of [Ru (dmp) 2 (dppz)] 2+ and [Ru (dmb) 2 (dppz)] 2+ with DNA: effects of the ancillary ligands on the DNA-binding behaviors. *Inorganic Chemistry*, *40*(19), pp.5045-5050.
13. Vijayalakshmi, R., Kanthimathi, M., Subramanian, V. and Nair, B.U., 2000. Interaction of DNA with [Cr(Schiff base)$(H_2O)_2$] ClO4. *Biochimica et Biophysica Acta (BBA)-General Subjects*, *1475*(2), pp.157-162.
14. Adeloye, D., Sowunmi, O.Y., Jacobs, W., David, R.A., Adeosun, A.A., Amuta, A.O., Misra, S., Gadanya, M., Auta, A., Harhay, M.O. and Chan, K.Y., 2018. Estimating the incidence of breast cancer in Africa: a systematic review and meta-analysis. *Journal of Global Health*, *8*(1).
15. https://www.cansa.org.za/womens-health/ (Breast Cancer).
16. Abrahams, S., Mosebi, S., Fish, M.Q., Papathanasopoulos, M.A. and Hewer, R., 2018. Screening of the NIH Clinical Collection for inhibitors of HIV-1 integrase activity. *South African Journal of Science*, *114*(3-4), pp.1-5.
17. Naher, S., Tognela, A., Moylan, E., Adams, D.H. and Kiely, B.E., 2018. Patterns of care and outcomes among triple-negative early breast cancer patients in South Western Sydney. *Internal Medicine Journal, 48*(5), pp.567-572.

18. Seburu, J.O., Romero-Canalon, I., Sullivan, N., Lapkin, A.A., and Barker, G.C., 2014. Comparative cytotoxicity of artemisinin and cisplatin and their interactions with chlorogenic acids in MCF7 breast cancer cells. *Chemical Medicine & Chemical Biology, 9*(12), pp.2791-2797.
19. https://www.sigmaaldrich.com/technical-documents/articles/biology/quantitation-of-oligos.html (DNA extinction coefficient).

CHAPTER 7: CONCLUSIONS AND FUTURE WORK

7.1 Conclusions

In this study, Schiff base and phenanthroline-based ligands (dppz) have been synthesized and chelated to copper(II) to produce five complexes (Figure 7.1). The copper(II) chelates were synthesized with the aim of producing a new class of potential chemotherapeutic agents that exert their cytotoxicity through DNA interaction and the catalytic production of ROS through the Cu(II)/Cu(I) redox couple. The Schiff base ligand and four complexes were synthesized using an environmentally friendly solid state procedure.

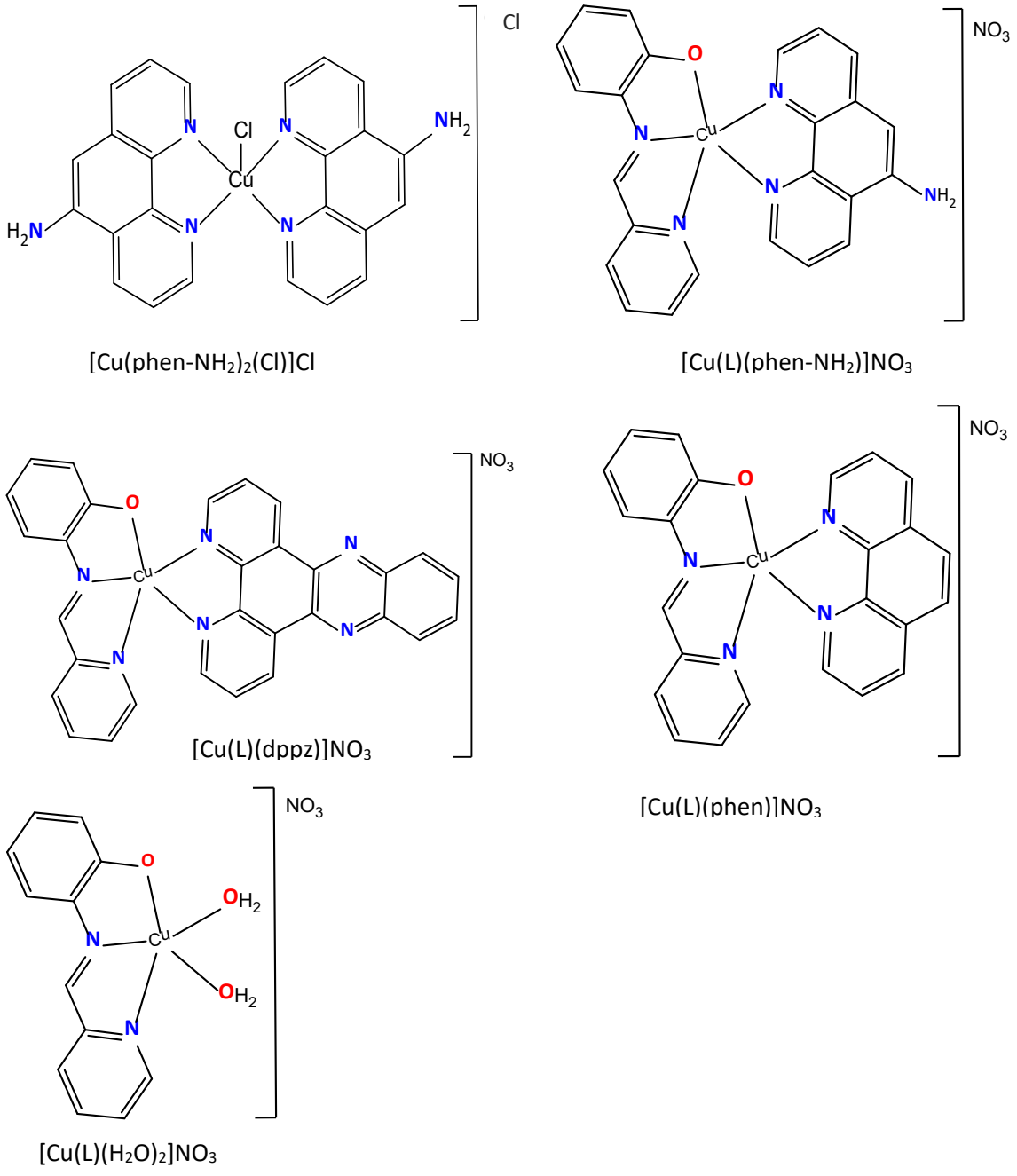

Figure 7.1: Structures of the copper(II) chelates successfully synthesized in this work.

The Schiff base ligand was synthesized in a one-step, solid state reaction involving the condensation of 2-pyridinecarbaldehyde and 2-aminophenol in a 1:1 ratio. This ligand was characterized by ^{1}H NMR spectroscopy with the signature peak of the azomethine group (CH=N) appearing at 8.75 ppm. The dppz ligand was synthesized *via* reflux of *o*-phenylenediamine and

1,10-phenanthroline-5,6-dione. The dppz ligand is symmetric with carbons and protons on each side of the molecule in equivalent chemical environments. Both ligands were further characterized by IR and ^{13}C NMR. In the synthesis of $[Cu(L)(H_2O)_2]NO_3$ chelate, the metal complex was synthesized by reacting the Schiff base ligand with $[Cu(NO_3)_2]$ in a 1:1 molar ratio. The isolated dark red crystals grew *via* slow evaporation of a solution of $[Cu(L)(H_2O)_2]NO_3$ and were then further reacted with three co-ligands: phen, phen-NH_2 and dppz to afford three secondary heteroleptic complexes ($[Cu(L)(phen)]NO_3$, $[Cu(L)(phen\text{-}NH_2)]NO_3$ and $[Cu(L)(dppz)]NO_3$). The $[Cu(phen\text{-}NH_2)_2Cl]Cl$ complex was synthesized by reacting the bidentate phen-NH_2 with $[CuCl_2]$ under reflux conditions in a 2:1 molar ratio.

Various spectroscopic techniques (IR, UV/vis, MS, EPR) and elemental analysis were employed to confirm the successful synthesis of the copper(II) chelates. Due to the large aromatic chromophores and extended conjugation of the ligands and complexes, interesting absorption spectra were noted. The spectra of the Schiff base ligand has a characteristic band at 283 nm ($\pi \rightarrow \pi^*$) which underwent a bathochromic shift in the spectra of $[Cu(L)(H_2O)_2]NO_3$ to 303 nm, due to the chelation with the metal ion. The secondary heteroleptic copper(II) complexes ($[Cu(L)(phen)]NO_3$, $[Cu(L)(phen\text{-}NH_2)]NO_3$ and $[Cu(L)(dppz)]NO_3$) are characterized by an increased number of $\pi \rightarrow \pi^*$ bands between 250-400 nm upon addition of the co-ligand. The EPR spectra of the primary heteroleptic complex ($[Cu(L)(H_2O)_2]NO_3$) and secondary heteroleptic copper(II) complexes have similar spectra. Substitution of the co-ligand appears to have little impact on the shape of the spectra, confirming the similar geometry of the complexes. The EPR spectrum of $[Cu(phen\text{-}NH_2)_2Cl]Cl$ complex is different to other complexes. This is expected since this complex has a square planar geometry in solution. X-ray crystallography showed that primary heteroleptic complexes ($[Cu(L)(H_2O)_2]NO_3$ and $Cu(L1)(H_2O)_2]$) had square pyramidal geometries with various combinations of N and O-donor ligands.

The DNA binding affinities of the chelates were measured using direct and fluorescence competitive binding DNA titrations. The direct DNA binding technique was used to determine the binding constant of the known intercalator ethidium bromide (EB). The fluorescence competitive binding DNA titrations were done to determine the binding affinity of the copper(II) chelates for ctDNA. During the DNA titration, with increasing concentration of complexes there was a quenching of the initial EB-ctDNA emission intensity. This is indicative of the complex displacing EB from the binding sites on the DNA. The DNA studies showed the influence of the structural features of the complexes on the DNA binding affinities. The K_{app} values ranges from 2.79×10^5 M^{-1} for $[Cu(L)(H_2O)_2]NO_3$ to 5.31×10^6 M^{-1} for $[Cu(phen\text{-}NH_2)_2(Cl)]Cl$. This shows that square planar complexes bind more effectively than square pyramidal complexes (in solution). The order of all complexes in terms of increasing binding strength is:$[Cu(L)(H_2O)_2]NO_3$ < $[Cu(L)(phen)]NO_3$ < $[Cu(L)(dppz)]NO_3$ < $[Cu(L)(phen\text{-}NH_2)]NO_3$ < $[Cu(phen\text{-}NH_2)_2(Cl)]Cl$. The addition of hydrogen bonding groups increased the binding affinity by stabilising the DNA/drug conjugate.

The five copper(II) chelates were screened against a panel of four human cell lines. These cell lines are: HEK293 (healthy embryonic kidney cells) which was used as a control, MDA-MB (triple negative cancer cells), HELA (cervical cancer cells) as well as SHSY5Y (human neuroblastoma cells). From the cell screening, the EC_{50} values were calculated. The complex $[Cu(L)(dppz)]NO_3$ had the

lowest EC_{50} values while $[Cu(L)(H_2O)_2]NO_3$ had the highest EC_{50} values. The results showed that four complexes are highly cytotoxic, more so than the well-known chemothepeutic agent, cisplatin. The primary heteroleptic complex $[Cu(L)(H_2O)_2]NO_3$ showed lower cytotoxicity than cisplatin, however, it has greater selectivity. It is noteworthy that the cytotoxicity of the compound varies with different cells; hence each has a unique cytotoxicity profile and could be used for specific type of cancer. There is little correlation between the binding affinities of complexes and their cytotoxicity, this suggest that the mechanism of action could include the production of ROS *in vitro*, which are known to cleave the DNA and induce apoptosis. Significantly, all the complexes synthesized in this work showed lower toxicity towards the healthy cell line than the tumour cell lines. It was also shown that the combination of the Schiff base ligand and co-ligand was an important factor in the cytotoxicity.

The objectives proposed in chapter one have been accomplished:

- The synthesis of Schiff base ligand and the co-ligand dppz which were fully characterized
- Five copper(II) chelates have been synthesized and characterized.
- The DNA binding affinities of the complexes were determined using direct and competitive DNA titrations.
- The copper(II) chelates were screened against a panel of different human cell lines and cytotoxicity was determined.

The synthetic procedures used in this study are unusual methods for coordination and condensation reactions. This work on copper(II) chelates shows good DNA binding affinities with good cytotoxicity and will be useful for future research, not only for designing chemotherapeutic agents, but also for the green synthesis of metal complexes. The Schiff base ligand and heteroleptic complexes were synthesized using a solid state technique. The binding affinities and cytotoxicity studies showed promising results, although the exact mechanism of action through which the complexes bind to DNA and exert their cytotoxicity is unknown. Hence, additional experiments such as gel electrophoresis and hydroxyl radical assays will be conducted in the future.

7.2 Future work

The main objective of this research was to synthesize and fully characterized copper(II) chelates and determine their potential as chemotherapeutic agents. The study showed that there is potential for the copper(II) chelates as chemotherapeutic agents. The primary goal has therefore been achieved, however there are a few structural features that could have been implemented to improve the cytotoxicity of the complexes. Some of the future avenues of research are briefly discussed below.

In the present study, phenanthroline-based ligands have been used as co-ligands in the synthesis of copper(II) chelates. The aromaticity and hydrogen bonding ability of this co-ligand appears to influence the binding affinities and cytotoxicity of the copper(II) chelates. Although the copper(II) chelates showed good selectivity towards different cell lines, it is necessary to develop tumour-

specific delivery agents for chemotherapeutic compounds that can recognize the intrinsic difference between tumour and normal cells to further improve selectivity. In general, a tumour-targeting drug delivery system (DDS) consists of a tumor recognition moiety and a phototoxic or cytotoxic agent connected through a suitable linker to form a conjugate.[2] The tumour targeting DDS should have a bio-essential constituent that is non-toxic prior to activation. In addition, the linker unit must be stable in blood circulation, but the conjugate may become cleaved to release a cytotoxic agent upon the internalization into tumour cells. There are many tumour-specific receptors that are overexpressed by cancer cells and could be used as biomarkers to deliver cytotoxic agents to tumour cells. Folic acid, transferrin, monoclonal antibodies, polysaturated fatty acid, aptamers and oligopeptides have all been used to design tumour-targeting drug conjugates.[1-3]

Since cancer cells require certain vitamins for their rapid growth, receptors involved in the uptake of these vitamins are overexpressed on the surface of cancer cells. Vitamin B_{12}, biotin, folic acid and riboflavin are essential vitamins for the development and growth of tumours. Biotin receptors are overexpressed more than any other vitamins and it has been reported that the high specificity of second-generation taxoid in leukaemia cells is due to conjugation of a drug to biotin through a self-immolative linker.[2]

Hence, by suitable modification of the substituents on the phenanthroline ligand, the cytotoxicity of the complexes can be highly modulated. This can be done by incorporating the biotin substituent appended to the phenanthroline scaffold *via* an amide linkage. The phen-biotin co-ligand will hopefully improve the biodistribution of the chelates by making them more selective toward neoplastic tissue. Also, biotin is water soluble, which enhances the absorption of the drug into the body. The proposed structure of the chelates $[Cu(L)(phen\text{-}biotin)]^{+}$ and $[Cu(phen\text{-}biotin)_2]^{2+}$ are shown in Figure 7.2.

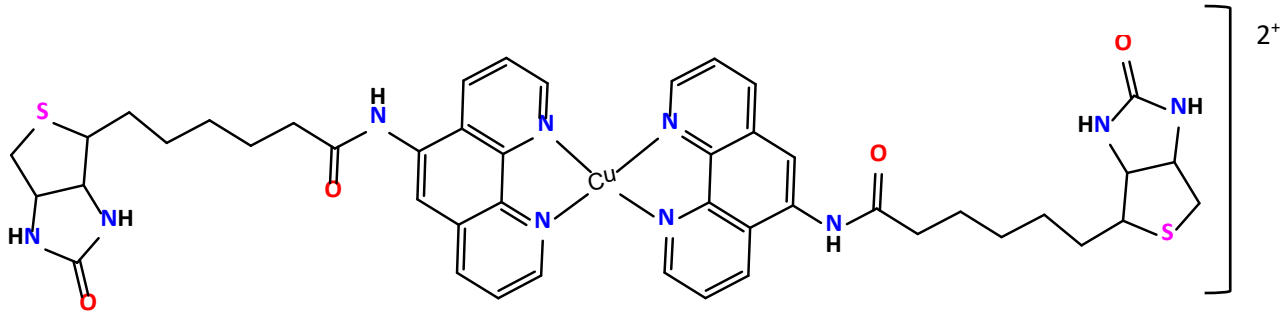

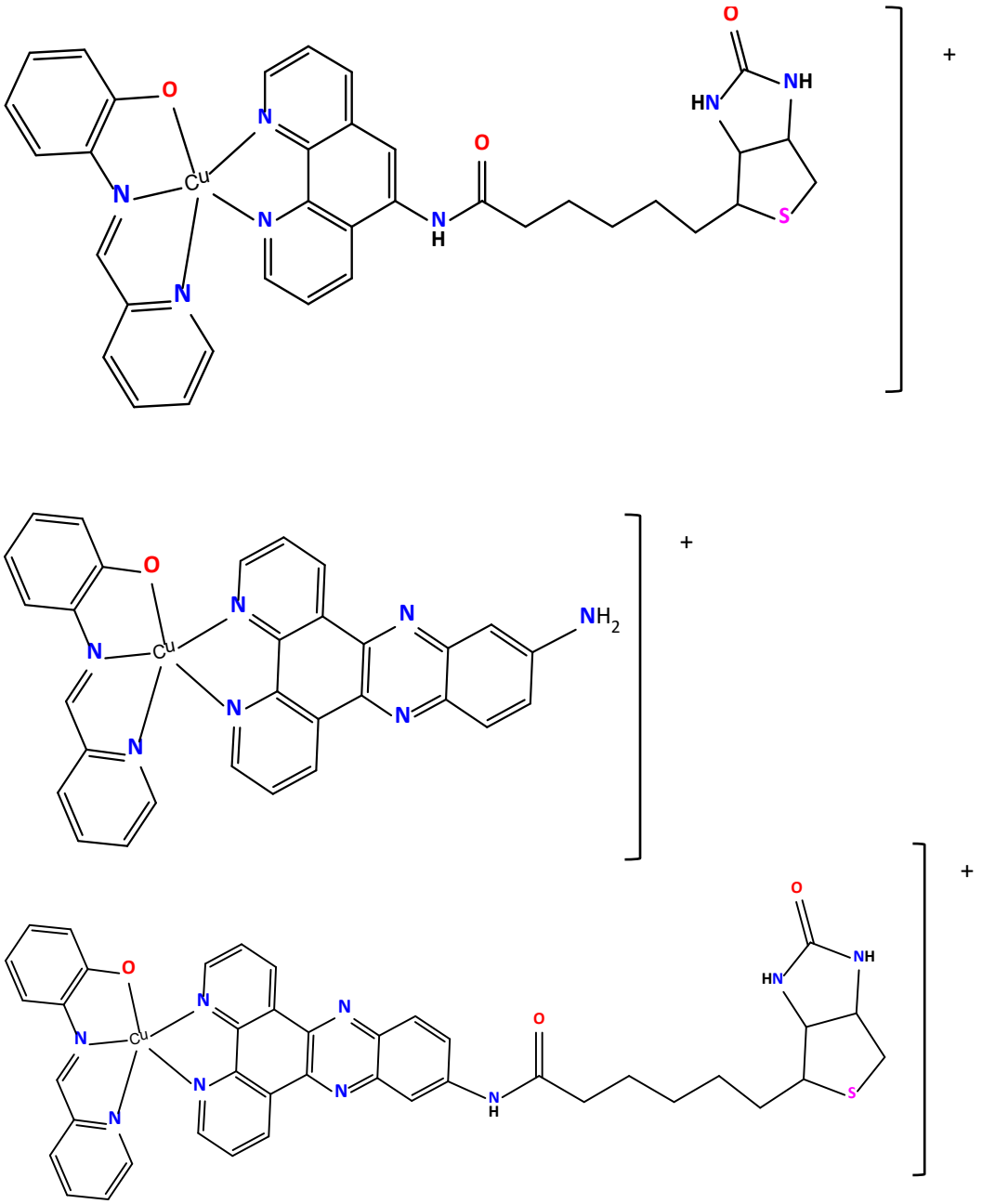

Figure 7.2: The structures of the proposed copper(II) complexes.

The phen-biotin ligand was synthesized, however, the ^{1}H NMR spectrum showed unwanted products of side reactions. Due to the impurities within the phen-biotin ligand, the coordination reaction was not conducted. If the compound can be isolated and purified in the future it could be reacted to form copper(II) chelates which are anticipated to be more target specific.

The presence of hydrogen bonding appears to improve the binding affinities, while extending the aromaticity appears to enhance the cytotoxicity of the complex. The co-ligand with both of these characteristics will be synthesized in the future development of heteroleptic copper complexes (Figure 7.2). A biotin-conjugated dipyridophenazine derivative has been reported to improve the target delivery of the complexes specifically to tumor tissues, and to reduce their accumulation

in normal tissues.[1] The biotin will also be linked to dppz forming a dppz-biotin co-ligand. This will be reacted to form the heteroleptic copper(II) chelate $[Cu(L)(dppz\text{-}biotin)]^{+}$.

In this future work, we will conjugate biotin to the phenanthroline-based ligand with an objective to increase target specificity and cytotoxicity of the copper(II) complexes towards tumours. The uptake of biotin by cells is known to occur through the sodium-dependent multi-vitamin receptors (SMVTs) and mono-carboxylate transporters.[4] No modification will be done on the single Schiff base complex, since the chelate showed good selectivity. Although it has low cytotoxicity, the addition of the co-ligand appears to improve the cytotoxicity.

The activity of many pharmaceuticals requires them to interact with and cross the biological membrane to reach their active site and induce the desired responses. So, it is important to study the physiochemical properties of the drug to achieve the desired pharmacokinetics behaviour of a drug without losing its pharmacodynamic features.[5] In order to move across the lipidic core of the membranes, molecules of a drug must be hydrophobic and also have the ability to lose their hydration sphere. Hence, the lipophilicity is a crucial parameter in the design and development of drugs. The measurement of lipophilicity is used to infer bioavailability of drugs and represents the affinity of a molecule in a lipidic environment. The most common measure is by molecule-distribution process in a biphasic system.[5,6] In the future work of this project the partition/distribution system to be used is octanol/water. The octanol/water coefficient (K_{ow}) is a prerequisite study for any drug since the biological properties such as toxicity and bioaccumulation depends on its K_{ow}. The K_{ow} will provide a measure of the ability of the compound to cross cellular membranes allowing it to reach the target and have the intended therapeutic effect.

In a biological system, one of the attributes of the toxicity of copper comes from its ability to participate in redox reactions and therefore catalyse the formation of reactive oxygen species (ROS). Copper(II) can be reduced to copper(I) with ascorbic acid *via* the Haber Weiss reaction, generating hydroxyl radicals from hydrogen peroxide as seen in Scheme 7.1.

$$HS\text{-}R\text{-}S^{-} + Cu^{2+} \rightarrow HS\text{-}R\text{-}S^{\cdot} + Cu^{+}$$

$$HS\text{-}R\text{-}S^{-} + O^{2} \rightarrow S\text{-}S\text{-}R + H^{+} + O_2^{-\cdot}$$

$$2O_2^{-\cdot} + 2H^{+} \rightarrow H_2O_2 + O_2$$

$$Cu^{+} + H_2O_2 \rightarrow OH^{\cdot} + OH^{-} + Cu^{2+}$$

$$OH^{\cdot} + DNA \rightarrow \text{fragments}$$

Scheme 7.1: The production of hydroxyl radicals catalysed by copper(II) for DNA degradation.

The production of ROS leads to DNA cleavage and will be investigated in future work. Hydroxyl radical assays will be carried out using the Rhodamine B dye which acts as a spectrophotometric indicator. During the experiment, the decrease in the absorbance will indicate the production of hydroxyl radicals and the corresponding decay of Rhodamine B dye. This will likely be one of the key steps in the cytotoxicity of the copper(II) chelates.

DNA binding studies of copper(II) chelates have been conducted by direct and competitive DNA binding titrations. However, the exact binding mode of the chelates is not known since this method does not distinguish between groove binding and intercalation. Gel electrophoresis will be carried out to investigate the DNA binding mode. The electrophoretic mobility shift assays (EMSAs) are usually used to analyse nucleic acid-protein interaction. This assay is based on the fact that when the nucleic acid is bound by protein, its electrophoretic mobility during gel electrophoresis is reduced when compared to the free state. Correspondingly, the final position of the protein within the complex is shifted when compared to the free state.[7] In gel electrophoresis, the mobility of DNA through the agarose gel is highly dependent on the length of the DNA. The DNA strand is lengthened by the intercalation of a molecule resulting in reduced mobility.

The copper(II) chelates in this research study showed good cytotoxicity when tested against four cell lines. However, a more accurate cytotoxicity profile can be achieved by screening the copper(II) chelates against a wider range of cell lines. Testing the complexes against different forms of cell lines will provide results that allow for the statistical comparison of the activity profile of these complexes with activity profile of a compound with well-known modes of action. This will give a likely mode of action of the potential chemotherapeutic agents.

7.3 References

1. Saha, S., Majumdar, R., Hussain, A., Dighe, R.R. and Chakravarty, A.R., 2013. Biotin-conjugated tumour-targeting photocytotoxic iron (III) complexes. *Philosophical Transactions of the Royal Society A: Mathematical, Physical and Engineering Sciences*, *371*(1995), pp.1-5.
2. Ojima, I., Geng, X., Wu, X., Qu, C., Borella, C.P., Xie, H., Wilhelm, S.D., Leece, B.A., Bartle, L.M., Goldmacher, V.S. and Chari, R.V., 2002. Tumor-specific novel taxoid− monoclonal antibody conjugates. *Journal of Medicinal Chemistry*, *45*(26), pp.5620-5623.

3. Farokhzad, O.C., Cheng, J., Teply, B.A., Sherifi, I., Jon, S., Kantoff, P.W., Richie, J.P. and Langer, R., 2006. Targeted nanoparticle-aptamer bioconjugates for cancer chemotherapy in vivo. *Proceedings of the National Academy of Sciences*, *103*(16), pp.6315-6320.
4. Russell-Jones, G., McTavish, K., McEwan, J., Rice, J. and Nowotnik, D., 2004. Vitamin-mediated targeting as a potential mechanism to increase drug uptake by tumours. *Journal of Inorganic Biochemistry*, *98*(10), pp.1625-1633.
5. Cumming, H. and Rücker, C., 2017. Octanol–Water Partition Coefficient Measurement by a Simple ^{1}H NMR Method. *ACS Omega*, *2*(9), pp.6244-6249.
6. Esteves, F., Moutinho, C. and Matos, C., 2013. Correlation between octanol/water and liposome/water distribution coefficients and drug absorption of a set of pharmacologically active compounds. *Journal of Liposome Research*, *23*(2), pp.83-93.
7. Stead, J.A. and McDowall, K.J., 2007. Two-dimensional gel electrophoresis for identifying proteins that bind DNA or RNA. *Nature Protocols*, *2*(8), p.1839.